STRENGTH ENHANCEMENT OF AUTOCLAVED AERATED CONCRETE (AAC) BLOCK AND ITS MASONRY

A Thesis Submitted in Partial Fulfillment of the Requirements
for the Degree of

DOCTOR OF PHILOSOPHY

By

Amit Raj

(Roll No. 156103044)

Department of Mechanical Engineering

Indian Institute of Technology Guwahati

Guwahati-781039

INDIA

November 2020

Department of Mechanical Engineering,

Indian Institute of Technology Guwahati,

Guwahati-781039, INDIA

CERTIFICATE

It is certified that the work contained in the thesis entitled **"Strength Enhancement of Autoclaved Aerated Concrete (AAC) Block and its Masonry"** is submitted by **Mr. Amit Raj** to the Indian Institute of Technology Guwahati for the award of the degree of Doctor of Philosophy. The work has been carried out under our supervision in the Department of Mechanical Engineering, Indian Institute of Technology Guwahati. This work has not been submitted elsewhere for the award of any other degree or diploma.

Dr. UDAY SHANKER DIXIT

Professor

Department of Mechanical Engineering,

Indian Institute of Technology Guwahati,

Guwahati-781039, INDIA

Dr. ARUN CHANDRA BORSAIKIA

Technical officer (Grade 1)

Department of Civil Engineering,

Indian Institute of Technology Guwahati,

Guwahati-781039, INDIA

Date: November 03, 2020

DECLARATION

I declare that,

a. The work contained in this thesis is original and has been done by me under the guidance of my supervisors.
b. The work has not been submitted to any other institute for any degree or diploma.
c. I have followed the guidelines provided by the institute in preparing the thesis.
d. I have confirmed to the norms and guidelines given in the ethical code of conduct of the institute.
e. Whenever I used materials (data, theoretical analysis, figure and text) from other sources, I have given due credit to them by citing them in the text of the thesis and giving their detail in references.

Signature of student
(Amit Raj)

Dedicated to God, My Teachers
and
My Parents

Acknowledgement

I would like to express my deep and sincere gratitude to **Prof. Uday Shanker Dixit** and **Dr. Arun Chandra Borsaikia**, who have inspired my academic and personal life with their guidance, encouragement, gracious support and care throughout my work. Their valuable suggestions, effusive co-operation, co-ordination and encouraging interactions were a great driving force for me to carry out this research work. I express my sincere gratitude to my doctoral committee **Prof. Baleshwar Singh**, **Prof. Debabrata Chakraborty** and **Prof. Pankaj Biswas** for their encouragement and valuable suggestions throughout the study. I express my sincere thanks to the former and present heads of the Department of Mechanical Engineering, **Prof. A.K. Das** and **Prof. S.K. Dwivedy**. I would also like to extend my gratitude to all my teachers for broadening and enriching my knowledge.

Financial assistance provided by the Ministry of Human Resource Development (MHRD), Government of India, is greatly acknowledged. I would like to acknowledge Department of Science and Technology (DST) Govt. of India, Indian Institute of Technology Guwahati for sponsoring a project entitled "Design and development of proper bonding mechanism for individual AAC block units in wall system of a structure" through grant number DST/TSG/AMT/2015/375 and M/s KD Infra Industry for providing all sorts of infrastructural facilities. Special thanks to all the technical and non-technical staff at Structural Engineering Laboratory, Central Workshop and Strength of Material Laboratory of IIT Guwahati for their unconditional and most-willing support during the experiments.

I wish to express my sincere thanks to Mr. Biswajit Debnath, Mr. Pranab Hazarika, Mr. Saurabh Kumar Mudoi, Mr. Sanjib Sarma, Mr. Pankaj Khakhlary, Mr. Suresh Boro and Mr. Prakash Mondal for helping me during the experimental studies. I would like to thank Research fellows (Mr. Sushrut Barman, Ms. Smita Kumari and Mr. Biswajeet Barman) for their supports during the experiments.

I express my sincere thanks to my friends/labmates Dr. Polash Pratim Dutta, Dr. Vinod Yadav, Dr. S.M. Kamal, Dr. Besufekad Negash Fetene, Dr. R. Kalidasan, Dr. W.G. Jiru, Dr. Rajkumar Shufen, Dr. Vikash Kumar, Mr. Sujoy Tikader, Mr. Faladrum Sharma, Mr. Nitish Bhardwaj, Mr. Nilkamal Mahanta, Mr. Kaustabh Chatterrjee, Mr. Shivam Mishra, Mr. Swapnil Sahoo, Mr. Vipul Kumar and Mr. Snehal Shende.

I would like to express my sincere gratitude to all those who have helped me in various ways directly and indirectly during the tenure of my Ph.D. work at IIT Guwahati. I shall always be grateful to all my IIT and childhood friends for their great encouragement and wishes.

I express my deep gratitude to my parents Shri Wakil Prasad Yadav and Mrs. Parvati Devi for their goodwill, motivation, supports and grace. I am thankful to all my family members and one related to this work up to any extent in the due course of time.

Amit Raj
IIT Guwahati

Abstract

Autoclaved Aerated Concrete (AAC) is a light-weight building-construction product of fly ash, sand, water, cement, lime and aluminum powder, used globally for brickwork. The AAC is now widely accepted as an innovative and high quality building-material. In the recent years, AAC has been widely used for the interior of industrial, commercial and residential buildings. The AAC blocks are used for both load bearing and non-load bearing masonry walls. The tensile bond and shear bond strengths of such walls are greatly affected by the bond strength of block-mortar interface. For a strong masonry, a perfect bond between masonry unit and mortar is crucial. The bond strength becomes significantly important when the masonry is subjected to in-plane and out-of-plane loading during seismic tremors. The masonry unit-mortar bond development is influenced by a large numbers of parameters related to the characteristics of masonry unit and mortar.

The AAC blocks are wire-cut as per the industrial practice, which results in smooth surfaces. Shear bond strength is low when the two blocks with smooth surfaces are joined with mortar. The presence of frog in clay brick imparts higher masonry shear bond strength. For this, in the present work, a grooved AAC block has been studied to enhance the shear bond strength of AAC masonry. The grooved AAC blocks were produced in an AAC manufacturing industry. Moreover, for adequate bond strength, an optimum amount of cementitious material is required at the interface. Hence, a cement slurry coating at the bed face of AAC has been used to enhance the bond strength of block-mortar interface. The thesis explores the various efficient techniques to enhance the strength of AAC masonry. The study of the AAC masonry behavior under compression load using finite element method (FEM) is also covered in this research work.

First, the mechanical properties of AAC block and its masonry were investigated. There is hardly any information available on the mechanical properties of AAC masonry based on a thick cement-sand mortar. Hence, the compressive, shear bond and tensile bond strengths of AAC masonry assemblage were evaluated. A simple analytical model has been also proposed to evaluate the elastic modulus of masonry prism. The elastic modulus of AAC masonry evaluated using a one-dimensional analytical model has a close agreement with experimental findings. It is observed that the bond strength of AAC masonry is quite less as compared to the clay brick masonry.

The bond strength may be enhanced by changing the bed face of AAC block from plain to rough texture. Here, the bond strength of a grooved AAC masonry was studied. Producing the grooved AAC block is found to be practically feasible in the existing manufacturing set-up through mold modification method. A large numbers of experiments on the sliding shear bond (along the bed joint) and compressive strengths of grooved AAC masonry have been carried out. The results are compared with those for conventional AAC blocks and masonry. Analytical models have been developed to estimate upper, lower and most likely estimates of strengths. Hypothesis testing has been carried out to support the experimental findings. The findings of this work strongly support the enhancement of shear

load carrying capacity of a masonry employing grooved AAC blocks; however, compressive strength does not change significantly.

Further, the bond strength of AAC block-mortar interface made of ordinary sand-cement mortar of different compositions and polymer modified mortars was investigated. A method of improving the bond strength (both tensile and shear) of ordinary sand-cement mortar without altering the block surface characteristics is proposed. In this method, the block surfaces are coated with a thin cement-slurry coating before applying a thick sand-cement mortar. The failure patterns during the bond strength tests were studied. Subsequently, costs were estimated for AAC walls of different types of interfaces. Considering the bond strength as well as cost, using a weak mortar (lean cement content) along with cement-slurry coating was found superior to the ordinary sand-cement mortar and polymer modified mortar.

The last part of this work deals with finite element (FE) modeling of AAC masonry for the estimation of compressive strength. The aim was to assess and analyze the experimental results. In this part of work, the finite element micro-modeling, governed by plastic-damage constitutive relation in tension and compression, has been used to model the AAC block and mortar, while cohesive zone modeling strategy is adopted to model the block-mortar interface. The developed model has been used for the estimation of compressive strength of AAC masonry. The nature of lateral stress developed due the application of axial stress is discussed. The comparative study on stress distribution in AAC block and clay brick masonries is also presented. The results obtained from modeling have good agreement with the experimental results.

Overall, this research accomplished the following tasks. A comprehensive study on the mechanical properties of AAC masonry was conducted through experiments. A simple analytical model has been proposed to evaluate the elastic modulus of masonry prism. Rigorous experiments on the shear bond and compressive strengths of grooved AAC masonry have been carried out. Using the interval arithmetic, analytical models have been developed to estimate upper, lower and most likely estimates of strengths. Hypothesis testing has been carried out to support the experimental results. A method of improving the bond strength (both tensile and shear) of ordinary sand-cement mortar without altering the block surface characteristics is proposed. Finally, the finite element (FE) modeling of AAC masonry for the assessment and analysis of the experimental results of compressive strength have been carried out. A good agreement between experimental and computational results is obtained. It is envisaged that the proposed techniques will enhance the shear bond strength of AAC blocks in the masonry.

Contents

List of Figures

List of Tables

Nomenclature

Roman letters

A	Bonding area
C	Cohesion
d	Diameter of groove
D	Diameter of cylindrical AAC specimen
d_c	Damage variable in compression
d_t	Damage variable in tension
E	Elastic modulus of masonry
E_0	Initial elastic stiffness of material
E_1	Elastic modulus of AAC block
E_2	Elastic modulus of mortar
E_{eq}	Equivalent elastic modulus of masonry
E_t	Tangent modulus
f_{bo}	Biaxial compressive strength
f_{co}	Uniaxial compressive strength
h	Height of masonry prism
I_1	First invariant of stress tensor
J_2	Second invariant of deviatoric stress tensor
J_3	Third invariant of deviatoric stress tensor
K	Temperature
K_{nn}	Stiffness coefficient in normal direction
K_{ss}	Stiffness coefficient in shear direction
K_{tt}	Stiffness coefficient in out of plane shear direction
l	Length of AAC block
L	Length of cylindrical AAC specimen
l_1	Thickness of AAC block

l_2	Thickness of mortar
l_{total}	Total height of masonry
n	Sample size
P_1	Shear load carrying capacity of PB masonry triplet
P_2	Shear load carrying capacity of SGB masonry triplet
P_3	Shear load carrying capacity of DGB masonry triplet
P_c	Maximum compression load
P_{DGB}	Compressive load carrying capacity of DGB block
P_{MDGB}	Compressive load carrying capacity of DGB masonry
P_{MPB}	Compressive load carrying capacity of PB masonry
P_{MSGB}	Compressive load carrying capacity of SGB masonry
P_{PB}	Compressive load carrying capacity of PB block
P_s	Peak shear load
P_{SGB}	Compressive load carrying capacity of SGB
P_t	Peak tensile load
r	Stress invariant measure of deviatoric stress
s	Standard deviation
T	Traction
t	Thickness of masonry prism
T_n	Traction in normal direction
T_t	Traction in tangential direction
w	Width of AAC block

Greek letters

ξ	Stress invariant measure of hydrostatic stress
ε_c	Strain in compression
ε_t	Strain in tension
$\tilde{\varepsilon}_c^{pl}$	Equivalent plastic strain in compression
$\tilde{\varepsilon}_t^{pl}$	Equivalent plastic strain in tension
$\dot{\tilde{\varepsilon}}_c^{pl}$	Equivalent plastic strain rate in compression
$\dot{\tilde{\varepsilon}}_t^{pl}$	Equivalent plastic strain rate in tension

t_α	t-value corresponding to significance level (α)
α	Significance level
β_i	Initial friction angle
δ	Separation
δ_{eq}	Equivalent deflection
δ_n	Separation in normal direction
δ_t	Separation n tangential direction
θ	Similarity angle
ρ_{dry}	Dry density
σ	Compressive strength
σ_b	Compressive strength of block
σ_c	Equivalent crushing strength of mortar
σ_{cu}	Ultimate stress in compression
σ_m	Equivalent compressive strength of mortar
σ_p	Pre-compression stress
σ_{split}	Splitting tensile strength
σ_{to}	Failure stress in uniaxial tension
σ_{xb}	Lateral stress in block in *x*- direction
σ_{xm}	Lateral stress in mortar in *x*- direction
σ_{yb}	Lateral stress in block in *y*- direction
σ_{ym}	Lateral stress in mortar in *y*- direction
τ	Shear bond strength
τ_t	Tensile bond strength

List of abbreviations

CDP	Concrete damage plasticity
CSCM1	Combination of cement slurry coating and SCM1
CSCM2	Combination of cement slurry coating and SCM2
CSCM3	Combination of cement slurry coating and SCM3
CV	Coefficient of variation
CZM	Cohesive zone modeling
DGB	Double-grooved block
ECZM	Elemental cohesive zone modeling
FEM	Finite element method
IRA	Initial rate of absorption
MOR	Modulus of rupture
PB	Plain block
PET	Polyethylene terephthalate
PMM	Polymer modified mortar
SCM1	Sand-cement mortar (cement to sand ratio by weight =1/2)
SCM2	Sand-cement mortar (cement to sand ratio by weight =1/4)
SCM3	Sand-cement mortar (cement to sand ratio by weight =1/6)
SCZM	Surface cohesive zone modeling
SGB	Single-grooved block
WA	Water absorption
XFEM	Extended finite element method

Chapter 1

Background and Scope

1.1 Introduction

Nowadays, awareness of environmental aspects has grown in the building and construction sectors. The conservation of natural resources, eco-friendly manufacturing, energy saving and comfort living have forced to search a sustainable manufacturing process for a sustainable building material. The manufacturing procedures of building materials contribute greenhouse gases like CO_2 to the atmosphere. There is a great concern and emphasis in reducing the greenhouse gases emission into the atmosphere in order to control adverse environmental impacts. The construction industry in India is responsible for the largest share of CO_2 (22%) emission into the atmosphere (Reddy and Jagadish, 2003).

Bricks are a widely used, and perhaps the oldest, construction and building material around the world (Zhang, 2013). Since 3000 BC, as humans started to settle, bricks registered as a remarkable, easily usable and workable product (Bories et al. 2014). Conventional (clay) bricks are produced from clay with high temperature kiln firing, and thus consume a lot of energy and have large carbon footprint. In many areas of the world, there is already a shortage of natural source material for the production of the conventional bricks (Zhang, 2013). Near about 10,000 hectares of top soil is lost every year for earth clay brick manufacturing (AACPA, 2017). Clay bricks are manufactured using top fertile soil causing soil infertility, soil erosion and also a concern of food production. Brick kilns are responsible for nearly 15% of total air pollution, which has become a major environmental concern for localities such as NCR-Delhi as per a study by IIT Delhi (India). On other hand, the solid waste in India has emerged as a great threat to the environmental health of the country. The urban India alone generates 1.5 lakh metric tons of waste per day and is increasing every year by 5% (India Today News, 2019). This increase in the solid waste generation is due to the rising population and consumption patterns.

The increase in industrial solid waste in India has also emerged as a great threat to the environmental health of the country. To increase the utilization of this solid waste for other application is the major concern of the modern era. During the year 2013-2014, around 172.87 million tons of ash was generated by burning coal. However, only 99.62 million tons of ash was utilized. The unutilized ash in the form of fly ash is usually disposed in open pond, forest and open land (AACPA, 2017). Dumping of fly ash lowers the soil fertility, contaminates the soil, corrodes the exposed metal and causes health hazards like bronchitis, silicosis, lung cancer and asthma (AACPA, 2017). For sustainable development and environmental protection, extensive research has been conducted on production of bricks from waste materials (Lingling et al. 2005, Menezes et al. 2005, Kayali 2005, Lin et al. 2006, Demer 2006, Aeslina et al. 2010, Turgut and Algin 2007, Chen et al. 2011, Rajamane et al. 2012 and Quesada et al. 2012). A wide variety of waste materials have been studied, including fly ash, slags, mine tailings, construction and demolition waste, cotton waste, wood sawdust, limestone powder, paper production residue, petroleum effluent treatment plant sludge, cigarette butts, waste tea, crumb rubber, cement kiln dust and rice husk ash.

Different methods have been used to produce bricks from waste materials in the past. The fly ash brick, autoclaved aerated concrete brick (AAC) or cellular lightweight concrete (CLC) are the types of brick made from the fly ash. These bricks have better quality than the burnt red clay bricks. The autoclaved aerated concrete (AAC) block/brick or unit has emerged as the best alternative of clay brick. The kilns meant for heat treatment source in clay brick create air pollution and is replaced by steam based heat treatment called autoclave in the AAC production industries. Hence, AAC is also known for a sustainable building material. A brief introduction, advantages, disadvantages, applications and manufacturing process of AAC are discussed in the further subsections.

1.2 Autoclaved Aerated Concrete (AAC) Block

Autoclaved Aerated Concrete (AAC) is a light-weight cementitious (of the nature of the cement) product of fly ash or sand, water, cement, lime and aluminum powder mix, used globally for brickwork. The AAC is now widely accepted as an innovative and high quality building material. In the recent years, AAC has been widely used for the interior of industrial, commercial and residential building. It safeguards against fire and seismic-hazard, provides good thermal and sound insulation. The manufacturing process of AAC is environmentally friendly (Wittmann 1992, Limbachiya and Roberts 2005).With growing pressure to adopt sustainable engineering practices, the use of AAC is expected to rise. It has extended a

widespread use in many areas of world including Europe, South America, Middle East and in Asian countries (Mathey and Rossiter 1990).The AAC block was invented in the mid-1920s by the Swedish Architect Dr. John Axel Eriksson and was patented in 1924 (Qu and Zhao 2017 and Habib et al. 2015). The first AAC blocks plant in India was setup in 1970s by Siporex at Pune. However, in the North-Eastern part of the country, it was produced in the year 2014 and opened for commercialization in 2015. The AAC block is a complete new product in North-Eastern part of the Indian subcontinent which falls in seismic zone V. AAC is a lightweight concrete whose cellular structure is obtained through the gas produced during exothermic chemical reaction of sand, cement and water. The aluminum powder is used as a gas producing or expansion agent for forming void or pore by introducing small air bubbles during the production of AAC (Narayanan and Ramamurthy 2000, Nambiar and Ramamurthy 2007).

1.3 Application of AAC

Autoclaved aerated concrete (AAC) are used in the form of block and panel for masonry wall structure (load-bearing and non-load-bearing), floors, roof insulation, trench fills and for other insulating purposes (Bisceglie et al. 2014). AAC has a wide range of application for construction of residential, commercial and industrial buildings. AAC block, being lightweight, is very suitable for the realization of masonry bearing wall of low to medium story building in the seismic zones for good seismic resistances (Ferretti et al. 2015). AAC panels are used directly in internal wall of concrete structures and steel structures, such as schools, hotels, offices, houses and market places etc. The internal walls such as, separation walls, household walls, partition walls in bathroom and kitchen also find the application of AAC panel. The AAC panels are also accepted in several countries for basement wall below the ground. The AAC blocks have application in both external and internal walls. There is an increasing use of this material for non-structural applications in the past decade such as infill panels and cladding. The photograph of AAC block and its building infill wall are shown in Figure 1.1.

Multi-story (high-rise) buildings are susceptible to wind loads (Longarini et al. 2017). Hence, the lateral wind load imposed on building is a governing factor in their structural design. Situation becomes even more complicated if the frequency of oncoming wind resonates with natural frequency of building which depends on structural properties of building. Although several researchers (Stathopoulos and Zhu 1988, Lam et al. 2008 and

Abuku et al. 2009) have examined the impact of high speed wind on the building made of conventional clay brick, but these studies in particular to AAC masonry building are very rare. However, few researchers have studied the seismic performance of AAC masonry. For example, Costa et al. (2011) have investigated the Seismic Performance of AAC masonry using both experiments and simulation.

According to findings of Costa et al. (2011), the unreinforced AAC masonry can face low to medium seismic events when the geometry of the building is regular. However, for severe seismic events, a significant damage can be expected in AAC multi-story buildings. This is due to lower lateral stiffness exhibits by AAC masonry as results of weak bond strengths of masonry and plain bed surfaces of block units. They have suggested that the AAC masonry must be used in combination with other structural systems using confined masonry or bed joint reinforced walls to achieve higher seismic performance. At present, AAC masonry is not used for supporting heavy loads, but with enhancement of its strength, it has potential of becoming a true replacement of load bearing masonry.

(a) (b)

Figure 1.1 Photographs of AAC block (a) stack of AAC block and (b) building infill wall made of AAC block (Dishang Boys' Hostel, IIT Guwahati, Assam, India)

1.4 Advantages and Limitations of AAC

The AAC has following decisive advantages over the conventional clay brick. Different researchers highlighted the following advantages of AAC (Bave 1983, Frey and Briesemann 1985, Mathey and Rossiter 1988, Mathey and Rossiter 1990, Mostafa 2005, Kurama et al. 2009, Bisceglie et al. 2014 and Hamad 2014)

- The AAC production is helpful for consuming the power plant by-products such as fly ash.

- The present AAC materials help in establishing a green environment due its environmentally friendly nature.
- In the AAC production process, no toxic by-products or pollutants are evolved and diffused in air.
- For the same shape and size, AAC weighs 30% of the traditional clay bricks. The lightweight cellular structure of AAC provides ease of handling, transportation and faster wall installation for the construction activities.
- The lightweight property of AAC material also provides high strength to weight ratio. AAC is typically a low density, porous and lightweight, by which it reduces the seismic inertia force acting on the structure as compared to the conventional concrete.
- With high porosity, thereby low density (~500 kg/m^3) and thermal conductivity (0.1 W/(m·K)), the AAC material can serve as a sound-proofing and thermal insulation material.
- AAC is non-combustible (fire resistant) and hence in case of fire, it can help to prevent the fire from transfer to other rooms. No toxic gases or vapors emits from the AAC at the time of fire.
- The AAC is energy efficient. The low weight of AAC units allows cuts in the energy consumption due to handling and assembly on construction site.
- AAC is as workable as wood and can be easily cut, shaped or directed to accommodate almost any design.
- AAC block and panel both are manufactured according to specification/dimension of the customer requirements. As AAC is a prefabricated product, it is of high precision and drillable.

Any of these aspects may argue strongly in favor of using the AAC block. However, there are some limitations too (Mathey and Rossiter 1990, Mallikarjuna 2017). They are as follows:

- The compressive and tensile strengths of AAC block are lesser than those of the conventional clay brick. The AAC blocks are wire-cut as per the industrial practice, which results in smooth surfaces. When the two blocks with smooth surfaces are joined with conventional sand-cement mortar, a high shear bond strength is not attained. The AAC material chips easily; the face of the block gets damaged easily during the scaffolding.

- One of the major concerns with AAC is the of internal and external cracking. The cracking may be caused by shrinkage, creep, moisture effect, settlement of foundation and deformation. The repair of cracks in the AAC wall houses or apartments can be difficult and expensive.
- Because of its low porosity and relatively low alkalinity, the AAC does not afford the same corrosion protection of reinforcement as that provided by dense concrete.
- The caution should be exercised in transporting and handling the AAC unit to avoid any damage at the construction site.
- In India, AAC is a very recent building material and is being used throughout the country. It is used in construction industries for less than thirty years. Thus, long term durability and threat to natural calamities is not ascertained.

1.5 Manufacturing Process of AAC

There are mainly five stages involved in the production of AAC block and panel units. They include mixing of raw materials, casting, expansion or rising, wire cutting and autoclaving. For both AAC blocks and AAC panels, the manufacturing steps are same. The only difference is in the cutting step, where the steel cages are plugged into the mould in case of AAC panel instead of wire cutting in AAC blocks. The detailed study on the manufacturing of AAC has been carried out in the ACC block manufacturing industry (KD Infra, Guwahati, India). All the stages for producing AAC are depicted in Figure 1.2. The detailed manufacturing stages are described in the following subsections.

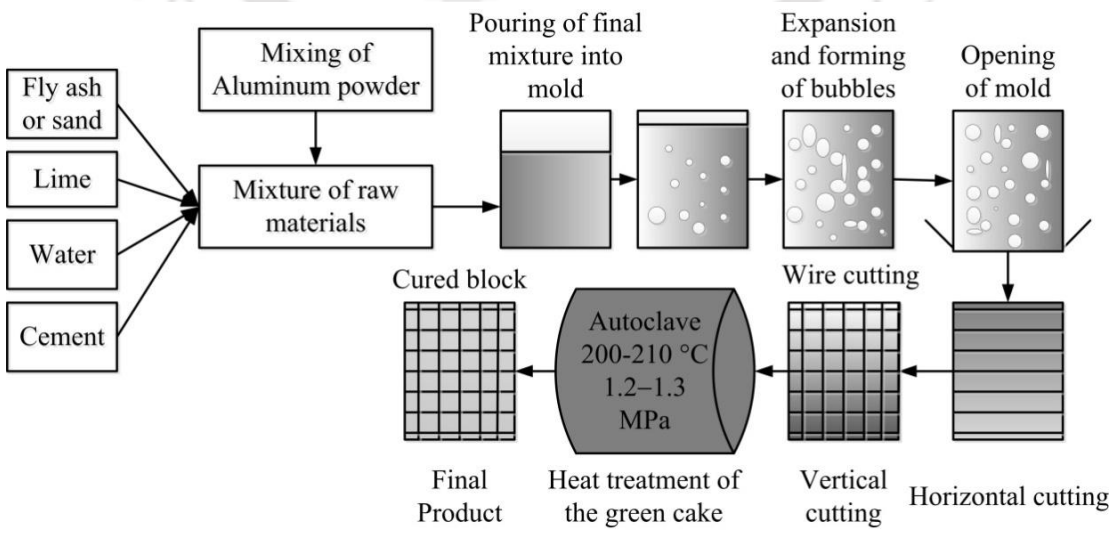

Figure 1.2 Block diagram representing the manufacturing stages of AAC block

1.5.1 Mixing of raw materials

Raw materials used for producing autoclaved aerated concrete are fine grade materials. Fly ash or sand, lime, cement, water and aluminum powder are main raw materials for producing AAC. A total of 3150 kg of mixture (43–45 % fly ash or sand, 36–38 % water, 13–14 % cement, 6–7 % lime, and 0.025–0.03 % aluminum powder by weight) is prepared for filling a single mold. Weighing of materials is carried out by an electronic scale controlled by programmable logic controller (PLC) system as shown in the Figure 1.3. The percentage of fly ash or silica sand used is the highest among other ingredients in aerated concrete mix, whereas the aluminum powder contributes the least. The variation of aluminum powder affects the final density of the AAC and hence, the strength of the final AAC products. After the addition of water to mix, the hydration starts with cement forming bond between fine aggregates and cement paste.

(a) (b)

Figure 1.3 Photographs of devices used for mixing process (a) PLC automatic system to control mix proportions and (b) machine for mixing raw materials

1.5.2 Pouring of final mix

After the preparation of the final mix with all its ingredients, the final mix slurry is poured into an empty oil-treated mold through up and down pouring device as shown in Figure 1.4. Presently, the mold used in the industry (KD Infra, Guwahati) is of size 4200 (length)×1200 (thickness)×600 (width) mm^3. The internal surface of the mold is treated with waste lubricating oil (waste from machines) for avoiding any sticking of mix on the surface of mold. The volume of raw material mixes allowed to occupy the mold is fixed to 60–65%

of mold volume. The remaining 35–40% volume of mold is kept unfilled for the expansion process to save the material spillage.

(a) (b)

Figure 1.4 Photographs of mold and pouring device (a) position of mold and pouring device and (b) pouring of the slurry into the mold

1.5.3 Expansion of the mix slurry

After the pouring process is completed, the filled mold is transferred to the pre-curing room by a ferry cart for pre-curing under constant temperature. The pre-curing of about 4–5 h is done in order to get required hardness for wire cutting. The pre-curing also allows the cake for its expansion and gaining initial hardness. The aluminum powder reacts with calcium hydroxide, which is the product of reaction between cement and water. This reaction causes forming of microscopic air bubbles which results in increasing of paste-volume. The formed hydrogen, which is a lighter gas rises and is replaced by air which is a denser gas. As a result, the hydrogen gas escape out of the material leaving the small air bubble in it. The volume increase is dependent upon the amount of aluminum powder added. The volume increases with increase in the amount of aluminum powder. The reaction can be written as

Aluminum powder + Hydrated lime + Water = Tricalcium hydrate + Hydrogen (1)

$$2Al\ (s)+3Ca(OH)_2+6H_2O = 3CaO.Al_2O.6H_2O+3H_2\ (g) \quad (2)$$

Lesser expansion will produce a higher strength (denser) material, while higher expansion will produce lower strength material (less dense). The whole expansion process takes about 4–5 h to complete depending upon the climate. Both the expansion and solidification process occur simultaneously. Figure 1.5 shows the expansion and solidification of slurry in the mold.

(a) (b)

Figure 1.5 Photographs of mold (a) mold partially filled with slurry just after pouring and (b) mold fully filled with slurry after the expansion or pre-curing process

1.5.4 Wire cutting of cake

A solidified soft green cake of size equivalent to the mold size of 4200 (length)×1200 (width)×600 (height) mm^3 is obtained after the final expansion process. The mold, with green cake in it, is transported to the locating position under tilting hoister by friction wheels, which take the mold to the cutting line. The tilting hoister turns the mold by 90 degrees and puts on the cart for demolding. After the demolding process, the large green cake is transferred to the wire cutting line. The wire used in this cutting process is highly tensioned by air pressure with help of pneumatic cylinder. The size of wire used is of 1–2 mm in diameter. A group of wires in both horizontal and vertical directions are adjusted according to the variable desired dimension of AAC block.

The size of AAC block generally produced in the industry are 600×250×200 mm^3, 600×200×200 mm^3, 600×150×200 mm^3, 600×100×200 mm^3 and 600×75×200 mm^3 corresponding to length, thickness and width dimensions. The variable sizes of the AAC block produced are as per the need for customer requirements. The wire cutting operations are carried out in two separate stages, horizontal cutting and then vertical cutting. The first cutting cart carries the large green mold to the horizontal cutting machine. The head of the large green cake is cut along the length direction (4200 mm). During the horizontal cutting, the large green cake is passed through the arrangement of 5 wires fitted in horizontal cutting machine. After the horizontal cutting, the large green cake gets divided into 6 slices of

dimension 4200×200×600 mm^3. After the horizontal cutting, the exchange device lifts the green cake and put on the second cutting cart for vertical cutting. During the vertical wire cutting, the cutting machine frame swings back and forth like a saw. Finally, the vertical cutting perpendicular to the length direction of large green cake are done after passing these stacked 6 slices through a vertical wire cutting machine. In the vertical cutting, a 4200 mm length side large cake is divided into 43 parts of different sizes. The AAC block of different thickness is obtained through the arrangement of 42 wires adjusted at a different distance in the vertical cutting machine.

Finally, a stack of 258 (43×6) AAC blocks of same length and width but of variable thickness (600×250×200 mm^3, 600×200×200 mm^3, 600×150×200 mm^3, 600×100×200 mm^3 and 600×75×200 mm^3) are obtained after the wire cutting. The total number of final AAC block obtained from a single mold may vary with desired dimension of individual AAC block and hence, accordingly the arrangements of wires are adjusted in the cutting machine. After the wire cutting, the stack of 258 AAC blocks is send to the autoclave for heat treatment or hardening. Figure 1.6 shows the wire cutting machines for cutting in horizontal and vertical directions.

(a) (b)

Figure 1.6 Photographs of wire cutting machine (a) wire cutting of large green cake in horizontal direction and (b) wire cutting of the large green cake in vertical direction

1.5.5 Autoclaving or hydrothermal treatment

After the final cutting operation, the stack of AAC block is transferred for heating or steam curing in an autoclaved chamber. This large steam-heated vessel is in fact a large pressure cooker by which the autoclaved aerated concrete is cured to gain strength. Autoclaving of AAC green cake is carried out with a steam at a high temperature ranging

from 190–210 ºC and high pressure ranging from 1.0–1.3 MPa. The whole autoclaving process completes in 16–18 h. During the autoclaving or hydrothermal treatment, the formation of tobermorite ($5CaO.6SiO_2.5H_2O$) occurs (Bisceglie et al. 2014). The formation of tobermorite, during the cooking period is affected by the presence of aluminum powder. The mechanical properties of final AAC are influenced by the formation of tobermorite. After the autoclaving, the cured or hardened stack of AAC blocks is pulled out from the autoclave chamber with the help of ferry cart. The final product is kept outside for cooling so as to attain the room temperature. Finally, the finished AAC blocks are taken to the storage yard with the help of fork lift. All the stages such as mixing of raw materials, pouring, expansion, wire cutting and autoclaving are carried out in a single industry with the help of mechanized transfer line and material handling equipment. Figure 1.7 represents the autoclave chamber for steam curing of the green cake.

(a) (b)

Figure 1.7 Photographs of hydrothermal treatment of green cake: (a) autoclave chamber and (b) final AAC block after autoclaving

1.6 Scope of the Present Thesis

The primary objective of the present thesis is to study the performance of AAC masonry used in the building wall system. The surface texture of the AAC bed face has great influence on the masonry bond strength. The AAC blocks are wire-cut as per the industrial practice, which results in smooth surfaces. When the two blocks with smooth surfaces are joined with mortar, high shear bond strength is not attained. The presence of frog in clay brick imparts higher masonry shear bond strength. For this, a grooved AAC block has been studied to enhance the strength (shear-bond and compressive strengths) of AAC masonry. Moreover, for adequate bond strength, an optimum amount of cementitious material is

required at the interface. Insufficient amount will lead to adhesive failures at interface, whilst the excessive amount will lower the cohesive or tensile strength of mortar layer adjacent to the interface. Hence, for this purpose, a cement slurry coating at the bed face of AAC has been used to enhance the bond strength of block-mortar interface. The thesis explores the various efficient techniques to enhance the strength of AAC masonry. The study of the AAC masonry behavior under compression load using finite element method (FEM) also forms the part of this research work.

1.7 Organization of the Thesis

The work performed in this thesis comprises eight chapters, which are organized as follows:

- The present chapter provides an introduction to AAC block along with the scope and organization of the thesis.
- Chapter 2 presents detailed literature review on mechanical and physical properties of AAC block and its masonry. In this chapter, various parameters related to the characteristics of AAC, mortar and brickworks are discussed. The relation between the various mechanical and physical properties of AAC and its masonry is presented. It also discusses the various factors responsible for the strength of AAC and its masonry. Subsequently, the major gaps in literature and objectives of thesis are presented.
- Chapter 3 describes the experimental facilities and specimen preparations methods used in this research work.
- Chapter 4 describes the evaluation of mechanical properties of AAC block and its masonry. This chapter describes the experimental evaluation and statistical variation of useful mechanical properties of AAC and its thick mortar (a mixture of cement, sand and water) based masonry. Based on basic of strength of materials, the simple analytical model has been also proposed to evaluate the elastic modulus of masonry prism.
- Chapter 5 discusses the compressive and shear bond strengths of grooved AAC blocks and masonry. In this chapter, a method of improving the compressive and shear bond strengths has been studied by altering the block surface characteristics. A groove is

produced at the bed surface of the block. The manufacturing procedure to obtain the grooved AAC block is described. In this chapter, simple analytical models are developed to estimate the masonry compressive and shear bond strengths. Significance tests (hypothesis test) are discussed to support the findings.

- Chapter 6 describes the bond strength of AAC masonry using various joint materials. In this chapter, a method of improving the bond strength (both tensile and shear) of ordinary sand-cement mortar without altering the block surface characteristics is proposed. In this method, the block surfaces are coated with a thin cement-slurry coating before applying a thick sand-cement mortar.
- In Chapter 7, the finite element modeling (FEM) of AAC masonry for estimation of compressive strength has been carried out. The finite element micro-modeling, governed by plastic-damage constitutive relation in tension and compression, has been used to model the AAC block and mortar, while cohesive zone modeling strategy is adopted to model the block-mortar interface. The nature of lateral stress developed due the application of axial compressive stress is discussed. The comparative study on stress distribution in AAC block and clay brick masonries is also presented.
- Chapter 8 summarizes the overall conclusion of the work and discusses the possibilities for future work.

Chapter 2

Literature Survey and Detailed Objectives

2.1 Introduction

Many researchers have been investigating AAC blocks since last three decades due to their advantages. Considerable research has been carried out on estimating the strength of AAC by experimental methods and with the help of a few theoretical models. A number of experimental studies are described in this chapter; theoretical studies on modeling of AAC strength are also discussed. The connectivity or relation between various relevant properties of AAC and its masonry are presented. The study also emphasizes to understand the various factors responsible for overall strength of AAC building walls under various loading conditions. The experimental studies, carried out by researchers on AAC and its masonry are described in Section 2.2. In this section, a brief discussion on physical properties of AAC is carried out. The relationships between various physical properties are discussed. In Section 2.3, the various mechanical properties of AAC are discussed. Section 2.4 discusses the different mechanical properties of AAC masonry. Finite element modeling methodology of masonry is described in Section 2.5. Based on literature review, Section 2.6 presents the major gaps that have to be explored for the strength of AAC masonry. Section 2.7 presents the detailed objective of the present thesis.

2.2 Physical Properties of Autoclaved Aerated Concrete (AAC)

Consideration of proper physical properties leads to conservative and capable building design and service. There are several physical properties of the AAC unit such as capillarity, permeability, porosity, shrinkage, thermal conductivity, thermal expansion, sound absorption, density, moisture content, water absorption (WA), sorption and initial rate of absorption (IRA) etc. Among these properties, the density, moisture contents, WA and IRA greatly affect the strength of AAC unit and masonry wall. In this Section, the relevant properties, much related to the strength of AAC masonry are discussed in brief. The connectivity or relation between various properties is also described.

2.2.1 Density

The density of autoclave aerated concrete material is generally measured for oven dry mass. The density is generally in the range of 300–1000 kg/m^3 (Narayanan and Ramamurthy 2000, Nambiar and Ramamurthy 2007, Aldolsun 2006, Hamad 2014, Qu and Zhao 2017). As per ASTM C1693 (ASTM 2017a) and RILEM (1993), the density of AAC is recommended to be in the range of 350–850 kg/m^3 and 300–1800 kg/m^3, respectively. Ferretti et al. (2015) reported the average density of 550 kg/m^3 tested in Italy (Europe), while the density of AAC in India (Asia) ranges from 562–810 kg/m^3 as reported by Researchers (Mallikarjuna 2017 and Bhosale et al. 2019). As per the standard procedure, the density of AAC block is evaluated based on the cubic specimen, extracted from top, middle and bottom portion of the block. The bottom cube shows the highest dry density followed by middle and top cube specimens. This difference arises because during the pre-curing process of manufacturing, the slurry in the mold expands or rises from bottom to top in the direction parallel to the mold height (Ferretti et al. 2015, Mallikarjuna 2017 and Bhosale et al. 2019). AAC blocks of around 350 kg/m^3 density can be used for roofs, floors and load bearing walls. The density is mainly governed by the dosage of aluminum powder in the raw material mix during the production of AAC in the plant (Kunchariyakun et al. 2015 and Habib et al. 2015). The aluminum powder being an expansion agent in the mix increases the numbers of pores, thereby increasing the porosity and decreasing the density and compressive strength.

2.2.2 Moisture content, water absorption and initial rate of absorption

The AAC block contains moisture from the manufacturing process (CEB manual). The moisture may also accumulate in the material during construction or after the construction is completed i.e., from rain and condensation. The average moisture content of the AAC blocks lies in the range of 2–18% of the specimen weight (Bhosale et al. 2019). Kunchariyakun et al. (2015) reported that AAC in equilibrium with normal environment (65% relative humidity and 20 ºC), tends to have a moisture content of about 3% of volume. Bhosale et al. (2019) reported that the average water absorption (WA) of AAC lies in the range of 28–53%. The WA is the amount of water required to saturate the masonry unit; it is a measure of porosity. The water/moisture may migrate through diffusion or through capillarity or both. Because of higher porosity and water absorption of AAC, as compared with the normal brick/concrete, the surface treatment should be considered for the exterior surfaces of AAC. The mortar with three coats not exceeding 20 mm is used as the surface

coating for the masonry wall. The unit moisture content and the water absorption (WA) play a key role in determining the bond strength of block-mortar interface. Highly absorptive specimens absorb more water from the adhesive joint and hence, reducing the masonry bond strength. In addition, the higher WA causes the damage to the wall finish as well as cracks on the plaster (Bhosale et al. 2019). IRA or suction is the amount of water absorbed per unit area per unit time, with SI units of $kg.m^{-2}.min^{-1}$. How quickly a masonry unit absorbs water from the mortar, is determined by IRA. The IRA of AAC ranged from 1.72 $kg.m^{-2}.min^{-1}$ to 4.91 $kg.m^{-2}.min^{-1}$.

Masonry units are said to be highly absorptive when IRA is greater than 1.5 $kg.m^{-2}.min^{-1}$ and hence, should be moistened prior to laying for realizing better bond strength. High IRA for AAC units may result, poor brick-mortar bond for thin mortar with less water-cement ratio because of rapid suction of water by brick from mortar. High value of WA and IRA of AAC may result because of its highly porous nature. For a dry density range of 390–630 kg/m^3, the porosity value for AAC material has been reported to be 74–84% (Aldolsun, 2006). Too high and too low IRA not only affects the bond strength of brick-mortar interface, but also the durability and water-resistance of bricks. Hence, it is important to control the porosity, which is negatively correlated with the density of AAC. Both WA and IRA is the indicator of bonding potential of brick/block-mortar interface. In United Kingdom, the WA is used to specify the bonding potential, while in Australia, the IRA is used to specify the bond potential of brick-mortar interface (Lawrence et al. 1994).

2.3 Strength of Individual AAC Unit

The strength of concrete is basically its ability to withstand various types of mechanical loads acting on it. The loads may be compressive, tensile, shear and flexural or their combinations; the strength corresponding to these loads are called compressive strength, tensile strength, shear strength and flexural strength, respectively. In this section, the different mechanical properties such as compressive strength, tensile strength and modulus of elasticity are discussed. Several factors affecting the mechanical properties of AAC are also described.

2.3.1 Compressive strength of AAC unit

The average value of compressive strength of AAC blocks range between 1.3– 8.5 MPa for a density range of 400–700 kg/m^3 (Hul et al. 1997, Narayanan and Ramamurthy 2000, Holt and Raivio 2005, Albayrak et al. 2006, Nambiar and Ramamurthy 2007, Aldolsun 2006, Hamad 2014, Qu and Zhao 2017, Mallikarjuna 2017 and Bhosale et al. 2019). The

compressive strength of AAC strongly depends on its density and porosity. With increase of porosity and decrease of density, the compressive strength gets decreased. An increment of small-size pores leads to higher compressive strength. In other words, the refinement of pore-size distribution can lead to obtain both high porosity and high compressive strength. The utilization of coarser sand during the manufacturing of AAC also leads to higher strength of the final products. The compressive strength of AAC varies inversely with moisture content (Houst et al. 1983). There is an increase in strength on drying the aerated concrete to equilibrium with normal atmosphere. Hence, the strength tests are recommended on AAC material that has attained the equilibrium with the surroundings (Svanholm, 1983). The compressive strength of AAC block reduces by 20–25% as the moisture content increases by 5–10%, respectively.

In addition to the porosity, dry density and moisture contents, the compressive strength also depends on the shape and size, direction of loading, age and characteristics of ingredients used during production. Habib et al. (2015) studied the compressive strength performance of aerated concrete by varying the aluminum powder content from 0.05% up to 0.25%. It was found that increase in the amount of aluminum powder decreases the compressive strength of aerated concrete. The presence of lower amount of aluminum powder tend to reduce the occurrence of aeration process that ultimately leads to the development of lesser amount of air voids, causing low expansion which finally yields hardened aerated concrete having lower porosity with higher compressive strength. On the other hand, inclusion of more aluminum powder promote the generation of higher amount of air bubbles trapped within the hardened aerated concrete forming higher expansion which finally leads to lower compressive strength.

Alexanderson (1979) found that the compressive strength of aerated concrete, especially cements and lime mixing, increases with the increasing amount of hydrates and with decreasing porosity. The strength of hydration products, overall porosity and pore structure i.e., shape, size and the connectivity of the pores play a key role for governing the compressive strength of AAC. The water to solid ratio (W/S) is a critical criterion for regulating the compressive strength of AAC. The W/S ratio is defined as the water to solid components of AAC (flyash, lime, cement, gypsum and aluminum powder) during production. Larger W/S ratio results in more microscopic pores and lower final strength (Narayanan and Ramamurthy 2000, Alexanderson, 1979). Ayudhya and Israngkura (2011) studied the compressive strength of AAC containing perlite aggregate and polypropylene

fiber subjected to high temperature. It is concluded that compressive and splitting tensile strength of AAC containing polypropylene fiber is not much higher than those containing no polypropylene fiber.

Several researchers have tested the compressive strength of AAC using different test specimens. Ferretti et al. (2014) investigated the compressive strength of AAC cube specimen of edge length 100 mm. They also performed the compressive strength test on AAC specimen of sizes and shape equivalent to actual AAC block, i.e., a rectangular block of size 625×100×250 mm^3. The strength of actual size AAC block specimen was 20% lower than that measured on cubic specimen. During the pre-curing at the time of manufacturing AAC, the slurry expands or rises from bottom to top in the direction parallel to the mould height. Hence, due to gravity, the bottom part of AAC is significantly denser and stronger than middle and top one. As a consequence, all the edges or corners of AAC specimen have different strengths. The cracks initiate near the weakest external corner. As the top part of AAC specimen is less dense, the crack initiates from the top part of AAC.

Based on the tests conducted on 12 cubic samples, Mallikarjuna (2017) reported the average compressive strength of AAC block as 2.61 MPa. The compressive strength of AAC is relatively low as compared to the conventional brick/block used in the building construction. This encouraged Farid et al. (2017) to propose AAC-concrete sandwich composite to enhance its compressive strength. Compression tests were conducted on three sets of plain sandwich specimens, each with a different combination of concrete thickness and AAC thickness. The proposed composite had a higher compressive strength than normal AAC. The highest strength-to-weight ratio was found for 100 mm cubic specimen with concrete sheet thickness of 25 mm and 20 mm. The failure cracks were first appered at the AAC-concrete interface. Hence, the interface bond strength enhancing techniques were also proposed by incoporating the groove at the AAC-concrete interface and by wrapping the block with wire mess. The study revealed that the wire mess provided a more effective bonding in comparison to plain sandwich block and grooved sandwich block. In general, AAC blocks are weak and soft as compared to normal burnt clay brick units (Kaushik et al. 2007) and fly ash brick units (Basha et al. 2014). The compressive strength of burnt clay brick and fly ash brick has been reported as 20.8 MPa (Kaushiket al. 2007) and 5.7 MPa (Basha et al. 2014), respectively.

2.3.2 Modulus of elasticity of AAC unit

The modulus of elasticity of AAC material is about one tenth of that of dense concrete and is a function of density and compressive strength. For a density range of 500–700 kg/m^3, the elastic modulus of AAC material has been reported as 1.1–2.8 GPa (Alexanderson 1979, Narayanan and Ramamurthy 2000, Aldolsun 2006, Hamad 2014, Ferretti et al. 2014, Qu and Zhao 2017, and Bhosale et al. 2019). In the study of Bhosale et al. (2019), the modulus of elasticity tested on the cubes of sizes 50 mm, 75 mm and 100 mm is reported to be in the range of 1.15–1.6 GPa. The elastic modulus can be positively correlated with compressive strength and density. The modulus of elasticity was found to vary from 220 to 820 times the compressive strength. Ferretti et al. (2014) reported a value of 1285 MPa evaluated with reference to stress level ranging between 2–33% of compressive strength.

Based on 12 AAC cube specimens collected from M/S K.D. Infra, India, the average modulus of elasticity was 266 MPa (Mallikarjuna, 2017); it varied between 63 to 151 times of the compressive strength of AAC block. These results differ significantly with the results of other researchers (Alexanderson 1979, Narayanan and Ramamurthy 2000, Aldolsun 2006, Hamad 2014, Ferretti et al. 2014, Qu and Zhao 2017and Bhosale et al. 2019).This may be due to the composition of raw material used to produce AAC block, individual strength of the raw material used and also differing climatic conditions. However, the tangent modulus obtained by the following empirical relation showed good agreement with the others:

$$E_t = k\rho_{\text{dry}}\sigma^{0.5}, \tag{2.1}$$

Where E_t is the tangent modulus (in MPa), ρ_{dry} is the dry density (in kg/m^3), σ is the compressive strength (MPa) and k is an empirical constant ranging between 1.5 to 2.

2.3.3 Tensile strength of AAC unit

The tensile strength of AAC is normally about one quarter to one sixth of the compressive strength and is significantly affected by the moisture gradient within the test specimen (CEB manual). Valore (1954) reported the ratio of direct tensile strength to the compressive strength of AAC to be 0.15–0.35. Ferretti et al. (2014) evaluated the tensile strength and its statistical variability through a three-point bending test on normal and deep beams of the AAC. The tensile strength for 6 AAC beams of size 625×100×250 mm^3 has been reported to be between 0.56 MPa to 0.64 MPa. However, in case of 7 deep beams of size 625×100×750 mm^3, the tensile strength has been reported to be 0.69–0.83 MPa. The

values agreed well with the design provisions suggested by researcher (Crisafulli, 1979). All the AAC beam specimens were characterized by brittle failure with main crack developed near the mid-span. However, deep beam showed a brittle failure characterized by the spreading of an inclined main cracks starting from the bottom of the specimen. The tensile strength increased with increase in the height of the AAC beam specimen. AAC is slightly stronger in flexural tension if the loads are oriented in parallel rather than perpendicular to the rising direction (Nambiar and Ramamurthy, 2006).

Małyszko et al. (2017) evaluated the splitting test results both experimentally and numerically on the cylindrical and cubic AAC specimen. The splitting tensile test is a simple and effective method of evaluating the indirect tensile strength of the AAC specimen. The failure mechanisms were discussed based on spatial finite element simulations and experiments with the digital image correlation and strain gauges. According to the theory of isotropic elasticity, the expression for the tensile strength for cylindrical AAC specimen is given in the form:

$$\sigma_{\text{split}} = \frac{2(P_{\text{t}})_{\max}}{\pi DL}, \tag{2.2}$$

where σ_{split} is the splitting tensile strength, $(P_t)_{\max}$ is the measured peak load, D is the diameter of the specimen and L is the length of the specimen. The modulus of elasticity and Poisson's ratio have been calculated by fitting the theoretical solution into the displacement field. An average tensile strength of 0.39 MPa and 0.42 MPa were found for cylindrical and cubic specimen, respectively.

Mallikarjuna (2017) reported the average splitting tensile strength of 0.26 MPa on a AAC specimen of size 200×110×75 mm^3. The test has been performed as per the ASTM C1006-07 (2013) on the specimen size equivalent to that of ordinary brick. Argudo (2003) studied the variation of splitting tensile strength with dry density and compressive strength of the AAC specimen. The linear regression analysis for splitting tensile strengths was carried out following ASTM C1006 test procedure. The empirical equations are given by

$$\sigma_{\text{split}} = 2\rho_{\text{dry}} - 10.3, \tag{2.3}$$

$$\sigma_{\text{split}} = 0.05\sigma + 30, \tag{2.4}$$

where σ_{split} and σ are the tensile splitting and compressive strengths in psi and ρ_{dry} is the dry density of AAC specimen in lb/ft^3. The modulus of rupture has been found more in case of loading parallel to rise direction than that with loading in perpendicular direction. The modulus of rupture for loading in parallel to rise and perpendicular to rise direction has been found to be 1.25 MPa and 0.98 MPa, respectively. As per the RILEM recommendation, the modulus of rupture can be roughly estimated according to the formula

$$MOR = 0.27 + 0.21\sigma, \tag{2.5}$$

where σ is the compressive strength of AAC in MPa. The results obtained by several researchers differ a lot. This may be due to variation in specimens and testing standards. The raw material compositions and climatic conditions (humidity) of different regions can be also the reason for large deviation in results. Moisture content within the AAC specimens also affects the overall tensile strength.

2.4 Mechanical Properties of AAC Masonry

Masonry is a nonhomogeneous, anisotropic and non-elastic material composed of two materials viz., unit and mortar/glue layer of different properties (Kaushik et al. 2007). The mortars or glues are generally stiffer than the AAC unit. The mechanical properties of AAC masonry are different from those of the individual AAC unit specimen. The presence of joints such as bed joint and head joint (see Figure 2.1) in the AAC masonry or wall affects its overall strength. In this section, all the mechanical properties viz., compressive strength, tensile bond strength, shear bond strength and fracture energy of AAC masonry are discussed under the following sub-sections.

2.4.1 Compressive strength of AAC masonry

The strength of brick-mortar masonry, loaded concentrically in the direction perpendicular to the bed joint is called its compressive strength (Crisafulli, 1997). In the masonry, different materials are distributed in a fixed interval and the bond between them is weak. The compressive strength of the masonry is generally investigated by testing prism specimens (Kaushik et al. 2007). The prism test specimen is the combination of 2–6 bricks units with required mortar layers stacked into one unit (see Figure 2.1 a). Many researchers reported the prism strength or compressive strength of AAC masonry (Ferretti et al. 2015, Mallikarjuna 2017 and Bhosale et al. 2019). The compressive strength of the masonry prism is observed to lie between the strength of individual AAC unit and mortar. Bhosale et al.

(2019) investigated the compressive strength of AAC masonry prism using 3 blocks stack-bonded with two layers of polymer based mortar of 2–5 mm thickness. The mean values of compressive strength and corresponding strain was found to be 2.12 MPa and 0.0018, respectively. A huge decrease (about 59%) in the compressive strength of masonry prism was found as compared to the compressive strength of individual AAC block. This may be due to the development of lateral stresses in the block and mortar layer. The lateral stresses are developed because of the differences in the mechanical properties (mainly elastic modulus and Poisson's ratio) of AAC unit and mortar material.

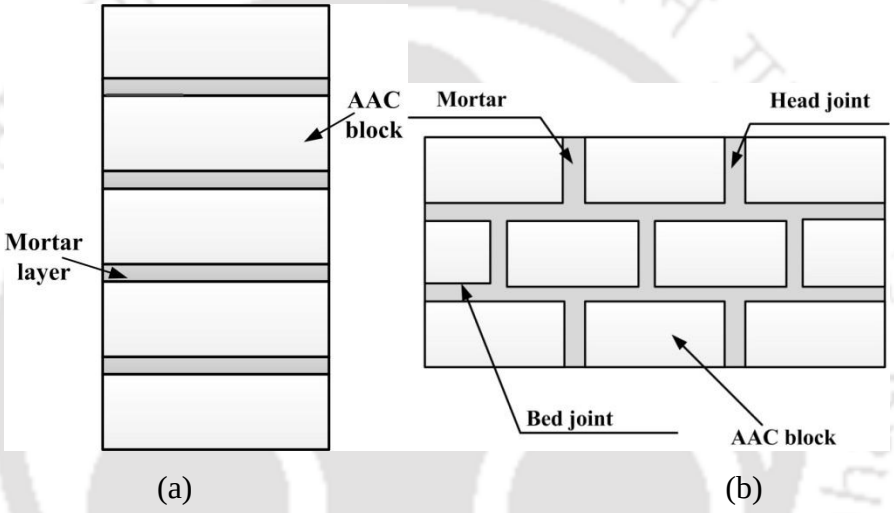

Figure 2.1 Schematic drawing of AAC masonry for compression test (a) prism specimen and (b) masonry wallette

Although the overall compressive strength of masonry can be observed using masonry prism test, but the effect of bed joint and head joint (Figure 2.1 b) are not considered in this type of specimens. Sometimes, the masonry wallette/wall specimens are constructed to observe the effect of head joint and bed joint on the compressive strength of masonry walls (Ferretti et al. 2015). The direct test on the wall specimen itself can be considered as an actual strength analysis for compression. An average value of compressive strength on the AAC wall or masonry panel specimen has been observed to be 2.60 MPa.

In general, the compressive strength of masonry depends on many factors such as mortar water retention, water absorptions of masonry unit, strength of masonry unit, mortar/glue strength, mortar/glue thickness and workmanship (Crisafulli, 1997). The masonry strength decreases with the increase in water absorption of the brick unit. A very low value of water absorption can lead to a reduction in the compressive strength because of lack of water

for necessary hydration for bond formation (Crisafulli, 1997). The excess water absorbed by the brick unit may result in lack of residual water essential for developing the strength of mortar. The masonry compressive strength can be increased by increasing the compressive and tensile strength of the brick units. The masonry strength is also related to the mortar/glue strength. The increase of mortar strength has significant influence on the compressive strength of masonry (Sarangapani et al. 2005).

2.4.2 Shear bond strength of AAC masonry

The proper evaluation of the shear bond strength of a masonry unit is required for the design of any masonry panel when subjected to the lateral loads. The lateral loads get induced due to earthquake vibration, shaking and due to wind pressure on the wall surface. In the study by Bhosale et al. (2019), the shear bond strength of AAC masonry triplet made of polymer based mortar, has been reported to be 0.22 MPa. In general, the shear bond strength of the masonry depends on the brick porosity, initial rate of absorption of brick, surface roughness of brick, sizes of frog on the brick surface, chemical reactivity of mortar, characteristics of sand in mortar, water retention of mortar, mortar strength, presence of additives in the mortar and on pre-compression load (Groot 1993, Walker 1999, Sarangapani et al. 2005, Reddy et al. 2007, Reddy and Vyas 2008, Singh and Munjal 2017 and Mallikarjuna 2017). Some comments about these factors are presented here. The shear bond strength of masonry increases with the increase in the moisture content in the brick (Sinha 1983). A dry brick absorbs water from the mortar and hence, there may be the insufficient water available for the hydration of cement. The shear bond strength of masonry increases with the increase in the compressive strength of mortar (Rahman and Anand 1994 and Malikarjuna 2017). The grading of sand also influences the shear bond strength. The sand graded as coarse-medium has shown the stronger bond strength between the brick and mortar (Sinha 1983). For adequate bond strength, an optimum amount of cementitious material is required at the interface. However, insufficient amount leads to the adhesive failures at interface, whilst the excessive amount will lower the cohesive or tensile strength of mortar layer adjacent to the interface (Sugo et al. 2001).

The AAC blocks are wire-cut as per the industrial practice, which results in smooth surfaces. When the two blocks with smooth surfaces are joined with conventional sand-cement mortar, a high shear bond strength is not attained (Mallikarjuna, 2017). The presence of frog in clay brick imparts higher masonry shear bond strength (Sarangapani et al. 2005, Reddy and Vyas 2007, Reddy et al. 2008, Singh and Munjal 2017). Mallikarjuna (2017)

performed the shear bond strength test on triplet test specimen of AAC unit masonry using 5 different mortar grades (different proportions of sand and cement). The mortar grades used were 1:2, 1:3, 1:4, 1:5 and 1:6 corresponding to cement: sand. The tests have been carried for a pre-compression load of 0.1 MPa, 0.3 MPa and 0.5 MPa and without any pre-compression load. The shear bond strength was found to increase with increase in compressive strength of mortar and with increase of pre-compression load. The behavior of AAC masonry bed joint and pre-compression has been observed and illustrated by the Coulomb's friction law. The relationship between shear bond strength (τ) and pre-compression stress (σ_p) is linear and is given by the following equation:

$$\tau = c + \sigma_p \tan \beta_i, \tag{2.6}$$

where c is cohesion i.e., shear bond strength of the brick-mortar interface when no pre-compressive stress is applied, σ_p is the pre-compression stress and β_i is initial friction angle. Mathematically, the shear strength for the triplet test specimens is calculated as

$$\tau = \frac{P_{\max}}{2A}, \tag{2.7}$$

$$\sigma_p = \frac{P_C}{A}, \tag{2.8}$$

where τ is shear bond strength in MPa, P_C is compressive load in N, $P_{\max}$ is maximum shear force applied in N; and A is the cross-sectional area of the specimen parallel to the shear force or the bonding area in mm^2. The average shear bond strength of AAC brick triplet specimen for 1:3 grade mortar have been reported to be 0.056 MPa, 0.226 MPa, 0.273 MPa and 0.40 MPa corresponding to pre-compression stress of 0 MPa, 0.1 MPa, 0.3 MPa and 0.5 MPa, respectively. Also, it was concluded that the shear bond strength of AAC masonry triplet increases with increase in the pre-compression stress.

2.4.3 Tensile bond strength of AAC masonry

The resistance of masonry to tensile stress when subjected to out-of-plane loading is an important aspect for the safe design of masonry wall system. The tensile strength of masonry is primarily governed by the bond strength of brick mortar interface (Crisafulli1997). Several researchers studied the tensile bond strength of AAC masonry. Bhosale et al. (2019) evaluated the tensile bond strength of AAC brick masonry based on the

Z-specimen tests and the failure patterns have been observed during the test. The AAC Z-specimen masonry was prepared using the polymer/block adhesive based mortar.

According to Khalaf (2005), the total joint strength can be obtained by linear stress distribution and parabolic stress distribution. Since the tensile bond strength calculated using the parabolic stress distribution is lesser than the value calculated using linear stress distribution, the assumption of parabolic stress distribution is safer and conservative. Bhosale et al. (2019) reported the average tensile bond strength of AAC masonry using the linear stress distribution and parabolic stress distribution as 0.28 MPa and 0.22 MPa, respectively. Mallikarjuna (2017) performed the test on cross-couplet specimens followed by the calculation of mode–I fracture energy. The load–displacement curves obtained from tests were used for the calculation of tensile bond strength ($_{T_j}$) and mode I fracture energy (G_f^I). Tensile strength of mortar-unit interface is given as

$$\tau_t = \frac{(P_t)_{\max}}{A}, \tag{2.9}$$

where τ_t is the tensile bond strength, $(P_t)_{\max}$ is the maximum value of the load applied, and A is the bonding area. The average tensile bond strength and the corresponding mode-I fracture energy were found to be 0.056 MPa and 0.01 N/mm, respectively. Ferretti et al. (2015) reported the tensile strength of AAC masonry beam and corresponding fracture energy in flexural loading using three-point bending test performed on 6 AAC small-scale masonry beams. The joint viz., head joint and bed material used for AAC masonry specimen preparation was grey glue of nominal joint thickness of 1.5 mm. The obtained tensile strength and fracture energy corresponding to 0º orientation of bed joint have been reported as 0.37 MPa and 0.007 N/mm, respectively. Similarly, for the bed joint inclination of 90º, it is reported as 0.30 MPa and 0.005 N/mm. The tensile strength test obtained on the AAC beam is the good realization of actual AAC masonry tensile strength. The presence of large number of bed joints and head joints in the AAC beam gives the actual representation of AAC masonry wall.

2.5 Finite Element (FE) Modeling of Masonry Strength

Understanding the theoretical behavior of any engineering materials and system is very important. This can be achieved through numerical or computational studies. In last few decades, there has been a lot of study in developing a new method of modeling and analysis of masonry structures. The aim is to provide efficient tools for better understanding the complex behavior of masonry structures. The basic mechanical properties of the masonry are

strongly influenced by its constituents namely, mortar and brick. Using the mechanical properties of unit, mortar and joint obtained from experiments, the behavior of masonry structure wall can be analyzed by Finite Element (FE) modeling. The FE Model has been developed to determine the strength, lateral displacement and stress distribution throughout the masonry wall system. Finite Element Method (FEM) is one of the most powerful tools for modeling a continuous masonry structure with the help of a number of complex elements.

The modeling is done by converting the structure into simple finite elements. There are generally two approaches for FE modeling of masonry structures called homogeneous or macro modeling and heterogeneous or micro modeling (Lourenço, 1994). In homogeneous approach, the mortar joints and brick units are smeared into a uniform composite material with average property of individual brick and mortar (Figure 2.2a). However, mortar joint and units are considered separately in heterogeneous approach (Figure 2.2b). The micro-modeling regards the masonry as a heterogeneous material and requires the determination of considerably higher number of parameters leading to expensive test (Bolhassani et al. 2015). Although the micro-modeling approach is more precise and can predict the local behavior of masonry, modeling becomes complicated by considering all the individual properties of masonry constituents. However, it needs more computational time.

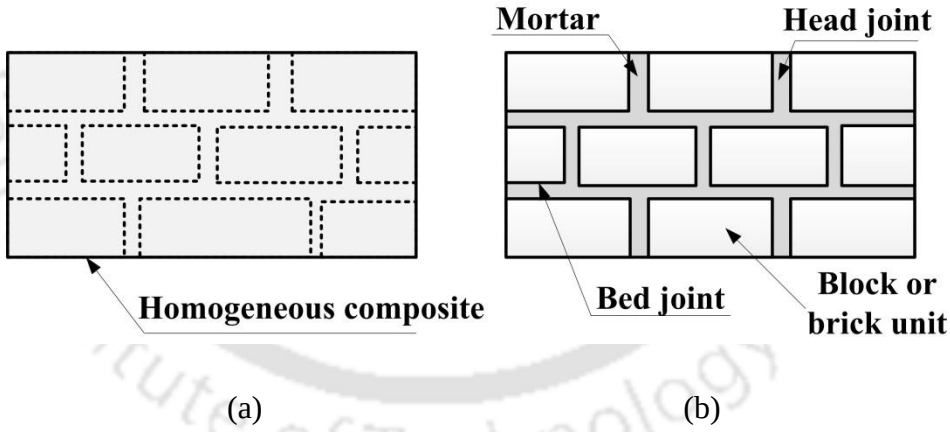

Figure 2.2 Modeling strategy of brick masonry: (a) macro-modeling and (b) micro-modeling

Lourenco (1994) used both micro modeling and macro modeling to study the behavior of masonry wall. The elastic model is used to represent the behavior of brick while the gradual softening model is used to represent the interface element. A three-dimensional FEM model using concrete damage plasticity (CDP) model for a partially grouted wall was developed by Minaie et al. (2010). Sejnoha et al. (2008) simulated a diagonal compression test using a continuum model for mortar and contact elements for the stone mortar interface.

The results were promising but the model did not account for the gradual loss of cohesion. Alberto et al. (2011) characterized the mechanical behavior of interface and predicted the de-bonding phenomena between brick and mortar through cohesive crack model.

Zhang et al. (2017) developed a detailed micro modeling method for the modeling of diagonal compression test for historical stone masonry structure using extrinsic cohesive element. Kowalewski and Gajewski(2015) determined the failure modes in the brick walls using a cohesive element approach. The micro modeling approach with the application of cohesive elements to describe the mortar joint was used in the analysis. Cohesive zone model was used for modeling the unit mortar interface. Since there is no any separate constitutive model for the finite element analysis of behavior of AAC beam or AAC masonry wall, many researchers (Ferretti et al. 2014, Ferretti et al. 2015, Mallikarjuna 2017 and Małyszko2017) adopted the macroscopic anisotropic constitutive model already developed for ordinary masonry (Sejnoha et al. 2008, Minaie et al. 2010, Alberto et al. 2011,Kowalewski and Gajewski 2015 and Zhang et al. 2017).

2.5.1 Concrete damage plasticity (CDP) for material modeling

The behavior of the masonry can be simulated in a commercial available FEM package such as ABAQUS using the CDP model, which can be used for concrete and other brittle materials (ABAQUS 6.13 Manual). The failure is caused by cracks in tension and crushing in compression. The concrete damage plasticity provides a general capability for modeling concrete and other quasi-brittle materials in all types of structures (beams, trusses, shells, and solids). In CDP model, the evolution of the yield (or failure) surface is governed by two hardening variables viz., compressive equivalent plastic strain ($\tilde{\varepsilon}_c^{pl}$) and tensile equivalent plastic strain ($\tilde{\varepsilon}_t^{pl}$), which are linked to failure mechanisms under compression and tension loading, respectively. The stress-strain behavior under uniaxial tension follows a linear elastic relationship until it reaches the failure stress (σ_{t0}). The stress corresponding to the onset of micro-cracking in the concrete material is the failure stress (ABAQUS 6.13 Manual). The formation of micro-cracks with a softening stress-strain response induces strain localization in the structure of concrete. However, under the uniaxial compression loading, the response is linear until it reaches the initial yield stress (σ_{c0}). The response is typically characterized by stress hardening followed by strain softening beyond the ultimate stress (σ_{cu}) in the plastic region. The uniaxial stress-strain curve can be converted into stress versus plastic-strain curves by ABAQUS from stress versus plastic strain data. Thus,

$$\sigma_t = \sigma_t(\tilde{\varepsilon}_t^{pl}, \dot{\tilde{\varepsilon}}_t^{pl}, f_i, \theta), \tag{2.10}$$

$$\sigma_c = \sigma_c(\tilde{\varepsilon}_c^{pl}, \dot{\tilde{\varepsilon}}_c^{pl}, f_i, \theta), \tag{2.11}$$

where the subscripts *t* and *c* indicate tension and compression, respectively. $\tilde{\varepsilon}_c^{pl}$ and $\tilde{\varepsilon}_t^{pl}$ are the equivalent plastic strains, $\dot{\tilde{\varepsilon}}_c^{pl}$ and $\dot{\tilde{\varepsilon}}_t^{pl}$ are the equivalent plastic strain rates, f_i (for i = 1, 2, 3,…) are the other predefined field variables and *K* is the temperature.

When the concrete specimen is unloaded from any point on the strain softening branch, the stiffness decreases. The elastic stiffness of the material seems to be degraded or damaged. The elastic stiffness damage is characterized by two damage variables, d_t (for tension) and d_c (for compression), which are the functions of the plastic strains, temperature and field variables. The damage variables can be varied from 0 to 1.

$$d_t = d_t(\tilde{\varepsilon}_t^{pl}, K, f_i); \quad 0 \le d_t \le 1, \tag{2.12}$$

$$d_c = d_c(\tilde{\varepsilon}_t^{pl}, K, f_i); \quad 0 \le d_c \le 1. \tag{2.13}$$

For undamaged materials, the damage variable is 0, whereas 1 indicates the total loss of strength (ABAQUS 6.13 Manual). Letting E_0 as the initial or undamaged elastic stiffness of the material, the stress-strain relations under uniaxial tension and compression become

$$\sigma_t = (1 - d_t)E_0(\varepsilon_t - \tilde{\varepsilon}_t^{pl}), \tag{2.14}$$

$$\sigma_c = (1 - d_c)E_0(\varepsilon_c - \tilde{\varepsilon}_c^{pl}). \tag{2.15}$$

A non-associative flow rule is considered to define the plastic strain rate in CDP model. The multiple-hardening Drucker-Prager type surface is adopted as a yield surface. The yield surface is governed by the parameters such as dilation angle (φ), ratio of biaxial compressive strength to the uniaxial compressive strength (f_{b0}/f_{c0}) and a constant *k* (Lubliner et al. 1989, van Zijl et al. 2004 and Daltri et al. 2019). The dilation angle or dilatancy is basically the measure of change in the volumetric strain with respect to the changes in shear strain. The dilation angle defines the amount of plastic volumetric strain induced in the body

during the plastic shear. The constant k is the ratio of second stress invariant on tensile meridian to that on the compressive meridian at the failure point. The tensile and compressive meridians are the intersection curves between the plane (meridian plane) containing the hydrostatic axis and the failure surface (Chen, 2007). The meridian plane along with theory of failure of concrete are briefly explained in Appendix A.

2.5.2 Cohesive Zone Modeling

Cohesive zone (CZ) models are widely used to investigate the behavior of interfaces between any two materials. This model, introduced by Dugdale and Barenblatt (1960), has attracted a growing interest to describe the failure and delamination process for composite materials in details. The cohesive interaction is the function of displacement or separation between the edges of cracks. The CZ model is generally applied to concrete and cementitious composites but can also be used for other materials. The application of CZ model may widen the knowledge of material properties and more powerful computer programs.

Previous researches have studied the parameters that affect the cohesive interaction performance for brittle materials. They have concluded that the mechanical behavior of cohesive elements can be defined by three methods: (1) uniaxial stress-based, (2) continuum-based and (3) traction-separation constitutive model. In this work, the third method is used. The traction-separation model represents the corresponding initial separation caused by pure normal stresses, in plane and out of plane shear stresses. The Coulomb frictional contact behavior is applied to the traction-separation model by introducing a coefficient of friction (μ), which prevents components penetration, especially for the normal contact behavior. For this study, surface-to-surface contact is chosen and the contacting properties for the tangential and normal behavior are specified. This type of contact is generally used to describe the behavior of two deformable surfaces connecting together. This focuses all the damage mechanisms in and around a crack tip on the interface, leading to a constitutive relation between the traction and opening displacement (separation). The crack initiation is related to the cohesive strength, also called the maximum traction on the traction separation law. The variation in traction in relation to separation or displacement is plotted as a curve and is called the traction-separation curve, as illustrated in Figure 2.3.

When the area under the traction-separation reaches the fracture toughness, the traction declines to zero and new crack surfaces are generated. The crack initiation is related to the cohesive strength, also called the maximum traction on the traction separation law.

From Figure 2.3, it can be observed that the material is initially bonded and the failure occurs after the maximum traction is reached, beyond which the traction starts decreasing.

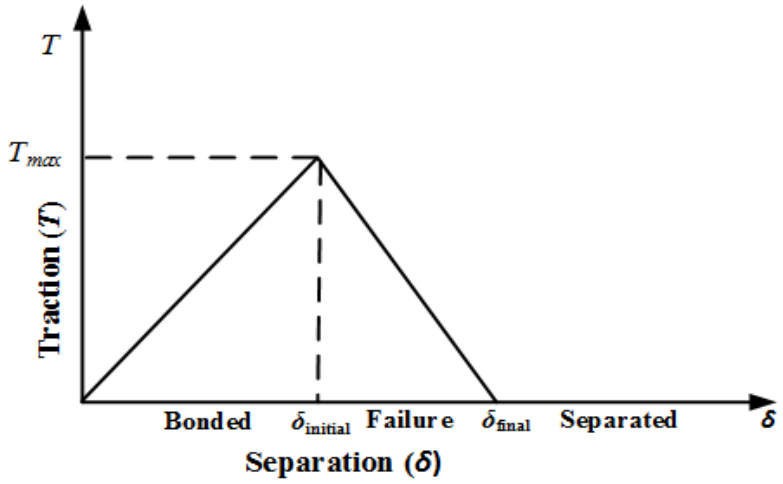

Figure 2.3 The effective linear traction-separation relationship

Cohesive zone modeling relates the relative displacement ("opening" δ) of two associated points of the interface to the force per unit of area ("Traction" *T*) needed for separation. A difference is made between normal (*n*) and tangential (*t*) direction. Hence, the cohesive zone law comprises two parameters i.e., T_n (δ_n) and T_t (δ_t). The cohesive zone laws can be uncoupled or coupled (Bolhassani et al. 2015). In an uncoupled cohesive zone law, the normal/tangential traction is independent of the tangential/normal opening, while both normal and tangential tractions depend on both the normal and tangential opening displacement in case of coupled cohesive zone law. Uncoupled laws are intended to be used when the debonding process occurs under normal (mode-I) or tangential (mode-II) loading. The majority of cohesive zone laws have a partial coupling between normal and tangential directions, which is achieved by introducing coupling parameters in the model. A large variety of cohesive zone laws are available in literature, e.g., (a) polynomial model, (b) piece-wise linear model, (c) exponential model and (d) rigid linear model.

The shear strength or bond strength of the masonry depends mainly on the interface between unit and mortar. The masonry interface modeling can be done using Cohesive Zone Modeling (Zhang et al. 2017). Cohesive zone model (CZM) can be used to predict the local fracture initiation and continued propagation in a material. It offers an alternative way to analyze failure along material interfaces. The CZM can be employed in FE analysis by relating the traction to displacement at interfaces.

Ramamurthi et al. (2013) studied the delamination between polyethylene terephthalate (PET) and polyvinyl chloride layers in polymer coated steel using two approaches to model cohesive zone for delamination viz., elemental cohesive zone model (ECZM) and surface cohesive zone model (SCZM). ECZM is a method for predicting the delamination process between the interface of bonded surfaces. However, SCZM is particularly used for zero or very thin interfaces, where the thickness effect is considered. The SCZM was found to be more desirable because of the advantages of reduced computational time, fewer input parameters and easy modeling (Ramamurthi et al. 2013). In this study, unit-mortar interface is modeled by adopting the surface based cohesive zone model. Turon et al. (2007) determined various constitutive parameters such as interface stiffness coefficient, length of cohesive zone for the simulation of delamination. The equation for the selection of interface stiffness parameter was derived. The expression to adjust the maximum interfacial strength used in the computations with a coarse mesh was presented.

Ferretti et al. (2014) performed an inverse extended finite element (XFEM) analysis to calibrate a proper cohesive law suitable for the AAC material. The XFEM is basically an extension of conventional FE method based on the concept of partition of unity, which takes into account the discontinuous structure of displacement field. The XFEM eases the difficulties in solving problems with localized features e.g., presence of main crack that are not efficiently resolved by mess refinement. Moslemi and Khoshravan(2015) proposed a new test methodology to determine the cohesive strength of the composite laminates. The various cohesive parameters such as cohesive strength and separation energy for mode I inter-laminar fracture of E-glass/epoxy woven fabrication was computed from the experimental tests. The results from the simulation were compared with experimental tests to confirm the adequacy of normal cohesive strength. Kowalewski and Gajewski (2015) determined the failure modes in the brick walls using cohesive element approach. The micro-modeling approach with the application of cohesive elements to describe the mortar joint has been used in the analysis. Małyszko et al. (2017) simulated the splitting test on cylindrical and cubic AAC specimens under the displacement control using the Mohr-Coulomb constitutive model of isotropic plasticity with the yield function expressed in terms of principal stress as

$$f(\sigma,k)=\frac{1}{2}(\sigma_1-\sigma_3)+\frac{1}{2}(\sigma_1+\sigma_3)\sin\theta-c(k)\cos\theta,\ \text{for}\ \sigma_1\geq\sigma_2\geq\sigma_3, \quad (2.16)$$

where $c(k)$ is the cohesion function of the internal state variable k with constant friction angle (θ), which is described by the hardening/softening diagram. Ferretti et al. (2015) used the

experimental results to calibrate a well-known macroscopic anisotropic constitutive model already developed for ordinary masonry. The behavior of AAC masonry and full-scale AAC wall were simulated for both tension and compression. Two different failure criteria were adopted for compression and tension, respectively "Hill-type" and "Rankine-type". Ferretti et al. (2015) concluded that the numerical anisotropic models proposed for traditional masonry can also be used for AAC masonry, if calibrated properly. Mallikarjuna (2017) carried out a two dimensional linear elastic finite element analysis of a masonry shear wall under a pre-compression load of 0.1 MPa. The aim was to study the normal stress and shear stress distribution in masonry units and AAC unit-mortar bond interface assuming plane-stress condition. The potential failure mechanism and collapse load were estimated from the analysis. It was concluded that the simplified micro-modeling is a convenient method for finite element modeling of the masonry shear wall. The stiffness of the wall depends mainly on brick-mortar interface bond strength rather than the strength of the mortar (Mallikarjuna 2017).

2.6 Major Gaps in the Literature

The information gathered from the review of published literature reveals a few research gaps and possibilities remaining for further investigation. The gaps found from the literature are summarized as follows:

- All the previous literatures are dedicated to study the mechanical properties of AAC masonry made of AAC block having smooth surfaces. However, the effect of surface roughness was not studied.
- The AAC blocks are wire-cut as per the industrial practice, which results in makes all the six surfaces smooth. No study was done to alter the bed face of AAC and feasibility of its implementation in the manufacturing industry.
- No researcher reported the study on enhancing the bond strength of AAC masonry by altering the unit surface characteristics.
- No researcher discusses the effect of mortar strength on the strength of AAC masonry.
- Various joining materials are used to form the AAC masonry such as conventional sand cement mortar and polymer modified mortar. No researcher studied the strength of AAC masonry using different joining materials.
- The nature of lateral stress developed in the block and mortar due the application of axial stress on AAC masonry for compression load is not presented till date.

- The joint thickness also affects the strength of ordinary (clay brick) masonry. In spite of it, the influence of mortar or glue thickness on the overall strength of AAC masonry is not present in the literature.

2.7 Detailed Objectives of the Present Thesis

Based on literature survey, the main objective was defined as design and development of proper bonding mechanism for individual AAC block units in wall system of a structure. To accomplish the main objective, four sub-objectives were adopted, which are also the objectives of the present thesis. The detailed objectives are as follows:

1. Evaluation of mechanical properties of autoclaved aerated concrete (AAC) block and its masonry

The first objective of this thesis is the experimental evaluation and statistical analysis of useful mechanical properties of AAC and its thick mortar (a mixture of cement, sand and water) based masonry. The following important physical properties of AAC blocks are evaluated: moisture content, initial rate of absorption, water absorption, dry density, compressive strength and tensile strength. For AAC masonry, the following properties are evaluated: compressive strength based on prism specimen test, tensile bond strength based on cross couplet specimen test and shear bond strength based on triplet specimen test. A simple analytical model is also proposed to evaluate the elastic modulus of masonry prism. The results indicate that there is a positive correlation between the strength of mortar and AAC masonry. The strength of AAC masonry increased with an increase in the strength of mortar. During the strength test of AAC masonry, the failure patterns were studied. The block-mortar interface failure was observed in most of the cases during the masonry bond strength test. A positive correlation was observed between masonry bond and compressive strengths. Further, a comparison of strengths of masonries made of AAC block and clay brick is presented. At the present level of manufacturing, AAC masonry cannot compete with clay brick masonry in terms of strength alone.

2. Compressive and shear bond strengths of grooved autoclaved aerated concrete blocks and masonry

The second objective of the present thesis asserts that the shear bond strength of AAC masonry can be enhanced by using grooved AAC blocks. The compressive strength of the grooved AAC block as well as the shear bond and compressive strengths of the masonry have been investigated experimentally and compared with conventional AAC blocks and masonry. The study clearly demonstrated the superiority of grooved AAC blocks to conventional AAC

blocks. Simple analytical models have been developed to estimate the masonry compressive and shear bond strengths. Analytical models are capable of obtaining lower, upper and most likely estimates of strengths. Significance tests have been carried out to support the findings.

3. Bond strength of autoclaved aerated concrete masonry using various joint materials

The third objective of this thesis investigates the bond strength of AAC block-mortar interface made of ordinary sand-cement mortar of different compositions and polymer modified mortars. A method of improving the bond strength (both tensile and shear) of ordinary sand-cement mortar without altering the block surface characteristics is proposed. In this method, the block surfaces are coated with a thin cement-slurry coating before applying a thick sand-cement mortar. For all types of interfaces, the shear bond strength of the masonry was studied using a triplet test, while the tensile bond strength was determined based on a cross-couplet test. The failure patterns during the bond strength tests were studied. Subsequently, costs were estimated for AAC walls of different types of interfaces. Considering the bond strength as well as cost, using a weak mortar along with cement-slurry coating was found superior to the ordinary sand-cement mortar and polymer modified mortar.

4. Finite element (FE) modeling of autoclave aerated Concrete masonry for the assessment and analysis of experimental results

The fourth objective deals with the finite element modeling of AAC masonry for the estimation of compressive strength. For a load bearing structure as well as framed structure, in-plane compression is an important mode of failure in the masonry walls. In this work, the finite element micro-modeling, governed by plastic-damage constitutive relation in tension and compression, has been used to model the AAC block and mortar, while cohesive zone modeling strategy is adopted to model the block-mortar interface. The developed model has been used for the estimation of compressive strength of AAC masonry. The nature of lateral stress developed due the application of axial stress is discussed. The comparative study on stress distribution in AAC block and clay brick masonries is also presented. The results obtained from modeling have good agreement with the experimental results. The flow chart of this thesis is presented in Figure 2.4.

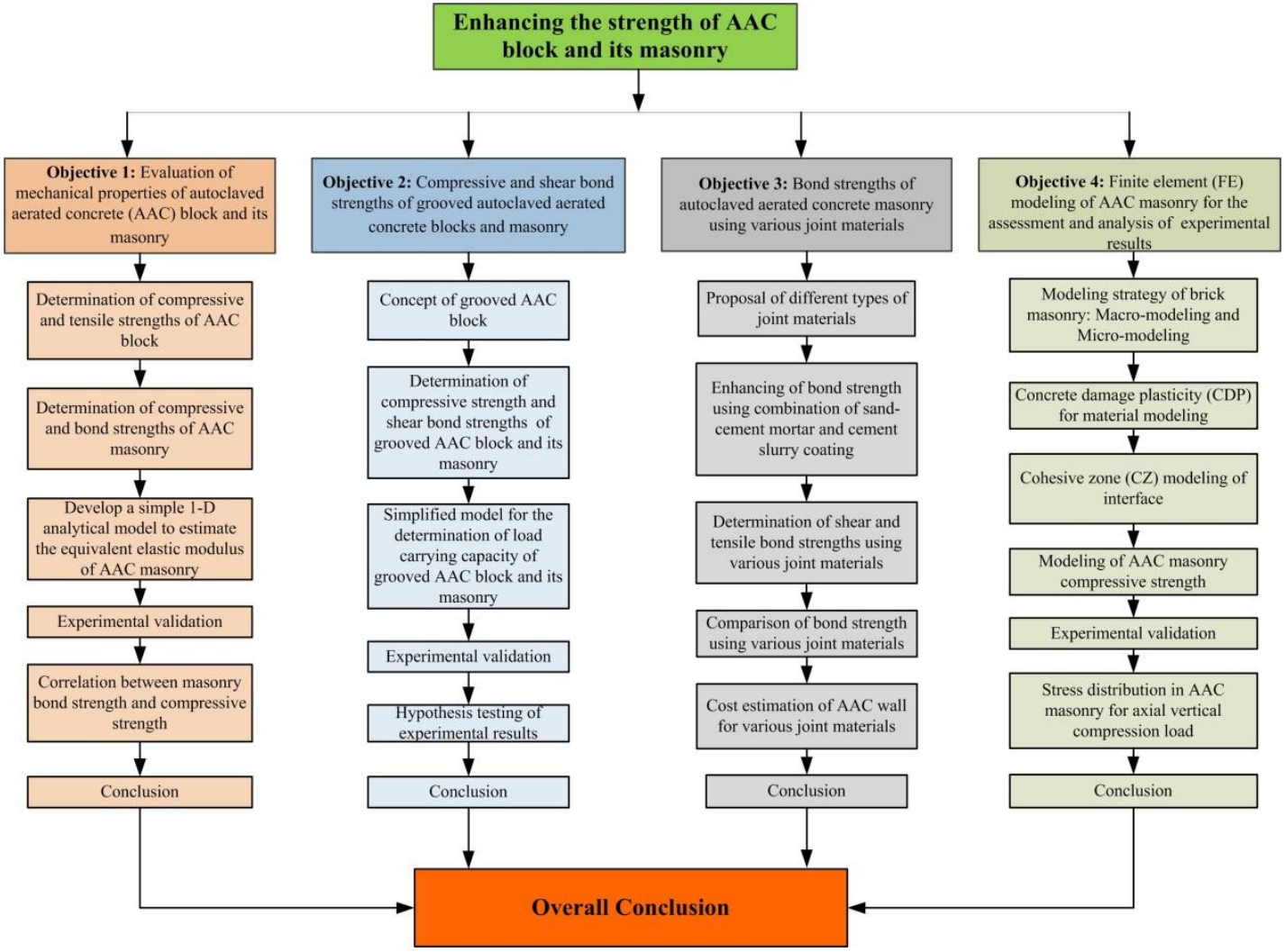

Figure 2.4 Flow chart of the present thesis

Chapter 3

Experimental Facilities used in this Research

3.1 Introduction

This chapter provides information about the experimental setups and equipment used during individual AAC block and its masonry test. In Section 3.2, details of the testing machines and accessories used for the evaluation of strengths of AAC masonry are provided. Section 3.3 discusses the various experimental set-ups and specimens used for the evaluation of strength of AAC block and its masonry.

3.2 Machines used for testing the strength of AAC masonry

Computerized Universal Testing Machine (UTM) was used to perform the compressive strength, tensile strength of individual AAC block and compressive strength of AAC masonry (assemblage of AAC block and mortar layer). The compressive strength and tensile strength of individual AAC block were determined using the AAC cubic specimen and AAC cylindrical specimen, respectively. The compressive strength of AAC masonry was evaluated using prism specimens. Further, a servo hydraulic actuator was used to evaluate shear bond strength and tensile bond strength of AAC masonry. The shear bond strength and tensile bond strength of masonry were evaluated using the triplet and cross-couplet specimens, respectively. The expected failure load for shear bond strength and tensile bond strength of AAC masonry is low (1 kN–12 kN). Therefore, a servo hydraulic actuator of lower least count, was used for these tests. The precise loading rate control facility gives the complete and clear visualization about specimen failure during the test. Laser extensometer was used to determine the transverse strain in order to evaluate the Poison's ratio of AAC block. All the equipment and accessories used in the experimental work are briefly described in the following sub-sections.

3.2.1 Universal testing machine (UTM)

A Universal Testing Machine (UTM) is used to test the mechanical properties such as tensile strength and compressive strength of a given test specimen by exerting tensile and compressive loads, respectively. Because of its versatility to perform tests of materials in both tension and compression, it is called UTM. Nowadays, computerized Universal Testing Machine that facilitates the automatic data capture, storage, graphical display and retrieval of results and other details is commonly used. Real time display of load-displacement graph can be obtained using computerized UTM. The computerized UTM are widely used for measuring the load range of 100 kN to 2000 kN with the loading accuracy of ± 1%, which conforms to IS: 1828. The various computerized UTM models commonly used worldwide are having capacity ranging from 100 kN to 2000 kN.

In UTM, the loading rate control is achieved through a hydraulic motor controlled by a specially designed flow control valve. The rate of increase of system hydraulic pressure is kept constant or variable as per the assigned program. The load rate can be controlled in the range of 0.35 kN/s to 35 kN/s for a 1000 kN capacity machine. In this study, a computerized UTM of capacity 1000 kN (Model: TUE-C-1000), as shown in Figure 3.1, was used to estimate the compressive strength of AAC block and its masonry. Moreover, the tensile strength of AAC was also evaluated using UTM. The important specifications of computerized UTM machine are given in Appendix B.

Figure 3.1 Photograph of computerized universal testing machine (UTM)

3.2.2 Servo hydraulic actuator

A servo hydraulic actuator was used to perform the tests for evaluating shear bond strength and tensile bond strength of AAC specimen. Servo hydraulic actuator is hydraulically powered pistons that can extend or retract to provide displacement or force into a test specimen or structure as shown in Figure 3.2. These actuators are used worldwide in a variety of demanding applications from structural fatigue and component testing to vehicle dynamics. Double-ended, fatigue-rated design (piston rod extends from both sides) combines balanced dynamic performance and robust side-load tolerance to maximize data accuracy.

The servo hydraulic actuators are available with or without displacement transducer to meet the specific application. The servo hydraulic actuator is comprised of actuator, servo valve, load cell and swivels. These actuators can apply loads in both displacement and load controlled mode to simulate various structural loading environment as per the requirement. Similar to UTM, the servo hydraulic actuator is also available for wide range of load applications e.g., from 100 kN to 2000 kN with a stroke length of 100 mm to 1500 mm. In this study, a servo hydraulic actuator (Make: MTS, USA; Model: 243.30T) with load carrying capacity of 250 kN and maximum stroke length of 500 (±250) mm was used to evaluate the shear bond and tensile bond strength of AAC masonry specimen. The important specifications of whole servo hydraulic system are given in Appendix C.

Figure 3.2 Photograph of hydraulic actuator

3.2.3 Laser extensometer

The laser extensometer is a high precision non-contact device used for measurement of the strain during materials testing. It uses high speed laser scanner to measure the spacing between reflective tape strips stuck on the sample. Strips of silver color reflective tape were stuck on the surface facing towards the front of the laser extensometer. The reflective tape can be used at temperatures up to 80 °C. The laser extensometer measure strain optically, without contacting the specimen, using laser diode technology. The extensometers are self-contained and portable. They can be interfaced with a variety of testing machines and data acquisition systems using the ±10V analog output or bi-directional RS-232 serial port. The measurement of extension ranges from 8 mm to 381 mm. The gauge length is set by the user. In this study, the laser extensometer (Make: Epsilon; Model: LE-15) has been used to determine the lateral displacement and thereby evaluate the lateral strain and Poisson's ratio. Figure 3.3 represents the photograph of laser extensometer setup. The important specifications of the LE-15 laser extensometer given in Appendix D.

Axial compressive load was applied on the AAC cubic specimen of edge length 150 mm for evaluating the Poisson's ratio of AAC block. The visible laser light was simply aimed at the AAC, which had small reflective tape strips set at the desired gauge length of 80 mm. The extensometer displays the actual measured gauge length. The laser extensometer records the changes in positions of the reflective tape during test and sense the data to the computing unit for storing. Thus, lateral elongation of the specimen due to axial vertical movement in perpendicular direction can be identified. The longitudinal or axial displacement was directly obtained from the hydraulic actuator system. Hence, using the lateral and axial displacements, the Poisson's ratio of AAC block was estimated.

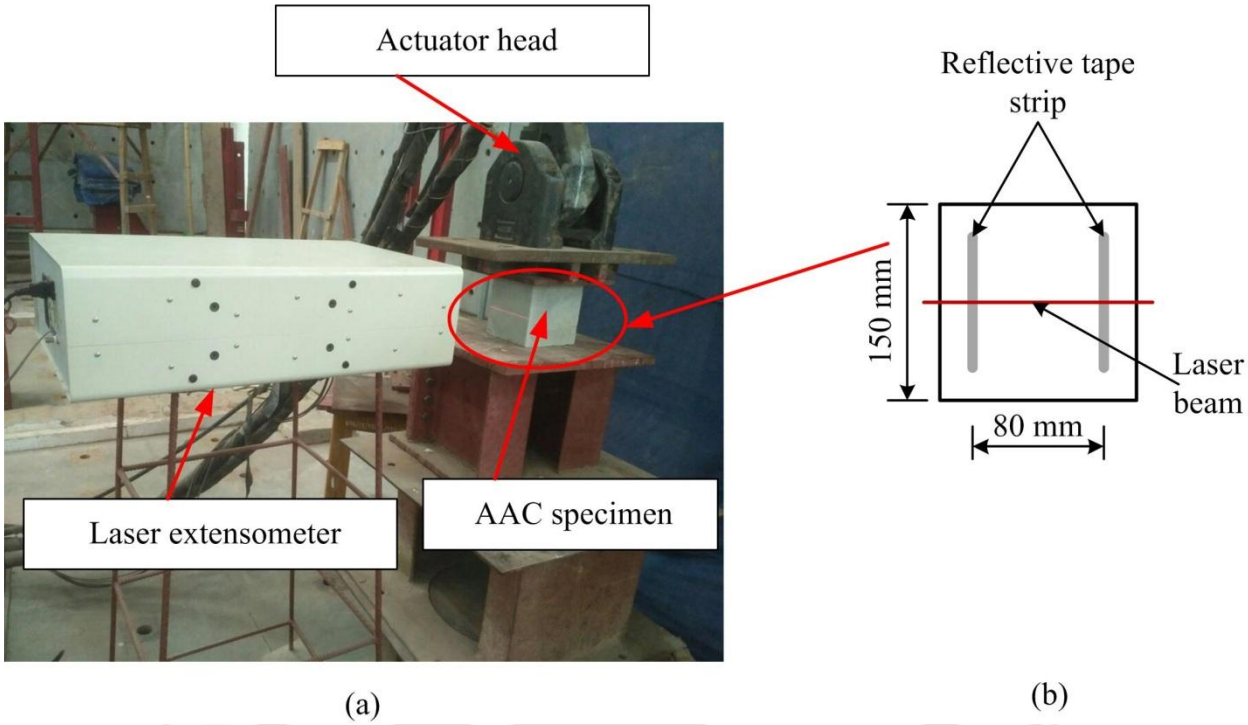

Figure 3.3 Photograph of laser extensometer during testing: (a) the complete experimental set-up and (b) exaggerated view of AAC cubic specimen with reflective tape strip and laser beam

3.3 Experimental Setup for Strength Test of AAC and its Masonry

Different types of test were conducted to evaluate the various properties of individual AAC blocks and their masonry. The compressive and tensile strength of individual AAC blocks were evaluated based on AAC cubic and AAC cylindrical specimens, respectively. The compressive strength of AAC masonry was determined using a prism specimen. The shear bond and tensile bond strengths of AAC masonry were evaluated using AAC triplet and AAC cross-couplet specimens, respectively. Various experimental setups are briefly described in the following sub-sections.

3.3.1 Experiment setup for compression test of AAC block

The compressive strength of AAC block was tested using individual AAC cubic specimen with edge length of 150 mm following IS 6441. During the test, the specimen was put between the upper and lower platens of UTM and clamped as shown in Figure 3.4. Further, the compression load with a loading rate of 1 kN/s was applied with help of a universal testing machine (UTM) of 1000 kN capacity. The compressive strength of AAC

sample was calculated by dividing the peak load with the area of the specimen surface normal to the load.

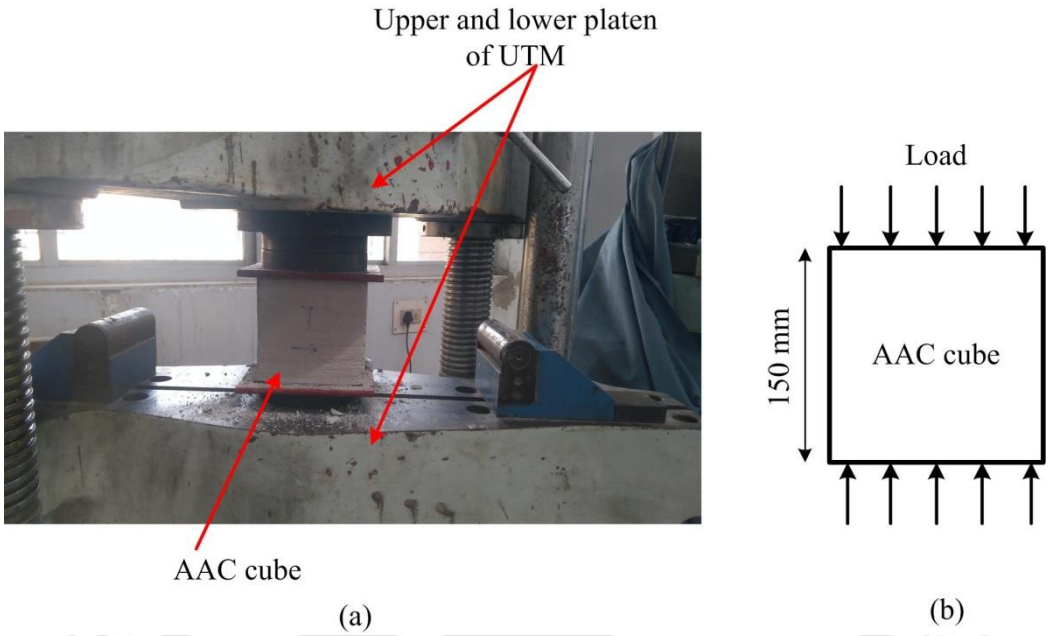

Figure 3.4 The experimental setup for compression test of AAC: (a) photograph and (b) schematic drawing of loading condition

3.3.2 Experiment setup for tensile test of AAC block

The tensile strength of AAC block was tested using AAC cylindrical specimens of size 75 mm diameter and 150 mm length as per ASTM C 1006-07. A compressive load was applied along the length of the specimen and on the diametrically opposite side of the cylindrical surface that causes lateral tensile stresses. Two plywood strips of 200 mm length and 3 mm thick were kept in between the test specimen and upper/lower crosshead of universal testing machine as shown in Figure 3.5. The purpose of plywood strip is to uniformly distribute the applied compressive load in the lines, which further causes the uniform lateral tensile stress in the test specimen. The tensile strength of AAC cylindrical specimen was calculated using the theory of isotropic elasticity.

Figure 3.5 The tensile test set-up of AAC cylindrical specimen: (a) photograph of test set-up and (b) schematic diagram of loading condition

3.3.3 Experiment setup for compression test of AAC masonry

Compressive strength is the most important parameter to quantify the characteristics of masonry. The compressive strength of masonry is primarily evaluated using a masonry prism. The prism is a small masonry wall built of one or two bricks in length and three or more bricks in height and is tested under compressive load perpendicular to the bed joint. In this study, AAC masonry prisms have been prepared using one block length and five blocks height assembled using mortar layers in between. Since the friction between bearing faces of the prism and loading platens restrains significantly the transverse deformation of the prism, higher aspect ratio or height-to-thickness (*h/t*) ratio of prism specimen has been used. The lower aspect ratio overestimates the compressive strength of the prism. IS: 1905 suggests a height-to-thickness (*h/t*) ratio between 2–5 and a minimum height of 40 cm.

Francis et al. (2017) reported that prisms with a height of five to six brick units can be considered to be free from effects of end platen during testing. Therefore, in this study the higher aspect ratio of 3.62 has been considered to eliminate the platen effect. The testing was carried out with help of a universal testing machine of 1000 kN capacity at a loading rate of 1 kN/s. During the test, the specimen was put between upper and lower platens of UTM and clamped properly. The experimental test setup for compressive strength of AAC masonry is presented in Figure 3.6.

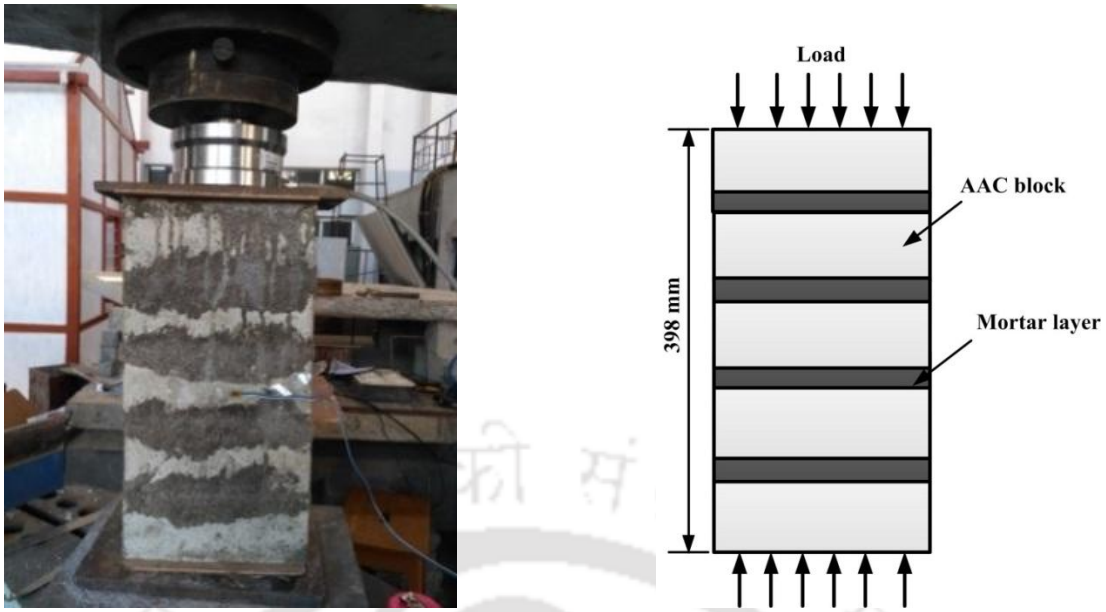

(a) (b)

Figure 3.6 Experiment test set-up for compressive strength of AAC masonry: (a) photograph of compression test set-up and (b) schematic diagram of loading condition

3.3.4 Experiment setup for shear bond strength test of AAC masonry

The shear bond strength of the AAC brick masonry can be evaluated through testing of the AAC triplets. Three block units and two mortar layers (10–12 mm thickness) were used to prepare the triplet specimen. A uniform vertical (without pre-compression) load was applied on the middle block using 20 mm thick mild steel plate and two rollers of 12 mm diameter, as illustrated in Figure 3.7. In order to reduce the eccentricity, the two side blocks were supported by mild steel roller at a location close to the mortar joint. The displacement controlled loading rate of 0.01 mm/s, corresponding to a strain rate of the order of 5×10^{-5} s^{-1}, was applied with help of a 250 kN servo hydraulic actuator. A photograph and schematic drawing of front view of the triplet test setup are shown in Fig. 3.7. Vertical compressive load on the middle brick is applied until the failing of bond between brick and mortar. The shear bond strength is calculated using the obtained peak load at failure during the test. The procedure mentioned by a number of researchers such as Alecci et al. (2013) and Singh and Munjal (2017) was followed to carry out the shear bond strength test for AAC masonry.

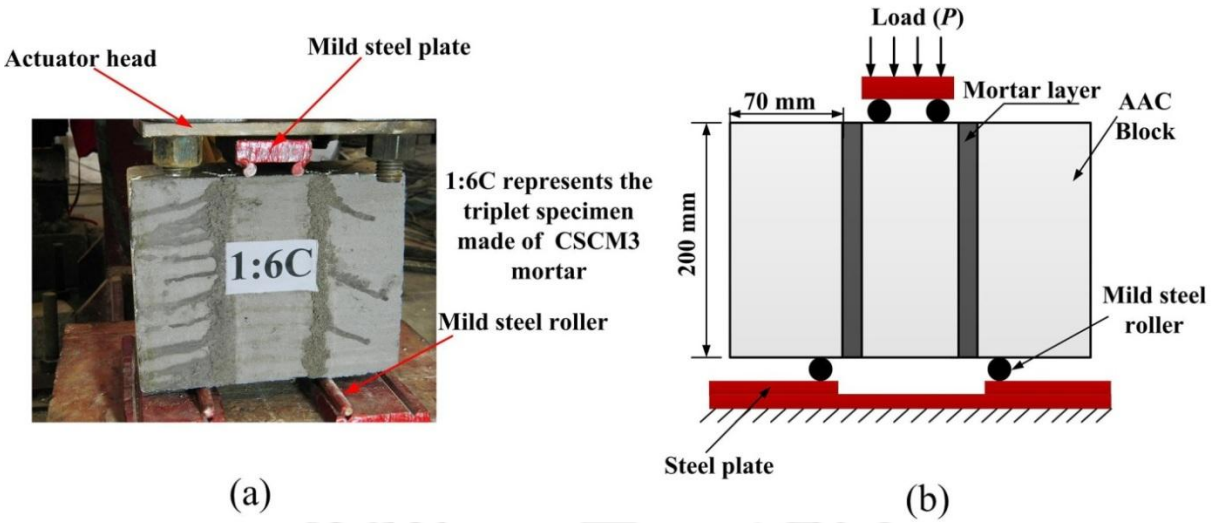

Figure 3.7 The triplet test setup: (a) a photograph (b) front view

3.3.5 Experiment setup for tensile bond strength test of AAC masonry

The resistance of masonry to tensile stress when subjected to out-of-plane loading is an important aspect for the safe design of masonry wall system. The tensile strength of masonry is primarily governed by the bond strength of brick mortar interface and is therefore called tensile bond strength (Crisafulli, 1997). In this work, the tensile bond strength of AAC block and mortar interface was determined using a cross-couplet test, which is a direct method of testing. The specimens were prepared using AAC block and mortar bed joint. It measures direct tensile strength of the bond between the mortar and AAC block unit.

The displacement controlled loading rate of 0.01 mm/s was applied with help of a 250 kN servo hydraulic actuator, which provides a strain rate of order of 10^{-3} s^{-1} during the test. Although the piston of the testing machine moves downwards at a controlled rate during testing, two specially made platens are used so as the compressive load applied n platen will be transferred to the specimen as tensile load. Specimen was placed on lower platen with lower surface of the upper block touching bars of the lower platen. Second platen was gently placed on lower block with its bars touching the upper surface of the lower block. There exists some gap between lower block and lower platen and also between upper platen and upper block. The whole setup is clearly depicted in Figure 3.8. The specimen preparation and the testing procedure were carried as per the guideline mentioned in ASTM C 952 (ASTM 1991). The tensile bond strength was calculated corresponding to the peak load at failure divided by block-mortar interface contact area.

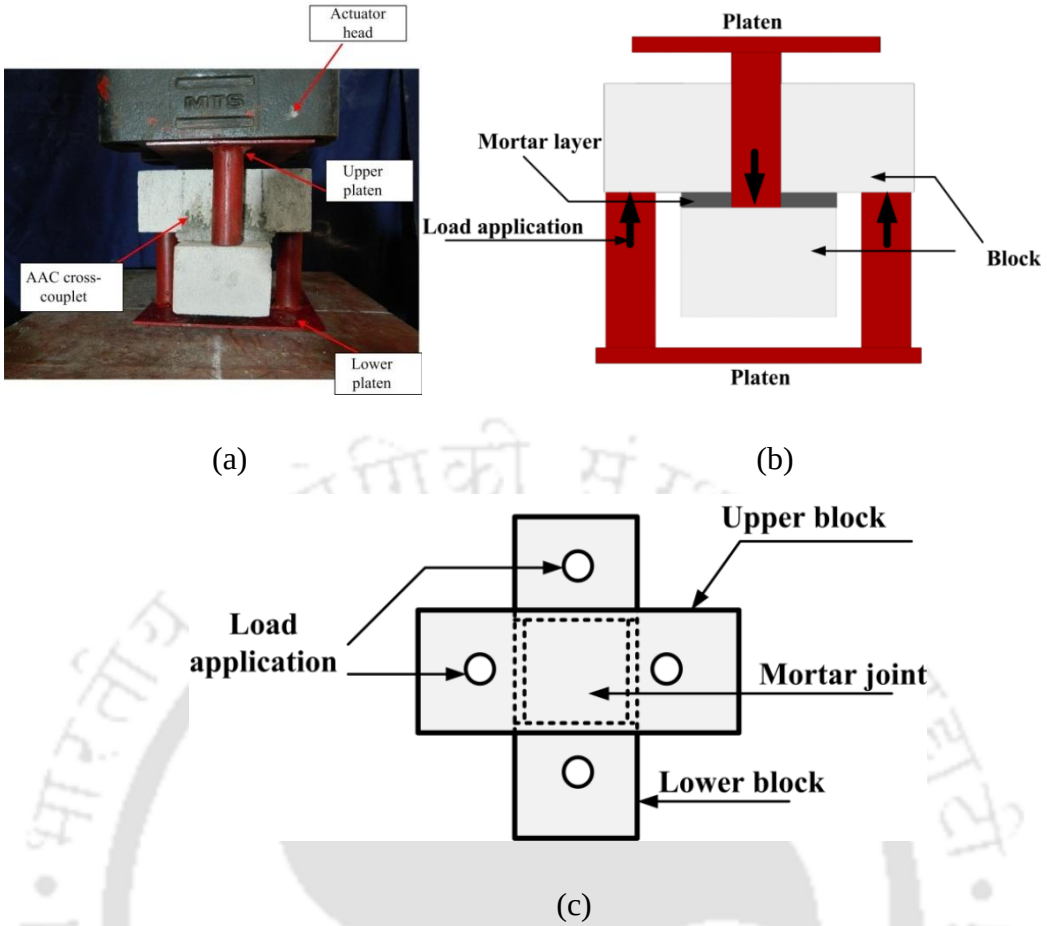

Figure 3.8 Experimental set-up for tensile bond strength test (a) photograph, (b) the loading condition and (c) top view of the cross-couplet test setup

3.4 Conclusions

In this chapter, details of testing machines and experimental set-ups are provided. Further, the test methodology and specimen adopted for the evaluation of various mechanical properties of AAC block and its masonry are discussed.

Chapter 4

Evaluation of Mechanical Properties of Autoclaved Aerated Concrete (AAC) Block and its Masonry

4.1 Introduction

Detailed literature review on AAC and its masonry described in Chapter 2 revealed that a large number of investigations on the physical, chemical and mechanical properties of AAC have been carried out in the past. The strength of AAC depends on the raw materials used and their proportions, processing methods and parameters, curing procedure, and atmospheric moisture content. AAC is a relatively new building material in Northeast India that falls in Seismic Zone-V of country's seismic map. Hence, there is an urgent need to evaluate the performance of AAC block manufactured for the benefit of Northeast region, in particular, and whole world, in general. The AAC masonry construction employing a thick conventional (cement-sand) mortar of 12 mm thickness is the general practice in India (especially in Northeast India), although the thin polymer-based mortar joint (2–5 mm thick) is also used occasionally.

There is hardly any information available on the mechanical properties of AAC masonry based on a thick layer of cement-sand mortar. Also, the effect of joint strength on the overall performance of AAC masonry has still not been properly investigated. This chapter attempts to fill up that gap. It discusses the useful mechanical and physical properties of AAC blocks. Furthermore, the experimental study on compressive strength, shear bond strength and tensile bond strength of AAC masonry using the thick conventional cement-sand mortar have been carried out. Three different proportions of cement-sand mortar have been used for the assemblage of AAC masonry specimens. The different mortars are having different compressive strength. The failure behaviors of individual AAC block and its masonry during the test are discussed. The effect of mortar strength on the mechanical properties of AAC masonry is highlighted. A comparison of strengths of masonries made of AAC block and clay brick is presented. Thus, the present chapter studies a comprehensive mechanical behavior of individual AAC block and its masonry.

The remaining sections of this chapter are arranged as follows. Section 4.2 describes the materials and the specimen preparation (for evaluating different mechanical properties) of AAC block as well as its masonry. Section 4.3 presents the experimental results with justification on mechanical properties of the AAC block and its masonry. Section 4.4 concludes the chapter.

4.2 Materials and Specimen Preparations

A total of 60 AAC blocks of actual size 600×200×200 mm^3 from the same lot were collected from a manufacturing industry to prepare the specimens. A total of 18 cubic specimens of edge length 150 mm were prepared in order to evaluate the compressive strength of AAC block following IS 6441. A total of 9 cylindrical specimens of 75 mm diameter and 150 mm length were used for evaluating the splitting tensile strength of AAC block. Although the size of AAC blocks can be as large as 625×250×200 mm^3, for the ease of testing and comparison with clay bricks, considering an AAC block of size equivalent to clay brick is appropriate. For example, the experiments of Ferretti et al. (2014) have shown that the use of scaled AAC unit specimen does not alter the compressive strength test results substantially. In another work, Ferretti et al. (2015) carried out the mechanical characterization of AAC masonry using the AAC unit of size 250×100×50 mm^3. Bhosale et al. (2019) evaluated the compressive strength of AAC masonry using the AAC unit of size 200×100×100 mm^3, cut from AAC block of size 600×200×100 mm^3. Hence, in this work, for the preparation of AAC masonry, the unit size was taken equal to the size of clay brick, i.e., unit of size 200×110×70 mm^3 was cut from larger (actual) AAC block of size 600×200×200 mm^3.

The masonry specimens for evaluating compressive, tensile bond and shear bond strengths were composed of AAC block and thick mortar joint of thickness 12 mm. The compressive strength, tensile bond strength and shear bond strength of AAC masonry were evaluated on prisms, cross couplet and triplet specimen, respectively. A dry AAC block can absorb most of the water content in mortar and retards the hydration process between cement and water. As a consequence, weak and improper bonds are formed in the masonry. To alleviate this problem, prior to the preparation of AAC masonry specimens, the blocks were immersed in the water tub for 24 hours. After removing from water tub, the blocks were air-dried at laboratory condition for 30 minutes. This action removed the water particle from the surface of the block ensuring proper bond formation at the block-mortar interface. Immersion in water simulated the prevailing condition in a high rainfall place like Assam, where the

most of the times, AAC blocks are already drenched with rain-water. The strength of masonry depends on the strength of the joining material, which is the mortar in this case. Three different proportions of cement-sand mortars were used as joining materials (Sarangapani et al. 2005, Kaushik et al. 2007, and Singh and Munjal 2017).

The different types of cement-sand mortar used in this study are as follows:

1. M1 (strong mortar); cement to sand ratio by weight=1/2
2. M2 (medium strength mortar); cement to sand ratio by weight=1/4
3. M3 (weak mortar); cement to sand ratio by weight=1/6

In India, the construction of the AAC wall is generally carried out using M2 and M3 cement-sand mortars. However, M1 mortar (strong mortar) was also used to investigate and compare masonry behavior with other mortars. Masonry strength was tested using 18 specimens in prism test, 18 specimens in cross couplet test and 18 specimens in the triplet test. Each masonry strength test used equal number of experiments with M1, M2 and M3 mortars. The prisms, triplets and cross couplet specimens were cured under moist condition using wet burlap for 28 days in the laboratory condition.

4.2.1 Test for physical properties of AAC block

The physical properties such as moisture content, dry density, water absorption (WA) and initial rate of absorption (IRA) of the blocks have been evaluated. The moisture content and dry density of block were evaluated as per IS 6441. In order to measure the dry density and moisture content, the specimens were completely dried out by maintaining a temperature of 105 ºC for about 36 hours. A total of 18 cubic specimens of edge length 150 mm were tested to examine the moisture content and bulk density. Average values and coefficient of variation (CV) are reported. Average moisture content and dry density of blocks were found to be 6.05% (CV= 0.27) and 621.23 kg/m^3 (CV= 0.05), respectively. Further, the WA and IRA were tested on six blocks of size 200×110×70 mm^3 as per IS 3495 and ASTM C 67-00 (ASTM 2001c), respectively. To determine the water absorption, the specimen was completely immersed in clean water at a temperature of 28 ºC for 24 hours. The specimen was removed and the traces of water were wiped out with damp clothes. The specimen was weighed just after 3 minutes of removal from water. The IRA was measured by placing the block in 3–4 mm deep water. The water level was kept constant by continuously adding the water during the test.

Here, WA ranged from 20.9% to 32.7% with an average of 25.4% (CV = 0.17). For clay bricks, WA typically ranges from 11% to 13% (Kaushik et al. 2007). The IRA of AAC

block ranged from 2.15 to 4.91 kg.m^{-2}.min^{-1} with an average of 3.21 kg.m^{-2}.min^{-1} (CV = 0.28). For clay bricks IRA ranges from 0.97 to 2.42 kg.m^{-2}.min^{-1}(Kaushik et al. 2007). Masonry units are said to be highly absorptive when IRA is greater than 1.5 kg.m^{-2}.min^{-1} and hence, should be moistened prior to laying for realizing better bond strength. High IRA for dry AAC block may result in poor block-mortar bond because of rapid suction of water by the block from the mortar.

4.2.2 Test of compressive and tensile strengths of AAC blocks

A total of 18 cubes of side 150 mm were cut from the bottom (the mold base side), middle and top (open side of the mold) portions of six actual AAC blocks of size 600×200×200 mm^3. During the test, the compression load with a loading rate of 1 kN/s was applied using a universal testing machine (UTM) of 1000 kN capacity as shown in Figure 3.1. The compressive strength of AAC sample was calculated as the peak load divided by the area normal to the load. The tensile strength of a masonry unit was evaluated using the splitting tensile strength test on the cylindrical specimens as per ASTM C 1006-07. A compressive line load was applied to the diametrically opposite side of the cylindrical surface that causes lateral tensile stresses. According to the theory of isotropic elasticity, the splitting tensile strength for the cylindrical specimen is expressed as

$$\sigma_{\text{split}} = \frac{2P_n}{\pi DL}, \tag{4.1}$$

here σ_{split} is the splitting tensile strength, P_n is the measured peak load, D is the diameter of the specimen and L is the length of the specimen. The compression and tension test set-up are shown in Figures 3.4 and 3.5, respectively.

4.2.3 Test for compressive strength of mortars

A total of 18 mortar cube specimens of edge length 70.6 mm, 6 of each, M1, M2 and M3 types, have been prepared. The specimen preparation and the testing protocol have been followed as per IS 2250. The Portland Pozzolana cement as a binder and local sand as a fine aggregate were used to prepare the mortar specimens. The cement was characterized by the compressive strength of 39.3 MPa, tested on three cubic specimens of size 70.6 mm as per the procedure available in IS 4031. The specimens were prepared by adding 0.33 kg water per kg of cement. The compression test was performed after curing the cement cube by immersing in water for 28 days. The sieve analysis was carried for the sand aggregate as per

IS 2386. A total of 6 sieves were arranged in the descending order of size with the largest sieve on top. The sieve sizes were 4.75 mm, 2.36 mm, 1.18 mm, 0.6 mm, 0.3 mm and 0.15 mm. After placing the dry sand aggregate on the top sieve, the complete sieve stack was vibrated on a sieve shaker for 5 minutes. The relationship between the sieve size and the percentage passing by weight of sand aggregate is depicted in Figure 4.1. As obtained from the sieve analysis, most of the sand particles lay in the range of 0.3–0.6 mm. The fineness modulus of the sand was found to be 2.4, which corresponds to fine sand aggregate. During the preparation of sand-cement mortar, the sand and cement were mixed in a dry condition for each types of cement-sand mortar, according to the required ratios by weight. To maintain a constant workable flow of 100%, the water-cement ratio of 58%, 70% and 91% was maintained for M1, M2 and M3, respectively. The compressive strength test of 70.6 mm cubes of these mortars was performed on a universal testing machine (UTM) of capacity 1000 kN after curing in water for 28 days and drying for 3 days.

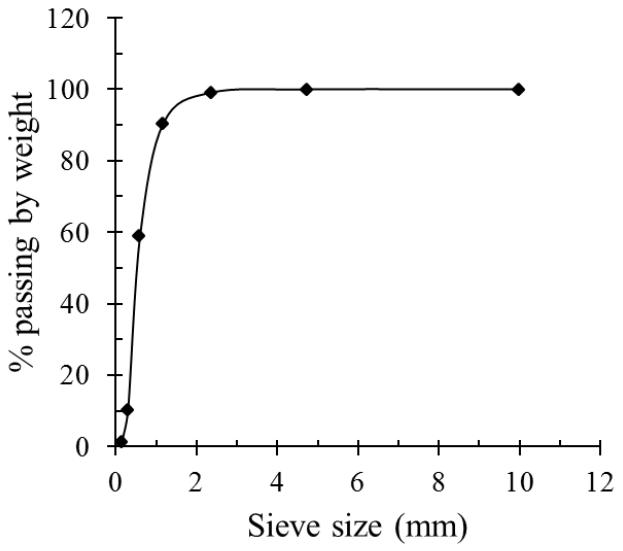

Figure 4.1 Relationship between sieve size and percentage passing by weight of sand aggregate

The average compressive strength, average modulus of elasticity and average failure strains of mortars are depicted in Table 4.1. The stress and strain corresponding to the failure load were considered as the compressive strength and failure strain, respectively. The modulus of elasticity of the mortar was measured as a slope of secant (ordinate from 5% to 33% of the ultimate strength of specimen) obtained from stress-strain data points (Kaushik et al. 2007).

Table 4.1 Summary of compressive strength test results for mortar

Mortar Types	Compressive strength (MPa)	Modulus of Elasticity (MPa)	Failure strain
M1	34.2 [0.09][a]	1913.3 [0.33]	0.021 [0.33]
M2	18.3 [0.11]	1046.0 [0.48]	0.020 [0.40]
M3	9.4 [0.20]	713.3 [0.28]	0.015 [0.43]

[a] Values in square bracket indicate the coefficient of variation.

4.2.4 Test for compressive and bond strengths of AAC masonry

The AAC brick masonry prisms have been prepared using one brick along the length and five bricks along height using three different combinations of cement-sand mortar. The capping using the neat Portland cement paste was applied both on the top and bottom surfaces of the masonry prism. The capping thickness of 2–3 mm was maintained during the application. The planeness of the capped surface and the uniform bedding was assured during the specimen preparation. Both the capped surfaces (top and bottom) were placed between two plywood sheets at the time of the test. During the test, the specimen was put between the upper and lower platens of UTM and clamped. Since the friction between bearing faces of the prism and loading platens restrains significantly the transverse deformation of the prism, higher aspect ratio or height-to-thickness (h/t) ratio of 3.62 has been used in this work to eliminate the platen effect. The lower aspect ratio overestimates the strength of the prism. IS: 1905 suggests a height-to-thickness (h/t) ratio between 2–5 and a minimum height of 40 cm.

The tensile bond strength of the AAC block and mortar interface has been determined using a cross couplet test, which is a direct method of testing. The specimens were prepared using the AAC block and mortar bed joint. Figure 1 (b) shows the schematic view of the cross couplet test setup. The specimen preparation and the testing procedure were carried out as per ASTM C 952 (ASTM 1991). During the test, the displacement controlled loading of 0.01 mm/s was adopted using a 250 kN servo hydraulic actuator as shown in Figure 3.2. The complete representation of the experimental test setup for the masonry cross-couplet test is depicted in Figure 3.8. The tensile bond strength was calculated corresponding to the peak load at failure. The tensile bond strength of the masonry is given by

$$\tau_t = \frac{(P_t)_{max}}{A}, \tag{4.2}$$

where $(P_t)_{max}$ is the peak load, τ_t is the tensile bond strength and A is the contact area. Three brick units and two mortar layers were used to prepare a triplet specimen. The shear bond strength test on the triplet was carried out in accordance with the tests carried out by a number of researchers (Mallikarjuna 2017 and Alecci et al. 2013). The complete representation of the experimental test setup for the masonry triplet test is depicted in Figure 3.7. The shear bond strength is given by

$$\tau = \frac{P_{max}}{2A}, \tag{4.3}$$

where P_{max} is the peak shear load, τ is the shear bond strength and A is the contact area.

4.3 Results and Discussion

The results obtained from the experiments are discussed in the following subsections. First, the results of the compressive and tensile strengths of AAC blocks are presented. Then, the compressive and bond strengths of AAC masonry are discussed.

4.3.1 Compressive and tensile strengths of AAC block

Prior to the compressive strength testing, the bulk density of AAC cubes was tested. The bulk density was found in the range of 569–684 kg/m^3 with a mean of 621 kg/m^3. The highest density i.e., 684 kg/m^3 was obtained for the bottom cube followed by 628 kg/m^3 for the middle and 569 kg/m^3 for the top cube. This difference in densities occurs because during the pre-curing process of manufacturing, the slurry expands or rises from bottom to top in the direction parallel to the mold height and the gravity effect dominates. In accordance with the variation in density, the average compressive strength of the bottom specimen was 3.82 MPa followed by 2.86 MPa of the middle and 2.31 MPa of the top cubic specimen. The overall average compressive strength of AAC was 2.99 MPa with the coefficient of variation of 0.25.

The average compressive strength of 2.60 MPa was reported by Mallikarjuna (2017), based on testing of 12 cubic specimens of side 150 mm. The AAC blocks are weak and soft as compared to normal clay brick units (Kaushik et al. 2007) and fly ash brick units (Basha et al. 2014). The compressive strengths of clay brick and fly ash brick have been reported as 20.8 MPa (Kaushik et al. 2007) and 5.70 MPa (Basha et al. 2014), respectively. Considering

the density of a typical clay brick as 2000 kg/m^3, its specific strength is 10.4×10^3 m^2/s^2. This value is significantly greater than the specific strength of the AAC unit obtained in this work, which is 1.5×10^3 m^2/s^2. The results of the compressive strength test of AAC cube are presented in Table 4.2. The modulus of elasticity (*E*) has been calculated with reference to a stress interval ranging between 2% to 33% of compressive strength (Ferretti et al. 2014). Its value is in the range of 152.0–317.2 MPa with an average value of 204.1 MPa. The average modulus of elasticity of the block was found to be about 68 times greater than that of the average compressive strength of the block. Substantial variation in the range of obtained modulus of elasticity is due to the significant change of properties from bottom to the top portion of the AAC block.

The very low weight and high deformability (low value of elastic modulus) tend to reduce the inertia force on the AAC building induced by the seismic motion during an earthquake (Costa et al. 2008). The elastic modulus of normal clay brick is high, 6095 MPa as per Kaushik et al. (2007), whereas for AAC block it is low, 266 MPa as per Mallikarjuna (2017). In present work, this value is found to be even lesser, i.e., 204.1 MPa. Such a low value of elastic modulus encourages the usage of AAC block in the seismic prone area like the northeast region of India.

Table 4.2 Compressive strength result of AAC cube

AAC cube specimens	Dry density (kg/m^3)	Compressive strength (MPa)	Modulus of elasticity (MPa)
Bottom	661.72 (0.02)[a]	3.82 (0.12)[a]	266.14 (0.13) [a]
Middle	613.33 (0.02)	2.86 (0.05)	180.20 (0.25)
Top	588.64 (0.05)	2.31(0.22)	166.04 (0.11)
Average	621.23 (0.05)	2.99 (0.25)	204.13 (0.29)

[a]Value in parenthesis represents the coefficient of variation.

The tensile strength of the AAC unit was evaluated using cylindrical specimens. The ultimate load i.e., the load corresponding to failure has been found in the range of 7.20–10.06 kN with a mean of 9.12 kN (CV=0.12). A typical load-displacement relation of three specimens is depicted in Figure 4.2. This figure provides an idea about the repeatability of results. The load-displacement behavior of all the specimens is similar with small deviation in quantitative values. The tensile strength, calculated using Eq. 4.1, varies in the range of 0.41 MPa to 0.57 MPa with an average of 0.52 MPa. The failure behavior for all specimens was

similar. A center vertical crack in line with applied load has been observed in the failed specimen. The failure initiated in the contact zone between a concrete specimen and a plywood strip. As the increased load reached the maximum, the plywood strip crushed the concrete specimen in the contact surface. The brittle failure was then followed by vertical crack and separation into two halves of concrete. Malyszko et al. (2015) reported an average splitting tensile strength of 0.39 MPa (CV=0.14), tested on 10 AAC cylindrical specimens.

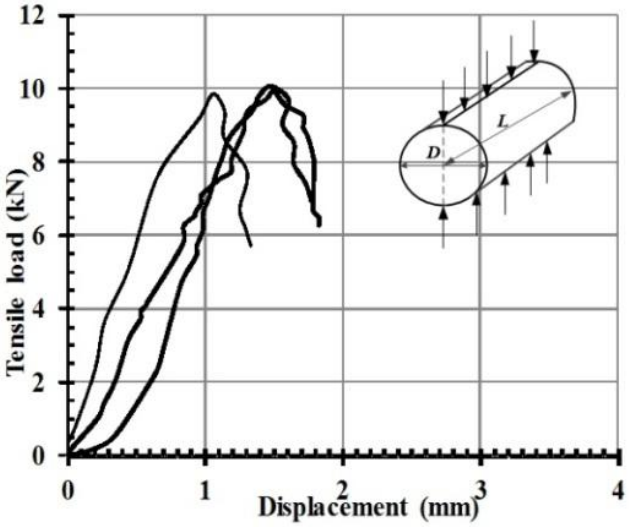

Figure 4.2 Load versus displacement curve after tensile testing of AAC cylindrical specimen

4.3.2 Compressive strength of AAC masonry

The AAC masonry prism was tested to evaluate the compressive strength. The results of the test are summarized in Table 4.3; the compressive strength of AAC masonry prism increases with an increase in the mortar compressive strength. The compressive strength of masonry based on M3 mortar has been found to be 24% lesser than that of masonry made of M1 mortar. The loading and the boundary condition of the masonry prism simulate the condition of uniaxial deflection of masonry under a monotonic compression load. Hence, using a one-dimensional Hooke's law, the mathematical expression for obtaining the total uniaxial deflection of AAC masonry, δ, is given by

$$\delta = \frac{Pl_1}{AE_1} + \frac{Pl_2}{AE_2}, \tag{4.4}$$

where$P$ is the total load applied to the AAC masonry prism, A is the area of masonry normal to the applied load, l_1 and l_2 are the total thickness of AAC unit and mortar, respectively, and E_1 and E_2 are the elastic moduli of AAC unit and mortar, respectively.

Further, the equivalent deflection (δ_{eq}) of the equivalent AAC masonry system, is given by

$$\delta_{eq} = \frac{P}{A}\left(\frac{l_{total}}{E_{eq}}\right) \tag{4.5}$$

wherel_{total} (= l_1+ l_2) is the total thickness or height of masonry and E_{eq} is the equivalent elastic moduli of masonry. For the two systems to be equivalent, the total static uniaxial deflection of the original and equivalent system must be same. Thus, using the Eqs. 4.4 and 4.5, the equivalent elastic modulus of masonry, $E_{eq}$is given by

$$E_{eq} = \left(\frac{l_1 + l_2}{\frac{l_1}{E_1} + \frac{l_2}{E_2}}\right). \tag{4.6}$$

Using l_1= 350 mm, l_2 = 48 mm, E_1 = 204.1 MPa and E_2 = 1913.3 MPa (from experiment, Tables 4.1and 4.2) in Eq. 4.6, the elastic modulus of AAC masonry prism made of M1 mortar comes out to be 228.70 MPa. Similarly, substituting E_2 for M2 mortar as 1046 MPa and M3 mortar as 713.3 MPa, the elastic modulus of AAC masonry made of M2 and M3 mortars come out to be 225.9 MPa and 223.2 MPa, respectively, as shown in Table 4.3. The relative errors with respect to the experimental findings for the masonry made of mortar M1, M2 and M3 are 14.8%, 13.5% and 15%, respectively. A typical failure pattern of the masonry prism observed under compression load can be classified into two types:

Type A: Vertical splitting cracks shown in Figure 4.3 (a, b)

Type B: Combination of cone and shear failure shown in Figure 4.3 (c, d)

During the test, the bond failure did not occur and the mortar joints were intact until the end of the test. However, lateral vertical crack in the mortar layer was found along with the block failure. As evident from Table 4.3, in most of the cases, vertical splitting cracks have been observed using M1 and M2 mortars. However, in the case of M3 mortar, the initiation of vertical splitting crack followed by cone and then shear mode has been observed in the majority of cases.

Table 4.3 The compressive strength test results of AAC masonry

Mortar Types	AAC Prism		Equivalent elastic modulus (E_{eq}) from the proposed 1D model (MPa)	Types of failure
	Compressive strength (MPa)	Elastic modulus (MPa)		
M1	2.58 [0.11][a]	268.50 [0.26] [a]	228.70	In five prisms, type A and in one prism, type B
M2	2.45 [0.13]	195.29 [0.55]	225.90	In four prisms, type A and in two prisms, type B
M3	1.96 [0.26]	189.61 [0.39]	223.20	In four prisms, type B and in two prisms, type A

[a]Value in parenthesis represents the coefficient of variation.

(a)

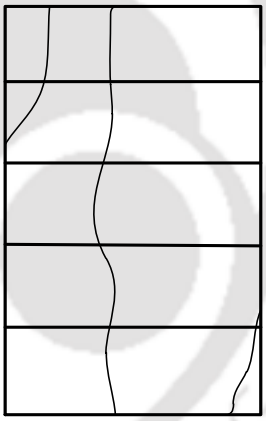

(b)

(c)

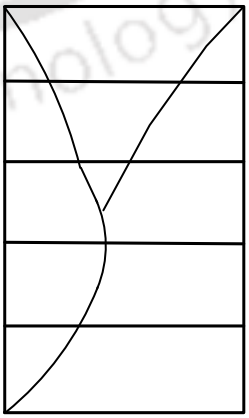

(d)

Figure 4.3 A typical failure behavior of AAC masonry (a, b) vertical splitting cracks and (c, d) combination of cone and shear failure

4.3.3 Bond strength of AAC masonry

The results of the tensile bond strength of masonry for various mortars lie in the range of 0.007–0.194 MPa. The tensile bond strength was calculated using Eq. 4.2 based on the contact area $A = 100 \times 100$ mm^2. The results of average tensile bond strength for all the mortars are tabulated in Table 4.4. The results show that the couplet specimen, using M1 mortar, has substantially better tensile bond strength than that by using M2 and M3 mortars. Thus, the use of a rich cement mortar such as M1 seems to be adequate in providing a good tensile bond of about 0.18 MPa. The bond strength falls to 0.020 MPa, when the leaner cement mortar M3 is used. It is observed that the tensile bond strength increases with the increase in mortar compressive strength. As obvious, the joint failure in the tensile bond test was brittle and sudden for all types of mortar. The failure patterns observed during the tensile bond strength test on the couplet specimens were as follows:

(1) Thorough block-mortar interface failure (Type A);
(2) Partial block-mortar interface failure (Type B) and
(3) Thorough block failure (Type C).

In the failure pattern of type A, the block and mortar is separated at the interface. This type of failure was observed in all AAC couplets using M3 mortar (Figure 4.4a) and in some cases using M2 mortar as well. This type of failure mainly occurs at the low joint strength of the interface. In partial block-mortar interface failure (type B), it can be noticed from Figure 4.4 (b) that a portion of one block (including mortar) gets stuck to other block. This type of failure mainly occurred in the couplet specimens while using M2 mortar and in some cases using M1 mortar. In case of thorough block failure (type C), the block fails completely at the interface due to the direct tension as shown in Figure 4.4 (c). This type of failure was mainly observed in the case of AAC couplet using M1 mortar, and in one case of M2 mortar. This type of failure is mainly due to the high joint strength at the block-mortar interface.

Table 4.4 The tensile bond strength test results of AAC masonry

Mortar Type	Displacement at failure (mm)	Peak tensile load (kN)	Tensile bond strength (MPa)
M1	1.35 [0.23][a]	1.82 [0.05]	0.182 [0.05]
M2	0.93 [0.47]	0.59 [0.39]	0.059 [0.39]
M3	0.43 [0.20]	0.20 [0.49]	0.020 [0.49]

[a]Value in square bracket represents coefficient of variation.

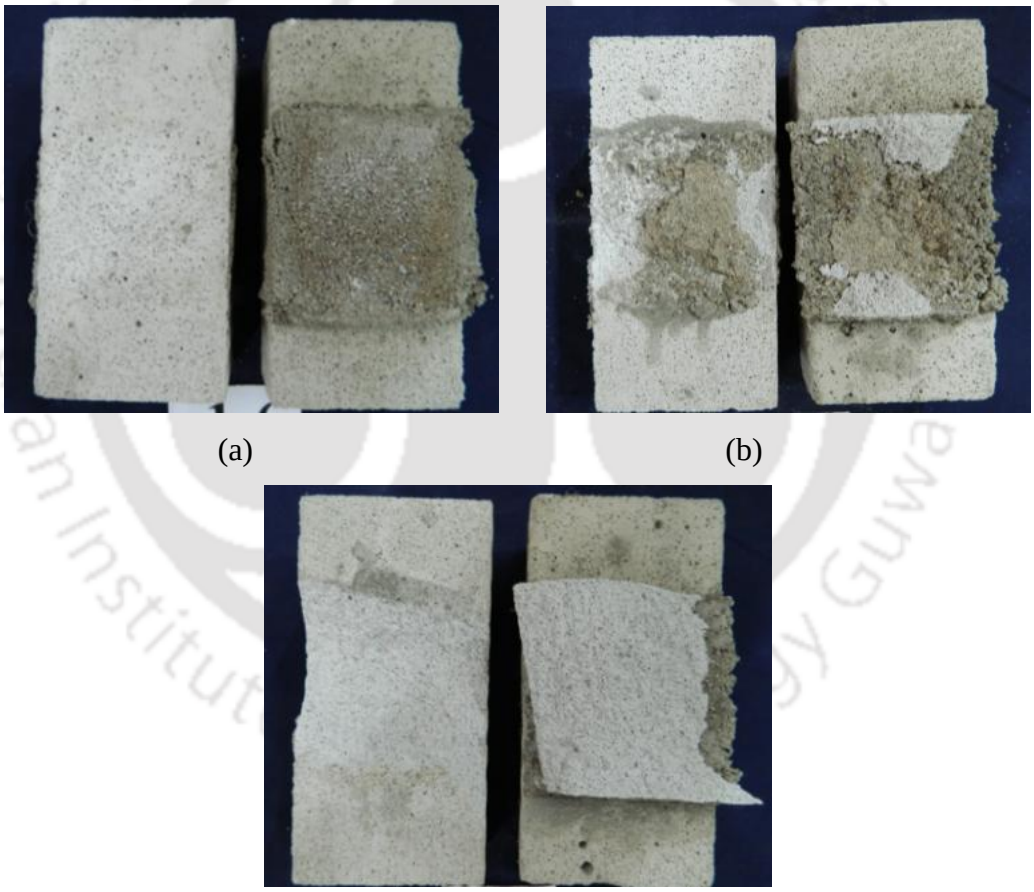

(a) (b)

(c)

Figure 4.4 Typical failure patterns observed during the couplet test (a) type A, (b) type B and (c) type C

The tensile bond strength of AAC masonry is quite less as compared to the clay brick masonry. The average tensile bond strength using M2 and M3 mortars are only 0.059 MPa

and 0.020 MPa, respectively. However, in the case of clay brick masonry, the tensile bond strength using M2 and M3 mortars was 0.205 MPa and 0.088 MPa, respectively (Sarangapani et al. 2005). Since the AAC block comprises smooth bed faces, it gets less contact area at the brick-mortar interface unlike a red clay brick. The frog present in the red clay bricks enhances the tensile bond strength, irrespective of the type of mortar used. The tensile bond strength may be increased by changing the bed face of AAC block from plain to rough texture. The introduction of rough bed surface, frogs and cement coating enhances the tensile bond as well as the compressive strength of masonry (Sarangapani et al. 2005).

The results of the shear bond strength tested on the masonry triplet are depicted in Table 4.5. From Table 4.5, it is observed that the shear bond strength of AAC masonry decreases with the decrease in the compressive strength of mortar, i.e., from M1 to M3 mortar. A relative reduction of shear bond strength by 24% has been found from M1 to M2 mortar. However, a more significant reduction has been observed (41%) from M2 to M3 mortar. The shear displacement (displacement at peak load) increases with an increase in the strength of mortar. In all the cases, irrespective of the mortar used, using all types of mortars, the AAC triplet has shown a similar type of failure behavior. The failure at the peak load is caused by the debonding of mortar-brick interfaces. The sliding shear occurred along the bed joints. In the majority of cases, the debonding of side (right or left) block-mortar interface was seen. However, the failure/debonding of the middle block-mortar interface has also been observed in some cases. No block failure was observed unlike in tensile bond test.

Table 4.5 The shear bond strength test results of AAC masonry

Mortar Type	Shear displacement (mm)	Shear Failure load (kN)	Shear bond strength (MPa)
M1	3.33 [0.12][a]	2.95 [0.13]	0.067 [0.13]
M2	2.96 [0.31]	2.23 [0.19]	0.051 [0.19]
M3	1.71 [0.35]	1.33 [0.30]	0.030 [0.30]

[a]Value in square bracket represents coefficient of variation.

The average shear bond strength of AAC masonry using M1 and M3 mortars is 0.067 MPa and 0.030 MPa, respectively. However, as reported by Sarangapani et al. (2005), in the case of clay brick masonry, the shear bond strength using M3 mortar was 0.054 MPa, which is around 44% higher as compared to AAC masonry. In another study conducted by Singh

and Munjal (2017), the shear bond strengths of clay brick masonry for mortar mix proportion (Cement: Lime: Sand) of 1:0:3, 1:1:4 and 1:0:5 were 0.169 MPa, 0.141 MPa and 0.107 MPa, respectively. Compared to clay brick masonry, the shear bond strength of AAC masonry is very less, which is quite discouraging. Similar to the tensile bond, the shear bond strength may be increased by changing the bed face of AAC block from plain to rough texture. The introduction of rough bed surface, frogs and cement coating enhances the shear bond as well as the compressive strength of masonry (Sarangapani et al. 2005).

During the compression test, the development of lateral tensile and compressive stresses in mortar and brick (or vice versa) plays a crucial role in the overall compressive strengths of masonry (Francis et al. 1971). However, the compressive strength of masonry prism also depends on the bond strength of block-mortar interface (Sarangapani et al. 2005). Figure 4.5 depicts the correlation between bond strength (shear and tensile) and masonry compressive strength with error bars. Both the compressive strength and the bond strength invariably increase with mortar strength increasing from M3 to M1. For instance, the shear bond strength of AAC masonry using mortar M1 is 0.067 MPa while the compressive strength of the masonry using same mortar is 2.58 MPa as shown in Figure 4.5 (a). However, in case of mortar M3, the shear bond strength was 0.03 MPa with corresponding compressive strength of 1.96 MPa. In the case of clay brick masonry also, the shear bond strength increases with the increase in the compressive strength of mortar (Sarangapani et al. 2005 and Singh and Munjal 2017). The shear bond strength and the compressive strength of AAC masonry decreased by 24% and 5% for mortar M1 to M2, respectively. However, the reduction is more significant i.e., 41.1% and 20% for mortar M2 to M3, respectively.

Figure 4.5 (b) represents the relation between tensile bond strength versus compressive strength of AAC masonry. Similar to the shear bond strength, the tensile bond strength also decreases with a reduction in the compressive strength of masonry. For instance, the tensile bond strength of AAC masonry with mortar M1 is 0.182 MPa, while the compressive strength of AAC masonry with similar mortar is 2.58 MPa. However, in the case of M3 mortar, as the tensile bond strength got lowered to 0.020 MPa, the compressive strength got lowered to 1.96 MPa. The ratios of tensile bond strength to shear bond strength are 2.72, 1.15 and 0.67 for mortars M1, M2 and M3, respectively. Hence, the tensile bond strength is usually greater than shear bond strength for strong mortar (M1), but it is lesser for the weak mortars (M2 and M3).

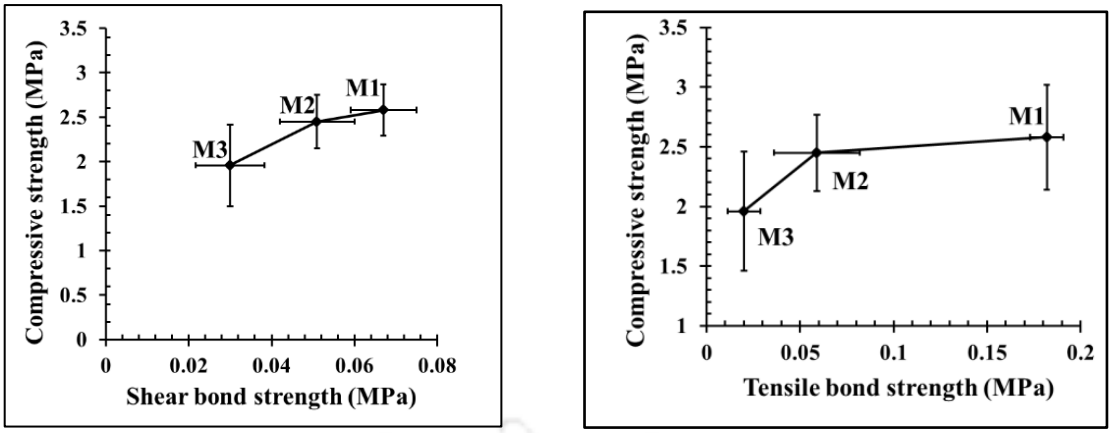

(a) (b)

Figure 4.5 Correlation between masonry bond strength and compressive strength: (a) shear bond strength versus compressive strength and (b) tensile bond strength versus compressive strength

4.4 Conclusions

In this chapter, the mechanical properties of AAC blocks and thick cement-sand mortar based masonry were tested. The important physical properties, viz., moisture content, dry density, water absorption (WA) and initial rate of absorption (IRA) were also evaluated. The influence of the mortar strength on compressive and bond strengths of the masonry has been discussed. A simple analytical model has been also developed to evaluate the elastic modulus of masonry prism.These findings can provide guidelines for structural analysis of the buildings made of AAC blocks. The experimental results can be used for validating finite element models of AAC structures. Some key observations from this study are as follows:

- The WA and IRA of AAC block are high as compared to the normal clay brick. In the AAC block, the WA and IRA ranged from 21–33% and 2.2–4.9 $kg.m^{-2}.min^{-1}$, respectively. However, for clay brick, the WA and IRA range from 11–13% and 0.97–2.42 $kg.m^{-2}.min^{-1}$, respectively. This implies that AAC unit requires moisturization at the time of masonry assemblage.
- The compressive strength of an AAC block increases with an increase in the dry density; it also increases from the top to bottom of the block. As the bottom portion of the block is denser than the middle and top portion, the bottom cube has shown the highest compressive strength. Also, the compressive strength of the ordinary clay brick is about 4–6 times that of the ordinary AAC block.

- The compressive strength of masonry is less than that of the compressive strength of individual AAC block. The average compressive strength of masonry using different proportions of cement-sand mortar ranged from 1.96–2.58 MPa, whereas the average compressive strength of individual AAC block is 2.99 MPa.
- The elastic modulus of AAC masonry evaluated using one-dimensional analytical model has a close agreement with experimental findings. The compressive and bond strengths of the masonry decrease with a reduction in the compressive strength of the mortar.
- An extensive increase in the tensile bond strength is achieved using M1 (high strength) mortar as compared to M2 (medium strength) and M3 (low strength) mortars. The use of M1 mortar changes the failure pattern, i.e., the block gets failed before the failure of mortar. Hence, M1 mortar is not recommended for AAC masonry.
- Since the present AAC blocks are smooth at all the six surfaces, the shear bond strength of AAC masonry is low as compared to the clay brick masonry, irrespective of mortar types. For the same cement-sand mortar, the shear bond strength of AAC masonry is 0.03 MPa, whereas for clay brick masonry, it is 0.05 MPa. It is suggested that high shear bond strength could be achieved by introducing the frog or rough textured bed face in the AAC block. Moreover, use of the combination of cement slurry coating and cement-sand mortar can also result in enhanced shear bond strength. All these aspects have been subsequently studied in Chapter 5 and Chapter 6.

Chapter 5

Compressive and Shear Bond Strengths of Grooved AAC Block and Masonry

5.1 Introduction

A perfect bond between brickwork unit and mortar is crucial for obtaining a strong brick work. The bond strength becomes significantly important when the masonry is subjected to in-plane and out-of-plane loading during seismic tremors. As discussed in literature survey (Chapter 2), the masonry unit-mortar bond development is influenced by a large numbers of parameters related to the characteristics of masonry unit and mortar. Masonry unit surface characteristics include the surface roughness of the bonding surfaces and dimensions of the frog, if any, in the brick/block. The water absorption and moisture content of the brick/block also influence the bond strength. Mortar related salient parameters are water retention capacity, compositions and workability (Sarangapani et al. 2005, Reddy et al. 2007, Reddy and Vyas 2008).

Autoclaved aerated concrete (AAC) blocks also known as light-weight concrete blocks or cellular concrete blocks are being used as a building wall material throughout the world. Light-weight AAC blocks can be employed to construct a multi-storey building. The AAC blocks are wire-cut as per the industrial practice, which results in smooth surfaces. When the two blocks with smooth surfaces are joined with mortar, a high shear bond strength is not attained (Mallikarjuna, 2017). The presence of frog in clay brick imparts higher masonry shear bond strength (Sarangapani et al. 2005, Reddy et al. 2007, Reddy and Vyas 2008 and Singh and Munjal 2017). Various researchers (Sinha 1967, Sarangapani et al. 2005, Reddy et al. 2007, Reddy and Vyas 2008) tried a number of techniques to enhance the masonry shear bond strength of clay brick and soil-cement block masonries. Some salient techniques are introducing multiple frogs, altering the brick surface texture and surface-coating using epoxy resin or fresh cement slurry.

Considering the present AAC manufacturing practice, it is difficult to produce AAC blocks with rough, textured or frogged bonding surface. However, the grooved bed face AAC block can be produced efficiently and economically. The grooved blocks will provide

significant increase in shear bond strength as observed through experimentations in this study. A detailed study on this aspect is the focus of the present Chapter. Moreover, the enhancement of bond strength using fresh cement slurry coating has been studied in the next chapter (Chapter 6)

This chapter reports rigorous experiments on the sliding shear bond (along the bed joint) and compressive strengths of grooved AAC masonry. The results are compared with those for conventional AAC blocks and masonry. Analytical models have been developed to estimate upper, lower and most likely estimates of strengths. Hypothesis testing has been carried out to support the experimental findings.

The remaining sections of this chapter are arranged as follows. Section 5.2 describes the concept of grooved AAC block. Section 5.3 presents the testing methods and specimen preparation to determine the compressive strength of grooved AAC block as well as compressive and shear bond strengths of grooved AAC block masonry. Section 5.4 describes the simplified model for the determination of load carrying capacity of grooved AAC block and its masonry. Concept of hypothesis testing is described in Section 5.5. Section 5.6 discusses the results and validation of experimental findings. Section 5.7 concludes the chapter.

5.2 Concept of Grooved AAC Block

The manufacturing process of AAC block is totally different from that of clay brick. For casting a clay brick, typically a mold of size 210 (length)×110 (width)×68 (height) mm^3 is used. The bottom surface of the mold contains a circular or rectangular raised pattern or design called emboss. As a result, the circular or rectangular frog/deboss is formed on the final clay brick surface. The frog is basically an indentation on the brick surface. In contrast to this, AAC block of size 600 (length)×200 (width)×150 (height) mm^3 is manufactured by wire cutting of a huge soft green cake cast in a mold of size 4200 (length)×1200 (width)×600 (height) mm^3 as discussed in Chapter 1. Thus, the final AAC block surface is smooth and there is no scope to form a frog on its surface. However, producing the grooved AAC block was found to be practically feasible in the existing manufacturing set-up through mold modification method. The mold modification is simple, economical and can be easily implementable in the existing AAC manufacturing industry.

Three different miniature molds of internal dimension 220×120×140 mm^3were fabricated to produce two blocks each of plain, single-groove and double-groove type. The

mild steel plates of 5 mm thickness were used to fabricate the mold. The photograph of mold is shown in Figure 5.1.

(a) (b) (c)

Figure 5.1 Photograph of miniature molds for producing (a) plain AAC block, (b) single geoove AAC block and (c) double groove AAC block

For the molds producing grooved blocks, holes of 30 mm diameter were made in the plates using stamping operation. The holes were for inserting steel cores. Fine grade materials were used to produce the AAC blocks in the following way:

(1) Initially, a slurry was prepared using 38% water, 14% cement, 7% lime, 0.03% aluminium powder and rest crushed fine sand by weight.

(2) The slurry was poured into oil treated miniature molds. The molds for producing grooved blocks contained 30 mm diameter cores spanning the entire width. Only 60% of the mold volume was filled with slurry to allow for the expansion of the slurry during casting process.

(3) After pouring, slurry was allowed to pre-cure and rise for about 4–5 h for getting a green cake with sufficient strength. During this time, the aluminum powder reacts with calcium hydroxide formed as a reaction between cement and water. As a result, hydrogen gets released and the pores are filled up with air, causing the expansion/rise of the slurry. The volume increases with increase in the amount of aluminum powder.

(4) After pre-curing, the top surface of the green cake was levelled by removing excess material. In case of grooved blocks, the core was removed gently, producing holes in green cakes. Green cake was taken out from the mold and wire-cut to make blocks of 70 mm height. As a result, two blocks could be prepared from each mold. Blocks from the molds with cores contained semi-circular grooves on one face.

(5) After wire-cutting, the blocks were placed in an autoclave chamber for hydrothermal treatment at the steam temperature and pressure of 200 ºC and 1.3 MPa, respectively. The temperature and pressure for hydrothermal treatment adopted was the same as used for manufacturing the conventional AAC blocks. Finally, the hardened plain as well as grooved AAC blocks were obtained after 18 h of autoclaving. The photograph of different stages to produce the grooved AAC blocks using the miniature is shown in Figure 5.2.

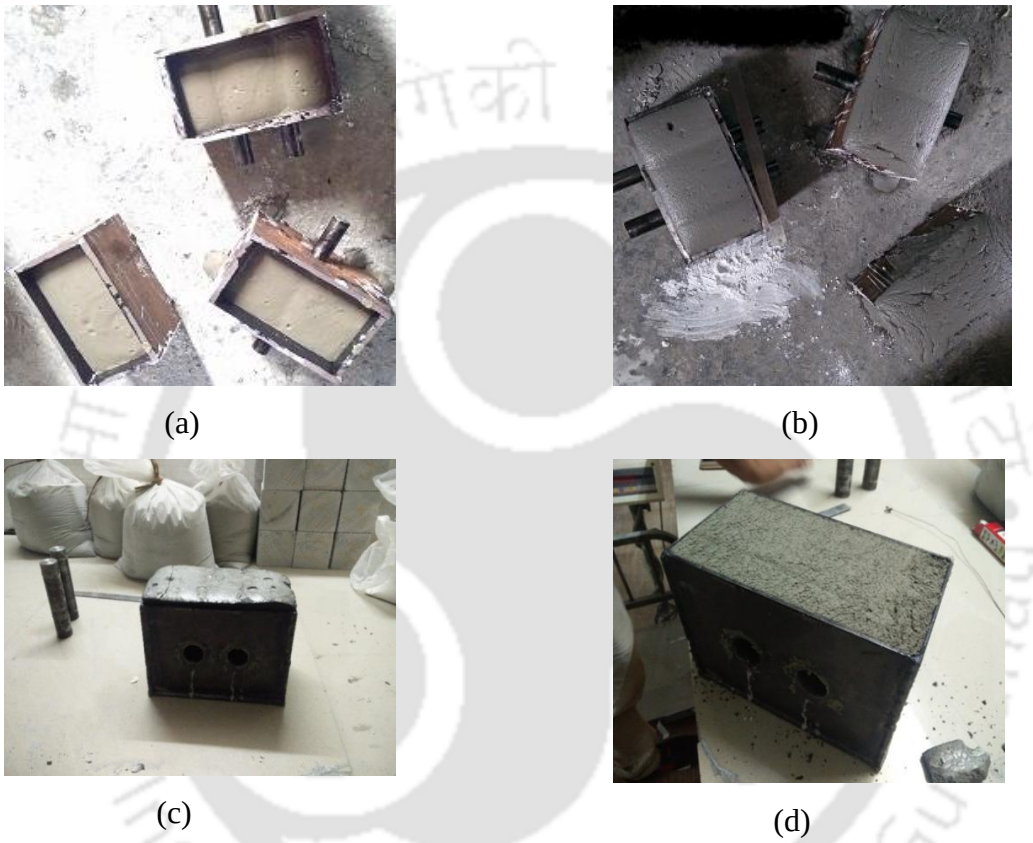

Figure 5.2 The photographs showing the different stages of manufacturing of grooved AAC block: (a) pouring of slurry mix into the miniature mold, (b) expansion/solidification of slurry in the miniature mold, (c) removal of core from mold leaving the hole inside the block and (d) levelling the top surface of green cake by removing extra material

Although AAC blocks are usually of size 625×250×200 mm^3, for the ease of testing and comparison, the sizes of AAC blocks in this study were of the clay brick size (220×120×70 mm^3). As per the I.S. 1077, clay bricks of 70–90 mm height have a rectangular or circular frog of 10–20 mm deep on one of its flat surfaces. Therefore, the AAC blocks with circular groove of depth 15 mm at one of its faces were used. The designations for plain

block, single-grooved block and double-grooved block are PB, SGB and DGB, respectively. The different grooved AAC blocks used in this study are depicted in Figure 5.3.

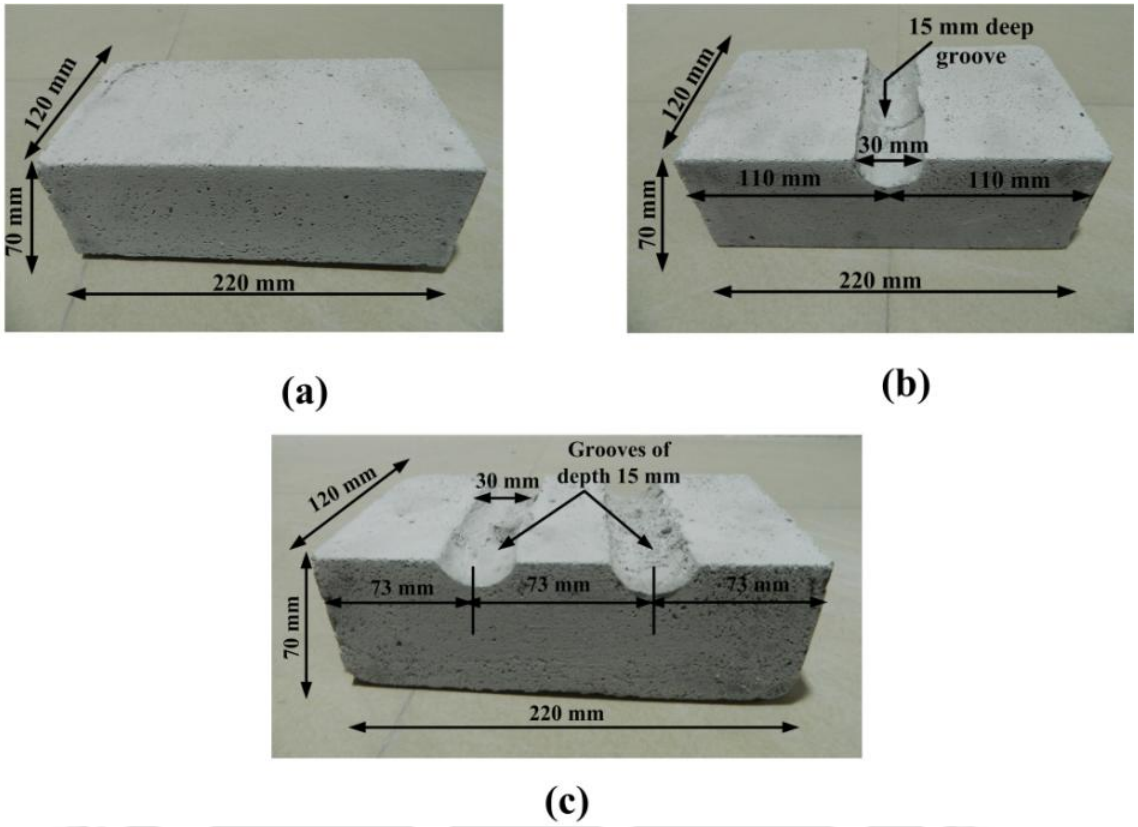

Figure 5.3 AAC blocks used in the study: (a) plain block, (b) single-grooved block and (c) double-grooved block

All the stages (pouring, rising, cutting and autoclaving) in production of grooved AAC block using the miniature mold were performed in an industry, manufacturing conventional AAC blocks following the usual industrial practice as discussed in Chapter 1. The moisture contents and the dry density of the final blocks were tested on each of six PB, six SGB and six DGB specimens. The moisture contents of PB, SGB and DGB blocks were found to be 8%, 9.4% and 9.2%, respectively, while the average dry densities of PB, SGB and DGB blocks were 658.2 kg/m^3, 665.3 kg/m^3 and 668.24 kg/m^3, respectively. The density of lower block was found to be marginally higher (4–9%) than that of upper block. However, the effect of groove on the moisture content and dry density of the block is very less.

5.3 Testing Methods and Specimen Preparation

The sand-cement mortar was used as a joining material. The cement to sand ratio by weight typically ranges from 1/2 to 1/6 (Sarangapani et al. 2005, Singh and Munjal 2017 and Mallikarjuna 2017). In this study, a mortar with cement to sand ratio of 1/4 was used to prepare all the AAC masonry specimens. The Portland Pozzolana cement as a binder and local sand as fine aggregate was used to prepare the mortar. The compressive strength of the mortar was evaluated using cubic specimens of 70.6 mm edge length. The mortar cubes were immersed in the water for curing for 28 days. After curing, the compressive strength testing of mortar specimens was performed. The mortar specimen preparation and the testing protocols were followed as per the guidelines provided in I.S. 2250. The stress and strain corresponding to the peak load was considered as the compressive strength and failure strain, respectively. The average compressive strength and failure strain of the mortar tested on 6 specimens were found to be 18 MPa (coefficient of variation, CV=12%) and 0.024 (CV=40%), respectively. Tests were conducted to obtain (a) compressive strength of AAC block, (b) shear bond strength of block-mortar interface, (c) compressive strength of masonry prism and (d) stress−strain behavior of AAC block and masonry under compression load. The procedures to evaluate the compressive strength of AAC block as well as shear bond and compressive strengths of masonry are discussed in the following sub-sections.

5.3.1 Determination of compressive strength of AAC block

The compression test of the blocks was performed on individual blocks. In order to obtain the uniform surface contact between the block surface and platens, the grooves of the blocks were filled with the mortar. Prior to mortar filling, all the blocks (including those without grooves) were soaked in normal water for 24 h. The specimens after mortar filling were kept in the moist condition, covering with burlap, for 28 days. A total of 18 specimens (6 each for PB, SGB and DGB) were tested using a Servo Hydraulic Actuator (Make: MTS, USA) of 250 kN capacity with a displacement controlled loading rate of 0.01 mm/s (Figure 3.2). The stress-strain behaviors were obtained from the tests. The loading condition for different types of AAC blocks is shown in Figure 5.4.

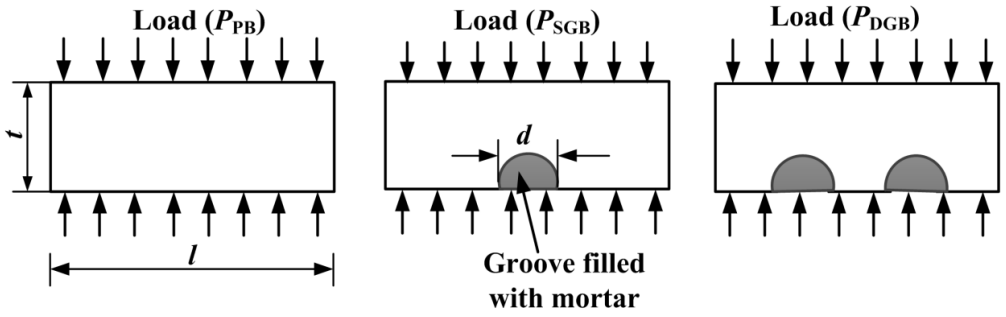

Figure 5.4 The free-body diagram of the AAC blocks under compression load for: (a) PB, (b) SGB and (c) DGB blocks.

5.3.2 Determination of shear bond strength of block-mortar interface

The shear bond strength of the block-mortar joints (without pre-compression) was studied through testing the AAC block triplets. Three blocks and two mortar layers (10–12 mm thickness) were used to prepare a triplet specimen. The displacement controlled loading of 0.01 mm/s was applied using the Servo Hydraulic Actuator (Figure 3.2). The shear bond strength test was carried out in accordance with existing practice for clay bricks (Singh and Munjal 2017 and Alecci et al. 2013). A total of 27 AAC triplet specimens, 9 each for PB, SGB and DGB, were prepared using the sand-cement mortar. Prior to the test, the prepared specimens were cured in the moist condition, covering with burlap, for 28 days. The shear bond strength was calculated corresponding to the peak load at the failure during the test. The loading and boundary conditions for different types of AAC masonries during the shear bond test is shown in Figure 5.5.

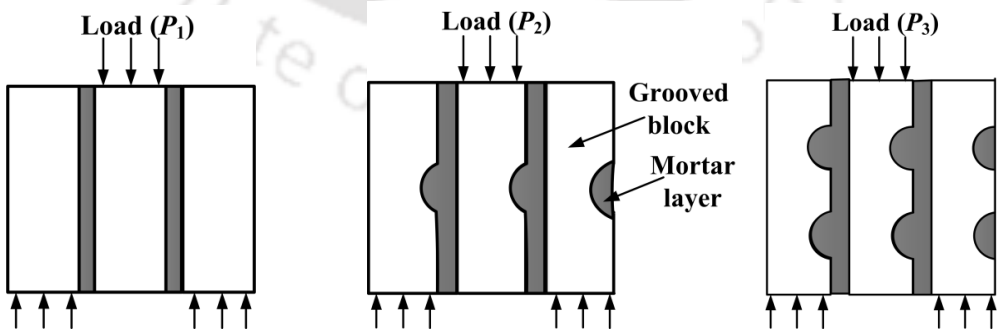

Figure 5.5 The loading and boundary conditions of masonry triplet for (a) PB, (b) SGB and (c) DGB masonry triplets

5.3.3 Determination of compressive strength of AAC masonry

The masonry compressive strength is primarily evaluated using a masonry prism. In this work, AAC masonry prisms were one-block long and five-block high and used cement-sand mortar as a joint material. To alleviate the effect of friction between bearing faces of the prism and loading platens, a high aspect ratio or height-to-thickness (*h/t*) ratio of prism specimen has been used; a lower aspect ratio would have overestimated the strength of the prism. The I.S. 1905 suggests a height-to-thickness (*h/t*) ratio in the range 2–5 and the minimum height of 40 cm. Therefore, in this study an aspect ratio of 3.32 with a total prism height of 40 cm has been used. The sample preparation has been carried out as per the guidelines available in ASTM C1314–16.

A total of 18 AAC prisms (6 each for PB, SGB and DGB) were prepared using 10–12 mm thick mortar layers. For SGB and DGB masonry prisms, grooves of bottom block were filled with mortar to obtain a uniform contact between bottom blocks with the end platens. Prior to the test, the prism specimens were cured in a moist condition, covered with the burlap for 28 days. The testing was carried out using the Servo Hydraulic Actuator with a displacement controlled loading of 0.01 mm/s (Figure 3.2). The compressive strength of the masonry was evaluated corresponding to the peak load at failure during the test. The stress-strain characteristics were obtained from the tests. The loading and boundary conditions for different types of AAC masonries during the compression test is shown in Figure 5.6.

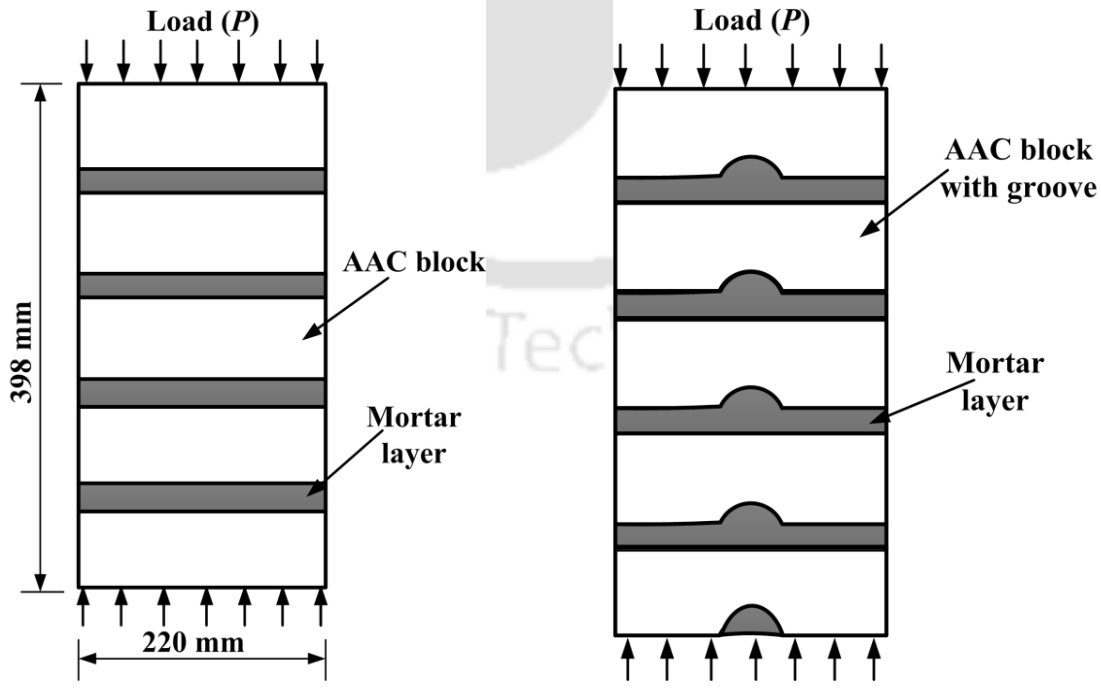

(a) (b)

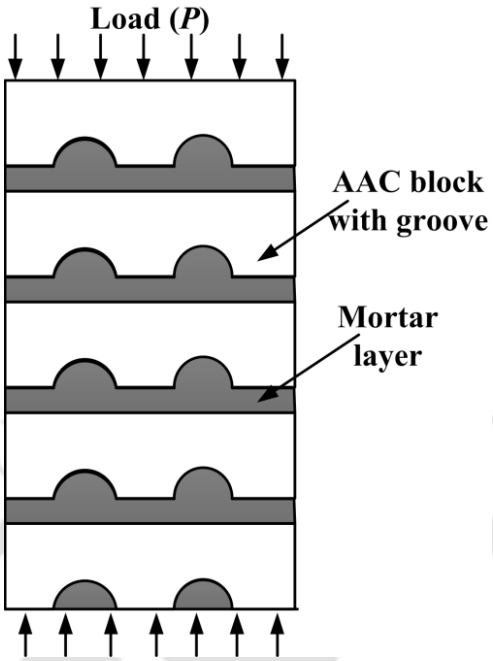

(c)

Figure 5.6 Experiment test setup for compressive strength of AAC masonry for (a) PB masonry, (b) SGB masonry and (b) DGB masonry

5.4 Simplified Models for the Determination of Load Carrying Capacity of Grooved AAC Block and its Masonry

The simplified models were developed to compute the compressive load carrying capacity of blocks and shear load carrying capacity of the masonry. The load carrying capacity of the plain block (PB) is given by

$$P_{PB} = \sigma_b lw, \tag{5.1}$$

where l is the length and w is the width of the block. From Eq.5.1, compressive strength σ_b of the AAC is estimated. The load carrying capacity of single-groove block (SGB) is given by

$$P_{SGB} = \left\{\sigma_b (l-d) + \sigma_m d\right\} w, \tag{5.2}$$

where σ_m is the equivalent compressive strength of the mortar portion. It is to be noted that σ_m is not the compressive strength of a mortar cube, which came out to be 18 MPa in this study. It will be significantly less than that value, as this case is similar to a small mortar half

cylinder resting on a softer AAC block. Moreover, during the experiment, the mortar cube specimens were prepared properly following the testing code discussed in Section 5.3. The air voids present inside the cube specimen were removed through the vibration and the uniform distribution of water and cement in the mortar was achieved. As a result, the mortar specimen had high compressive strength as compared to the mortar in the masonry. Hence, it was decided to estimate σ_m in an inverse manner from Eq. 5.2. Once the values of σ_b and σ_m are known from the tests conducted on PB and SGB, they can be used for estimating the load carrying capacity of a multi-grooved AAC block. For example, for a double-groove block (DGB) the load carrying capacity is given by

$$P_{DGB} = \left\{\sigma_b (l - 2d) + \sigma_m 2d\right\} w. \tag{5.3}$$

Similar equations can be developed for the blocks with more than two grooves. Using the similar method, the simplified models for the compression load carrying capacity of AAC masonry are developed, which are presented in Result and Discussion section.

The mathematical model for determining the shear load carrying capacity of a masonry triplet is also developed on similar lines. The corresponding free body diagrams of the middle block are shown in Figure 5.7. Figure 5.7 (a) shows that for PB masonry triplet

$$P_1 = 2\tau A_c, \tag{5.4}$$

where P_1 is the shear failure load, τ is the shear bond strength of mortar with AAC and A_c is the bonding area. Eq. 5.4 is used to estimate τ. Figure 5.7 (b) shows the free body diagram of the middle block. Here, the load P_2 is supported not only by the shear stress at the mortar-AAC interface, but also by the crushing strength σ_c of the mortar. As a simplification, the vertical force produced by crushing component is obtained by multiplying σ_c with the projected contact area of mortar on AAC. Thus,

$$P_2 = \tau A_c + \sigma_c \frac{d}{2} w + \tau (A_c - dw), \tag{5.5}$$

$$= 2\tau (A_c - dw) + \sigma_c \frac{d}{2} w. \tag{5.6}$$

Eq. 5.6 is used for estimating σ_c, which is different from σ_m and the compressive strength of the mortar block. Considering the simplification made, σ_c should be considered as only an

equivalent crushing strength and not the real one. Once τ and σ_c are known, the shear load carrying capacity of a multi-grooved masonry triplet can be estimated. For example, for a DGB masonry, it is given by

$$P_3 = \tau A_c + \sigma_c dw + \tau(A_c - 2dw), \tag{5.7}$$

$$= 2\tau A_c + (\sigma_c - 2\tau)dw. \tag{5.8}$$

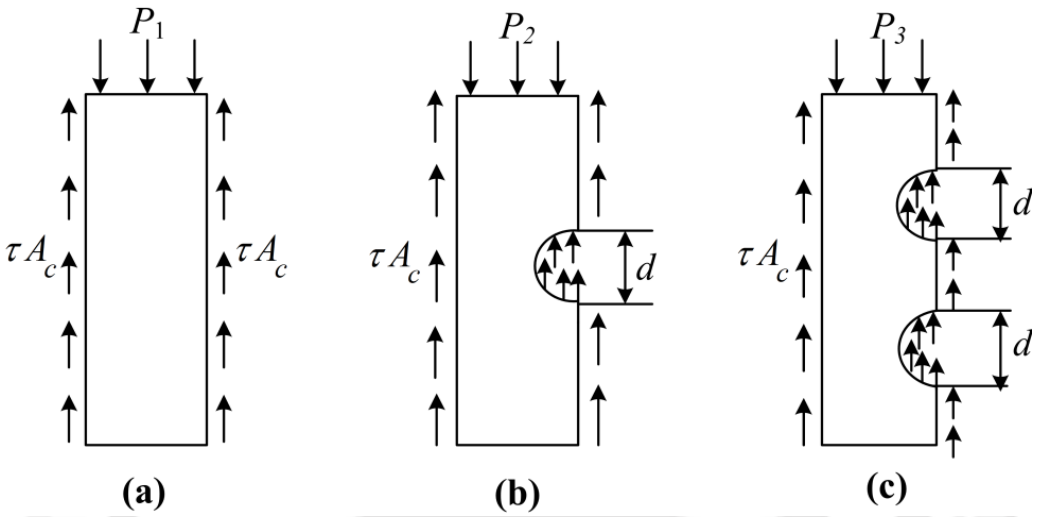

Figure 5.7 The free body diagram of the middle block under shear loading for (a) PB, (b) SGB and (c) DGB masonry triplet

In general, there are a lot of statistical variation in the experiments. It is preferable to find out the upper and lower estimates of load carrying capacities along with most likely estimates. Most likely estimates can be obtained by putting average experimental data in Eqs. 5.1–5.8. For upper and lower estimates, the method of interval arithmatic can be used, in which all the varaibles are treated as interval numbers. Interval arithmetic is a well-established discipline of mathematics and the procedure will be clear in Results and Discussion section.

5.5 Hypothesis Testing

A hypothesis test or confirmatory data analysis is a technique to obtain the statistical inferences of experimental data. It is a method or practice of testing the validity of a null hypothesis. The null hypothesis is a statement about a single population characteristics usually having a specific value (Dixit and Dixit 2008).The null hypothesis is rejected only if its probability of its being true falls below a predetermined threshold. In this work, the null

hypothesis is that the population means of two measurable quantities do not differ. Student's t-test is employed to assess the significance level of null hypothesis. Significance level is the probability by which a hypothesis gets rejected even if it is true. The hypothesis test has been carried out to check the significanct difference of the obtained experimental results. Let $\bar{x}$and $\bar{y}$ are the means of two quantities, then the following *t*-value is calculated:

$$t = \frac{\bar{x} - \bar{y}}{s\sqrt{1/n_1 + 1/n_2}}, \tag{5.9}$$

where

$$s = \sqrt{\frac{(n_1 - 1)s_1^2 + (n_2 - 1)s_2^2}{n_1 + n_2 - 2}}, \tag{5.10}$$

where $s_1$and s_2 are the standard deviations of two quantities with sample sizes of n_1 and n_2, respectively. The *t*-value is compared with t_α-value, obtained from the statistical table corresponding to the significance level (α). In this work, the hypothesis test is employed at 0.05 and 0.01 significance levels. If $|t|<t_\alpha$, the observed means have no significant difference, while if $|t|>t_\alpha$ the observed means have significant difference. In this study, a test of hypothesis has been employed to assess the significance level of experimental results for compressive strength of blocks as well as for the shear bond and compressive strength of AAC masonry.

5.6 Results and Discussion

The results of compressive load carrying capacity of blocks, shear load carrying capacity of the masonry triplet and the compressive load carrying capacity of the masonry prism are discussed. The stress-strain behavior of AAC block and its masonry under compression load is discussed. Subsequently, the hypothesis testing for the significant differences in the experimental results is presented.

5.6.1 Compressive load carrying capacity of AAC blocks

The experimental results of load carrying capacity of AAC blocks were used to validate the developed simplified models. The compressive load carrying capacity of PB and SGB were used to predict the load carrying capacity of DGB. Using average P_{PB} = 62.04 kN (from experiments), l= 220 mm and w = 120 mm in Eq. 5.1, the average compressive strength of PB block (σ_b) was found to be 2.35 MPa. Again, using average P_{SGB} = 64.42 kN (from

experiments) and σ_b = 2.35 MPa in Eq. 5.2, the average compressive strength of the mortar (σ_m) was found to be 3.01 MPa. Further, using σ_b = 2.35 MPa and σ_m = 3.01 MPa in Eq. 5.3, the average load carrying capacity of DGB block was estimated to be 66.79 kN against the experimental result of 70.22 kN. The result of average load carrying capacity obtained from the experiments has a good agreement (5.14% error) with the developed analytical model. Thus, it is possible to carry out reasonable prediction for DGB based on tests conducted on PB and SGB.

The AAC block with double groove has shown the highest average compressive load carrying capacity, while the plain AAC block has shown the least. The typical stress-strain responses of three specimens from each type of blocks are depicted in Figure 5.8. During the test, the cracks initiated from the bottom portion of the block. After reaching the peak compressive load, the load started decreasing suddenly due to crushing failure of the blocks, which indicates highly brittle nature of the AAC material after the peak load. The results of compressive load carrying capacity of the AAC blocks and the corresponding compressive strengths are presented in Table 5.1. The obtained compressive strength of PB blocks has good agreement (relative difference 10%) with the results of Mallikarjuna (2017) who reported the average compressive strength of 2.61 MPa, tested on 12 cubic specimens of side 150 mm extracted from bottom, middle and top portion of the AAC block.

Table 5.1 The compressive strength test results of AAC block

AAC block type	**Load carrying capacity (kN)**	**Compressive strength (MPa)**	**Failure strain**
PB	62.04 [12.52][a]	2.35 [12.52]	0.109 [48.50]
SGB	64.42 [27.40]	2.44 [27.40]	0.096 [18.90]
DGB	70.22 [06.60]	2.66 [06.60]	0.105 [26.30]

[a]Value in parenthesis represents the coefficient of variation in percentage.

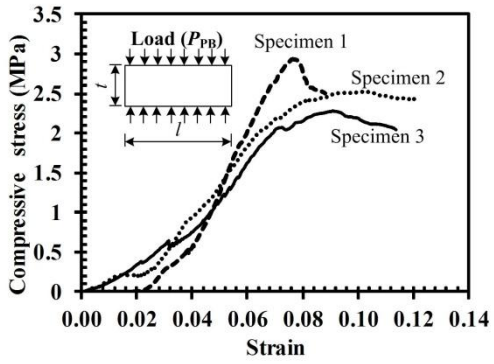

(a)

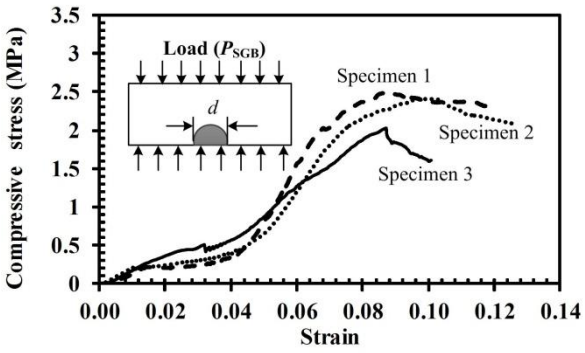

(b)

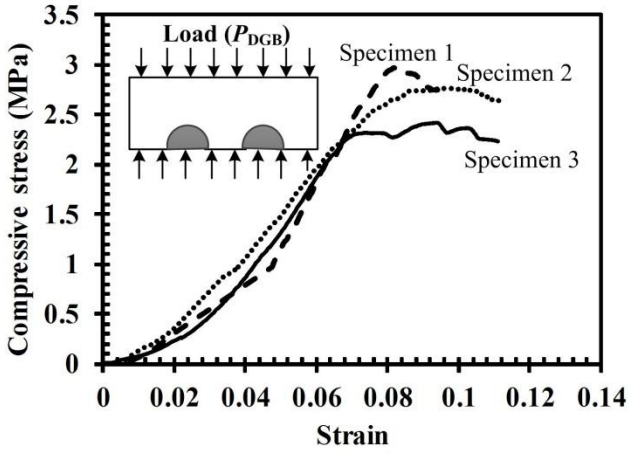

(c)

Figure 5.8 Stress-strain relationship under compressive load for (a) PB, (b) SGB and (c) DGB blocks

The lower and upper estimates of compressive load carrying capacity of the blocks were evaluated by applying the interval arithmetic in the simplified models. First, the lower and upper estimates of load carrying capacity of PB blocks were observed from the experiments. The entire experimental data is provided in Appendix E. The lower and upper estimates of the compressive strength of the PB blocks (from Eq. 5.1) are given by

$$\sigma_{\text{bmin}} = \frac{(P_{\text{PB}})_{\text{min}}}{lw}, \tag{5.11}$$

$$\sigma_{\text{bmax}} = \frac{(P_{\text{PB}})_{\text{max}}}{lw}, \tag{5.12}$$

where $(P_{PB})_{min}$ and $(P_{PB})_{max}$ are the lower and upper estimates of load carrying capacity of PB blocks, respectively. The σ_{bmin} andσ_{bmax} calculated using Eqs. 5.11 and 5.12 were 2.11 MPa and 2.93 MPa, respectively. The experimental results of $(P_{SGB})_{max}$= 100.58 kN, $(P_{SGB})_{min}$ = 44.10 kN, $(\sigma_b)_{max}$ = 2.93 MPa and $(\sigma_b)_{min}$ = 2.11 MPa were used to compute the lower and upper estimates of mortar compressive strength. (The $(P_{SGB})_{min}$and $(P_{SGB})_{max}$ are the lower and upper estimates of compressive load carrying capacity of SGB blocks.) The lower and upper estimates of the mortar compressive strength (from Eq. 5.2) are given by

$$(\sigma_m)_{min} = \frac{(P_{SGB})_{min}}{dw} - \sigma_{bmax}\left\{\frac{l}{d} - 1\right\}, \tag{5.13}$$

$$(\sigma_m)_{max} = \frac{(P_{SGB})_{max}}{dw} - \sigma_{bmin}\left\{\frac{l}{d} - 1\right\}. \tag{5.14}$$

The $(\sigma_m)_{min}$ and $(\sigma_m)_{max}$ calculated using Eqs.5.13 and 5.14 were found to be –6.31 MPa and 14.58 MPa, respectively. Since the lower estimate of mortar compressive strength cannot be negative, the $(\sigma_m)_{min}$has been assumed to be equal to the lower estimate of compressive strength of the PB block i.e., $(\sigma_m)_{min}$ = $(\sigma_b)_{min}$ = 2.11MPa. Further, $(\sigma_b)_{max}$ = 2.93 MPa, $(\sigma_b)_{min}$ = 2.11 MPa, $(\sigma_m)_{max}$= 14.58 MPa and $(\sigma_m)_{min}$= 2.11 MPa were used to compute the lower and upper estimates of load carrying capacity of DGB blocks. The lower and upper estimates of compressive load carrying capacity of DGB block (from Eq. 5.3) are given by

$$(P_{DGB})_{min} = \left\{\sigma_{bmin}(l-2d) + 2(\sigma_m)_{min}\, d\right\} w, \tag{5.15}$$

$$(P_{DGB})_{max} = \left\{\sigma_{bmax}(l-2d) + 2(\sigma_m)_{max}\, d\right\} w. \tag{5.16}$$

The $(P_{DGB})_{min}$ and $(P_{DGB})_{max}$ using Eqs. 5.15 and 5.16 were found to be 55.70 kN and 161.23 kN, respectively. The lower and upper values of compressive load carrying capacity of DGB block from the experiments are 63.88 kN and 78.40 kN, respectively. It is to be noted that estimated intervals are quite wider compared to experimental observations. It is because interval arithmetic provides a higher conservative estimate, because it considers the possibility of all favourable circumstances at one hand, and all unfavourable circumstances on the other hand. Moreover, experimental load carrying capacities are more inclined towards lower estimate, because it is difficult to achieve favourable conditions during the experiments.

5.6.2 Shear load carrying capacity of AAC masonry triplet

The experimental results of shear load carrying capacity of the masonry-triplet were used to validate the developed simplified models. The shear load carrying capacity of PB and SGB masonry triplets were used to predict the shear load carrying capacity of DGB masonry triplet. Using average P_1 = 2.44 kN (from experiments) and $A_c = w \times l$ in Eq. 4, the average shear bond strength of mortar with block (τ) was found to be 0.046 MPa. Again, using average P_2 = 3.39 kN (from experiments) and τ= 0.046 MPa in Eq. 5.6, the average compressive/crushing strength (σ_c) of the mortar was found to be 0.63 MPa. Here, P_2 is the average shear load carrying capacity of SGB masonry triplet. Further, using τ= 0.046 MPa and σ_c = 0.63 MPa in Eq. 5.8, the average shear load carrying capacity (P_3) of DGB masonry triplet was estimated to be 4.37 kN against the experimental result of 4.50 kN. The result of average shear load carrying capacity obtained from the experiments has good agreement (3% error) with the developed analytical model. Thus, it is possible to carry out reasonable prediction for shear load carrying capacity of DGB masonry based on tests conducted on PB and SGB masonries.

The masonry-triplet made of DGB has shown the highest average shear load carrying capacity, while the PB masonry-triplet has shown the least. Comapred to a PB masonry-triplet, the shear load carrying capacities of DGB and SGB masonry-triplets were greater by 45.60% and 28%, respectively. The shear load carrying capacity increased with increase in the number of grooves.Because of smooth surface and absence of any grip in the plane block, the shear load carrying capacity of PB masonry is the least as compared to the grooved AAC block masonry. The results of shear load carrying capacity and corresponding shear displacement of the masonry-triplet are shown in Table 5.2.

Table 5.2 The results of masonry-triplet test for shear failure load

Triplet type	Shear load carrying capacity (kN)	Shear displacement (mm)
PB	2.44 [14.30][a]	2.04 [43.70]
SGB	3.39 [11.90]	3.20 [23.80]
DGB	4.50 [24.89]	3.86 [26.48]

[a]Value in parenthesis represents coefficient of variation in percentage.

The lower and upper estimates of shear load carrying capacity of the AAC masonry triplet were evaluated by applying the interval arithmetic in the simplified models. Initially, the lower and upper estimates of shear load carrying capacity of PB block masonry triplet were obtained from the experiments. The lower and upper estimates of the shear bond strength of the PB masonry triplet (from Eq. 5.4) are given by

$$\tau_{\min} = \frac{P_{1\min}}{2A_c}, \tag{5.17}$$

$$\tau_{\max} = \frac{P_{1\max}}{2A_c}, \tag{5.18}$$

where $P_{1\min}$ and $P_{1\max}$ are the lower and upper estimates of shear load carrying capacity of the PB masonry triplet. The $\tau_{\min}$ and $\tau_{\max}$ calculated using Eqs. 5.17 and 5.18 were 0.028 MPa and 0.051 MPa, respectively. The experimental results of $P_{2\max}$ = 4.13 kN, $P_{2\min}$ = 2.91 kN, $\tau_{\min}$= 0.028 MPa and $\tau_{\max}$ = 0.051 MPa were used to compute the lower and upper estimates of mortar crushing strength. The $P_{2\min}$ and $P_{2\max}$ are taken as the lower and upper estimates of shear load carrying capacity of SGB block masonry triplet. The lower and upper estimates of the mortar crushing strength (from Eq. 5.6) are given by

$$\sigma_{c\min} = \frac{P_{2\min} - \tau_{\max}\{2A - dw\}}{dw/2}, \tag{5.19}$$

$$\sigma_{c\max} = \frac{P_{2\max} - \tau_{\min}\{2A - dw\}}{dw/2}. \tag{5.20}$$

The $\sigma_{c\min}$ and $\sigma_{c\max}$ calculated using Eqs. 5.19 and 5.20 were found to be 0.22 MPa and 1.53 MPa, respectively. Finally, the lower and upper estimates of shear load carrying capacity of DGB masonry triplet (from Eq. 5.8) are given by

$$P_{3\min} = (2A - 2dw)\tau_{\min} + \sigma_{c\min} dw, \tag{5.21}$$

$$P_{3\max} = (2A - 2dw)\tau_{\max} + \sigma_{c\max} dw. \tag{5.22}$$

The $P_{3\min}$ and $P_{3\max}$ using Eqs. 5.21 and 5.22 were found to be 2.07 kN and 7.57 kN, respectively. The lower and upper values of shear load carrying capacity of DGB masonry triplet from the experiments are 2.88 kN and 6.20 kN, respectively.

For all types of masonry triplet, similar failure behavior was observed. The failure at the peak load was caused by perfect (adhesive) debonding of block-mortar interfaces. The failure/debonding of middle block-mortar interface was observed in 56% (5 out of 9)

specimens in case of PB masonry triplet. For the rest of specimens, the failure was observed as debonding of side (left or right) block-mortar interface. However, in case of SGB and DGB, the debonding of side (right or left) block-mortar interface was observed in 67% (12 out of 18) specimens, while debonding of middle block-mortar interface was observed for the rest of the specimens. The typical failure behavior of masonry triplet is shown in Figure 5.9.

(a) **(b)**

Figure 5.9 Failure behavior of AAC masonry triplet: (a) debonding of middle block-mortar interface and (b) debonding of side block-mortar interface

5.6.3 Compressive load carrying capacity of AAC masonry prism

The experimental results of load carrying capacity of AAC masonry prism were used to validate the developed simplified models. The compressive load carrying capacity of PB and SGB masonry prisms were used to predict the load carrying capacity of DGB masonry prism. Similar models have been employed for the masonry prism to predict the compressive load carrying capacity as well as its lower and upper estimates as that of developed for the AAC blocks in the previous Sections. The load carrying capacity of PB masonry prism is given by

$$P_{\mathrm{MPB}} = \sigma_{\mathrm{mb}} lw, \tag{5.23}$$

where σ_{mb} is the compressive strength of PB masonry prism. Using average P_{MPB} = 32.52 kN (from experiments) in Eq. 5.23, the average compressive strength of PB block masonry prism (σ_{mb}) was found to be 1.23 MPa. Again, using average P_{MSGB} = 33.79 kN (from experiments) and σ_{mb} = 1.23 MPa, the average compressive strength of the mortar (σ_{mm}) in the masonry prism is given by

$$P_{\mathrm{MSGB}} = \left\{\sigma_{\mathrm{mb}}(l-d) + \sigma_{\mathrm{mm}} d\right\} w, \tag{5.24}$$

The average compressive strength of the mortar in the masonry prism is found to be 1.60 MPa. Further, using σ_{mb} = 1.23 MPa and σ_{mm} = 1.60 MPa, the average compressive load carrying capacity of the DGB masonry prism is given by

$$P_{\mathrm{MDGB}} = \left\{\sigma_{\mathrm{b}}(l-2d) + \sigma_{\mathrm{mm}} 2d\right\} w. \tag{5.25}$$

The average compressive load carrying capacity of DGB masonry prism was estimated to be 35.13 kN against the experimental result of 36 kN. The result of average compressive load carrying capacity obtained from the experiments has a good agreement (2.5% error) with the developed analytical model, again verifying that tests on plain and single-groove cases can carryout predictions for double-groove cases.

The masonry prism with DGB has shown the highest average compressive load carrying capacity, while the PB masonry prism has shown the least. The percentage increase in the load carrying capacity of DGB and SGB masonry over PB masonry was found to be 9.6% and 4%, respectively. However, the increase is marginal. A huge difference in the compressive load carrying capacity of the individual blocks and the masonries has been found in the study (refer Tables 5.1 and 5.3). For instance, the compressive load carrying capacity of PB masonry prism is 32.52 kN, while the compressive load carrying capacity of PB block is 62.02 kN.Also, the compressive load carrying capacity of masonry prism was found to increase with increase in the shear load carrying capacity. The results of compressive load carrying capacity of the AAC blocks and the corresponding compressive strengths (in terms of load carrying capacity) are presented in Table 5.3.During the test, the small cracks initiated from the multiple portions of the masonry prism. For all the types of masonry prisms, after reaching its peak load, the load started decreasing suddenly and the small cracks grew to a multiple large vertical splitting cracks.

Table 5.3 The results of compressive strength test for AAC masonry

Masonry type	load carrying capacity (kN)	Compressive strength (MPa)	Failure strain
PB	32.52 [23.30][a]	1.23 [23.30]	0.008 [41.70]
SGB	33.79 [18.50]	1.28 [18.50]	0.017 [26.60]
DGB	36.00 [13.40]	1.36 [13.40]	0.015 [24.40]

[a]Value in parenthesis represents coefficient of variation in percentage.

The lower and upper estimates of compressive load carrying capacity of the masonries were evaluated by applying the interval arithmetic in the simplified models. Initially, the lower and upper estimates of load carrying capacity of PB masonry prism were achieved from the experiments. All the relevant experimental data are shown in Appendix E. The lower and upper estimates of the compressive strength of the PB masonry prism (from Eq. 5.23) are given by

$$\left(\sigma_{\mathrm{mb}}\right)_{\min} = \frac{\left(P_{\mathrm{MPB}}\right)_{\min}}{lw}, \tag{5.26}$$

$$\left(\sigma_{\mathrm{mb}}\right)_{\max} = \frac{\left(P_{\mathrm{MPB}}\right)_{\max}}{lw}, \tag{5.27}$$

where $(P_{\mathrm{MPB}})_{\min}$ and $(P_{\mathrm{MPB}})_{\max}$ are the lower and upper estimates of load carrying capacity of the PB masonry prism, respectively. The $(\sigma_{\mathrm{mb}})_{\min}$ and $(\sigma_{\mathrm{mb}})_{\max}$ calculated using Eqs. 5.26 and 5.27 were found to be 0.90 MPa and 1.76 MPa, respectively. The experimental results of $(P_{\mathrm{MSGB}})_{\max}$= 43.30 kN, $(P_{\mathrm{MSGB}})_{\min}$ = 25.08 kN, $(\sigma_{\mathrm{mb}})_{\max}$ = 1.76 MPa and $(\sigma_{\mathrm{mb}})_{\min}$ = 0.90 MPa were used to compute the lower and upper estimates of mortar compressive strength in the masonry. The $(P_{\mathrm{MSGB}})_{\min}$and $(P_{\mathrm{MSGB}})_{\max}$ are the lower and upper estimates of compressive load carrying capacity of SGB masonry prism. The lower and upper estimates of the mortar compressive strength (from Eq. 5.24) are given by

$$(\sigma_{\mathrm{mm}})_{\min} = \frac{\left(P_{\mathrm{MSGB}}\right)_{\min}}{dw} - \left(\sigma_{\mathrm{mb}}\right)_{\max}\left\{\frac{l}{d} - 1\right\}, \tag{5.28}$$

$$(\sigma_{\mathrm{mm}})_{\max} = \frac{\left(P_{\mathrm{MSGB}}\right)_{\max}}{dw} - \left(\sigma_{\mathrm{mb}}\right)_{\min}\left\{\frac{l}{d} - 1\right\}. \tag{5.29}$$

The $(\sigma_{\mathrm{mm}})_{\min}$ and $(\sigma_{\mathrm{mm}})_{\max}$ calculated using Eqs. 5.28 and 5.29 were found to be –4.50 MPa and 6.33 MPa, respectively. Since the lower estimate of mortar compressive strength cannot be negative, the $(\sigma_{\mathrm{mm}})_{\min}$has been assumed to be equal to the lower estimate of compressive strength of the PB masonry prism i.e., $(\sigma_{\mathrm{mm}})_{\min}$ = $(\sigma_{\mathrm{b}})_{\min}$ = 0.9 MPa. Further, $(\sigma_{\mathrm{mb}})_{\max}$ = 1.76 MPa, $(\sigma_{\mathrm{mb}})_{\min}$ = 0.9 MPa, $(\sigma_{\mathrm{mm}})_{\max}$= 6.33 MPa and $(\sigma_{\mathrm{mm}})_{\min}$= 0.9 MPa were used to compute the lower and upper estimates of compressive load carrying capacity of DGB masonry prism. The lower and upper estimates of compressive load carrying capacity of DGB masonry prism (from Eq. 5.25) are given by

$$\left(P_{\mathrm{MDGB}}\right)_{\min} = \left\{\left(\sigma_{\mathrm{mb}}\right)_{\min}(l-2d) + 2\left(\sigma_{\mathrm{mm}}\right)_{\min} d\right\} w, \tag{5.30}$$

$$\left(P_{\mathrm{MDGB}}\right)_{\max}=\left\{\left(\sigma_{\mathrm{mb}}\right)_{\max}(l-2d)+2\left(\sigma_{\mathrm{mm}}\right)_{\max}d\right\}w. \tag{5.31}$$

The $(P_{MDGB})_{min}$ and $(P_{MDGB})_{max}$ using Eqs. 5.30 and 5.31 were found to be 23.76 kN and 79.36 kN, respectively. The lower and upper estimates of compressive load carrying capacity of DGB block from the experiments are 31.15 kN and 44.08 kN, respectively. The typical stress-strain responses of three specimens from each type of blocks are depicted in Figure 5.9. For all types of masonry prism, similar failure behavior was observed. The failure at the peak load was caused by vertical splitting cracks. The typical failure behavior of different masonry prism is depicted in Figure 5.10.

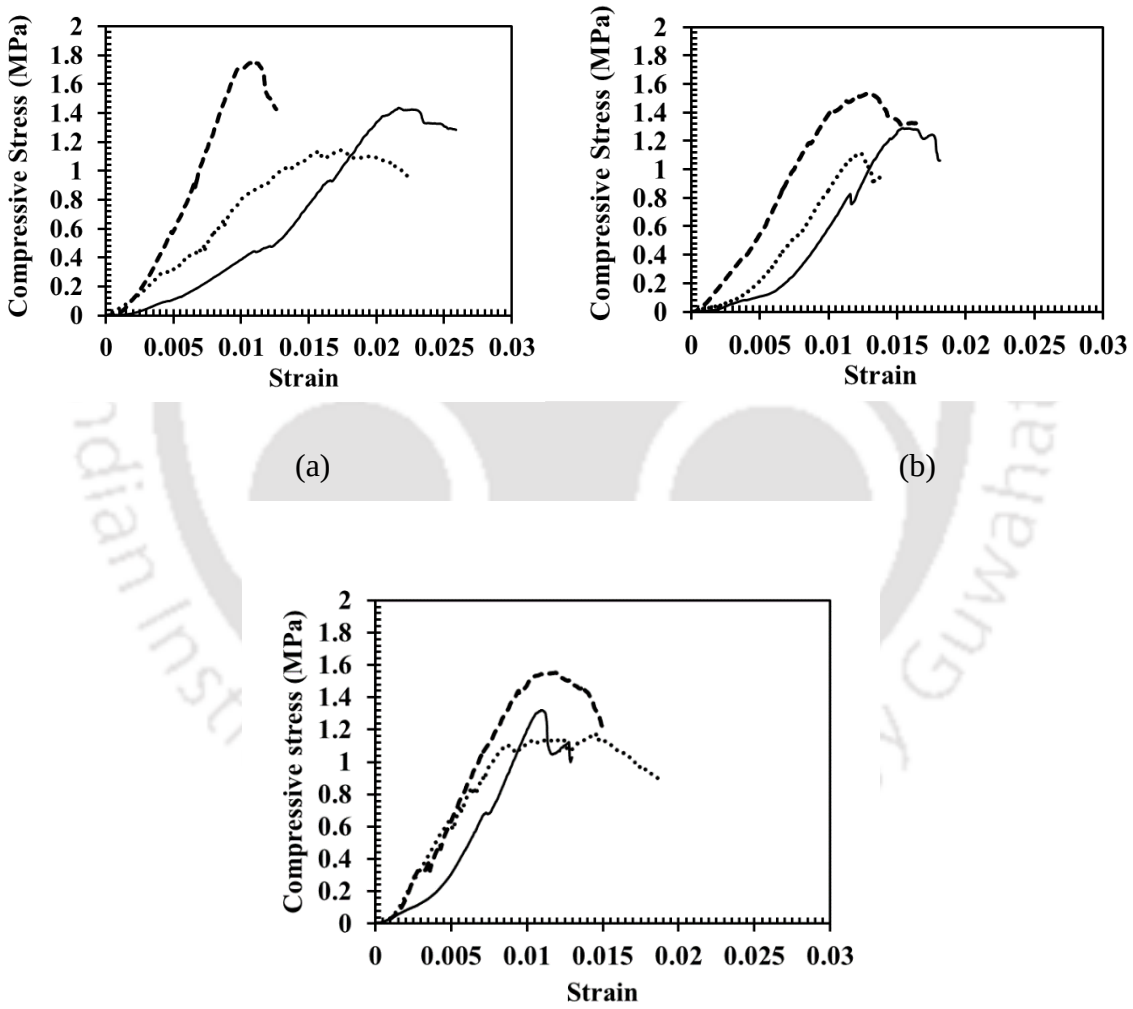

Figure 5.10 Stress-strain relationship of masonry in compression load: (a) PB masonry, (b) SGB masonry and (c) DGB masonry

(a) (b) (c)

Figure 5.11 Masonry prism specimens after the test: (a) PB masonry, (b) SGB masonry and (c) DGB masonry

5.6.4 Hypothesis testing of experimental results

The hypothesis testing, as discussed in Section 5.5, has been employed to assess the significance level of experimental results for compressive strength of blocks as well as for the shear bond and compressive strength of AAC masonry. The compressive strength results of PB, SGB and DGB blocks were compared for the significance level. For example, the mean compressive strength of PB and SGB blocks are $\bar{x}$= 2.35 MPa and $\bar{y}$= 2.44 MPa for six number of observations in each case (Table 5.1). Using s_1 = 0.29 and s_2 = 0.67 as the standard deviations corresponding to each of six (n_1= n_2 = 6) observations from the experiments, t-value obtained from Eq. 5.9 is 0.29. The t_α-value, corresponding to 10 (=n_1+n_2−2) degrees of freedom for 0.05 and 0.01 significance levels are 2.23 and 3.17, respectively. Since $|t|<t_\alpha$, the difference of compressive strength results of PB and SGB is not significant at both significance levels. Similarly, in the case of compressive strength results of SGB and DGB blocks, using $\bar{x}$= 2.44 MPa, $\bar{y}$= 2.66 MPa, s_1 = 0.67 and s_2 = 0.18 in Eq. 28, $|t|$ = 0.77. Hence, the difference of compressive strength results of SGB and DGB is not significant at both significance levels. However, in case of compressive strength results of PB and DGB block, considering $\bar{x}$= 2.35 MPa, $\bar{y}$= 2.66 MPa, s_1 = 0.29 and s_2 = 0.18 in Eq. 5.9, the modulus of t-value obtained from the t-test is 3.34. Since $|t|>t_\alpha$, the difference of compressive strength results of PB and DGB is significant at both 0.05 and 0.01 significance levels.

The shear load carrying capacity of PB, SGB and DGB masonry triplet were compared for the significance level. For example, the mean shear load carrying capacity of PB and SGB masonry triplet are $\bar{x}$= 2.44 kN and $\bar{y}$= 3.40 kN for nine number of observations in each case. Using s_1 = 0.35 and s_2 = 0.37 as the standard deviation corresponding to each of nine (n_1= n_2 = 9) observations, t-value obtained from Eq. 5.9 is 5.673. The t_α-values, corresponding to the (n_1+n_2–2=16) degree of freedom for 0.05 and 0.01 significance level are 2.12 and 2.92, respectively. Since $|t|<t_\alpha$, the difference of compressive strength results of PB and SGB masory triplet is significant at both the significance levels. Similarly, in case of shear load carrying capacity of SGB and DGB masoney triplets, using $\bar{x}$= 2.44 kN, $\bar{y}$= 3.40 kN, s_1 = 0.35 and s_2 = 0.37 in Eq. 5.9, $|t|$ = 2.82. Since $|t|>t_\alpha$ for 0.05 significance level, the difference in the shear load carrying capacity is significant. However, the difference is insignificant for 0.01 significance level because $|t|<t_\alpha$. Also, the difference in shear load carrying capacity for PB and DGB masonry triplet, considering $\bar{x}$= 2.44 kN, $\bar{y}$= 4.50 kN, s_1 = 0.37 and s_2 = 1.11 in Eqs. 5.9 and 5.10, $|t|$ = 5.35. Since $|t|>t_\alpha$ at both the significance levels, the difference in the shear load carrying capacity of PB and DGB masonry triplet is significant.

The compressive strength results of PB, SGB and DGB masonry prisms were also compared. For example, the mean compressive strengths of PB and SGB masonry prism are $\bar{x}$= 1.23 MPa and $\bar{y}$= 1.28 MPa for six number of observations in each case. Using s_1 = 0.30 and s_2 = 0.24 as the standard deviation corresponding to each of six (n_1= n_2 = 6) observations, t-value obtained from Eq. 5.9 is 0.32. The t_α-value, corresponding to the (n_1+n_2–2=10) degree of freedom for 0.05 and 0.01 significance level is 2.23 and 3.17, respectively. Since $|t|<t_\alpha$, the difference of compressive strength results of PB and SGB masonry prism is not significant at both significance levels. Similarly, in case of compressive strength results of SGB and DGB masonry prism, considering $\bar{x}$= 1.23 MPa, $\bar{y}$= 1.28 MPa, s_1 = 0.30 and s_2 = 0.24 in Eqs. 5.9 and 5.10, $|t|$ = 0.66. Hence, the difference of compressive strength results of SGB and DGB masonry prism is insignificant at both significance levels. Similarly, in case of compressive strength results of PB and DGB masonry prism, using $\bar{x}$= 1.23 MPa, $\bar{y}$= 1.36 MPa, s_1 = 0.29 and s_2 = 0.18 in Eq. 5.9, the t-value obtained from the t-test is 0.95. Since $|t|<t_\alpha$, the difference of compressive strength results of PB and DGB masonry prism is insignificant at 0.05 as well as 0.01 significance levels. The inference from hypothesis testing of ACC blocks and masonries are also depicted in Table 5.4

Table 5.4 Inference from hypothesis testing of ACC blocks and masonries

Comparison	Sample size	Sample means	Sample standard deviations	*t*-value	Inference
Compressive strengths of PB and SGB	6	2.35 and 2.44 MPa	0.29 and 0.67 MPa	0.29	Insignificant difference at α=0.05 and 0.01
Compressive strengths of SGB and DGB	6	2.44 and 2.66 MPa	0.67 and 0.18 MPa	0.77	Insignificant difference at α=0.05 and 0.01
Compressive strengths of PB and DGB	6	2.35 and 2.66 MPa	0.29 and 0.18 MPa	3.34	Significant difference at α=0.05 and 0.01
Shear load carrying capacity of PB and SGB masonries	9	2.44 and 3.39 kN	0.35 and 0.37 kN	5.67	Significant difference at α=0.05 and 0.01
Shear load carrying capacity of SGB and DGB masonries	9	3.39 and 4.5 kN	0.37 and 1.1 kN	2.82	Significant difference at α=0.05 but not at α=0.01
Shear load carrying capacity of PB and DGB masonries	9	2.44 and 4.50 kN	0.35 and 1.1kN	5.53	Significant difference at α=0.05 and 0.01
Compressive strengths of PB and SGB masonries	6	1.23 and 1.28 MPa	0.30 and 0.24 MPa	0.32	Insignificant difference at α=0.05 and 0.01
Compressive strengths of SGB and DGB masonries	6	1.28 and 1.36 MPa	0.24 and 0.18 MPa	0.66	Insignificant difference at α=0.05 and 0.01
Compressive strengths of PB and DGB masonries	6	1.23 and 1.36 MPa	0.30 and 0.18 MPa	0.95	Insignificant difference at α=0.05 and 0.01

5.7 Conclusions

The compression and shear load carrying capacities of grooved AAC block masonries have been studied. The developed simplified models help to predict the load carrying capacity of double-groove AAC block/masonry based on the tests conducted on plain as well as single-groove blocks and masonries. There is a definite advantage in replacing the existing plain surface AAC blocks with grooved surface AAC blocks. The manufacturing of AAC blocks with grooves at the bed face is very simple and is easily implementable in the existing production setups of the industry. The major conclusions from the study are as follows:

- The AAC block with double-groove has shown the highest average compressive load carrying capacity, while the plain AAC block has shown the least. The compressive strength of double-groove block evaluated from the experiment has the close agreement (5% error) with that of developed analytical model (requiring the data from tests on plain and single-groove blocks).
- As per Student's t-test, the difference between the compressive strengths of PB and DGB is significant even at 0.01 significant level. There is no significant difference between the compressive strengths of PB and SGB as well as SGB and DGB.
- The DGB masonry triplet has shown the highest shear load carrying capacity, while the PB masonry triplet has shown the least.
- The shear load carrying capacity of DGB masonry triplet was 45.60% more than that of the PB masonry triplet. On the other hand, the percentage increase of shear load carrying cappacity of SGB masonry over PB masonry triplet is 28%. The shear load carrying capacity of DGB masonry triplet evaluated from the experiment has the close agreement (3% error) with that of developed analytical models.
- The difference of shear load carrying capacity results of PB and DGB masonries was significant as per Student's t-test. In the case of SGB and DGB masonry triplet, the difference was significant at a significance level of 0.05 but not at 0.01. This indicates a clear enhancement of the shear load carrying capcity of in DGB masonries over that of PB masonries. Difference between the shear load capacities of SGB and DGB masonries is somewhat uncertain due to large amount of statistical variation within the samples.
- The masonry with DGB block has shown the highest average compressive strength, while the PB masonry has shown the least.

- The percentage increase in compressive strengths of DGB and SGB masonries over PB masonry is found to be 9.6% and 4%, respectively. However, Student's t-test indicated insignificant difference among these compressive strengths. Thus, the findings of this work strongly support the enhancement of shear load carrying capacity of a masonry employing grooved AAC blocks; however, no strong claim can be made for the enhancement of compressive strength.

Chapter 6

Bond Strength of Autoclaved Aerated Concrete (AAC) Masonry using various Joint Materials

6.1 Introduction

The brick unit-mortar bond development is influenced by many factors. These include the surface roughness of masonry unit, unit initial rate of absorption, unit moisture content, sand grading, water retention of mortar, mortar consistency, mortar composition and the cleanliness of the bonding surfaces (Walker 1999). A number of investigations on the bond strength of masonry were carried out in the past. Groot (1993) reported the influence of surface texture on the brick-mortar bond development; the bricks with rough surface texture provided better bond strength than the bricks with smooth surface. Rao et al. (1996) studied the dependency of the flexural bond strength of masonry on frog size, mortar type and mortar composition. The major observations of this study are as follows:

1. The masonry unit with deeper and wider frog in brick units provided higher bond strength.
2. Composite mortars i.e., cement-soil mortar and cement-lime mortar can result better bond strength than pure cement mortar.
3. The masonry bond strength increases with the increase in the strength of cement mortar irrespective of brick type.

A number of researchers (Sarangapani et al. 2005, Reddy et al. 2007 and Reddy et al. 2008) tried various techniques to enhance the bond strength of clay brick and soil-cement block masonries. Some salient techniques are introduction of multiple frogs, altering the brick surface texture, and surface coating using epoxy resin or fresh cement slurry. The influence of bond strength on masonry compressive strength and the stress-strain relationship have been studied.

Autoclaved aerated concrete (AAC) blocks have been extensively used for the construction of load bearing masonries in India (especially in north-eastern part for the last 4–5 years). The AAC blocks are wire cut as per the industrial practice, which results in smooth surfaces. When the two AAC blocks with smooth surfaces are joined with ordinary

sand-cement mortar, bond strength is poor (Mallikarjuna 2017). High content of sand in the mortar is used as an inert material to increase the volume of mortar for economy. However, the presence of fine silica particle in the mortar can clog the surface pores of the brick and prevent it from effective mechanical interlocking, thus forming a weak bond (Lawrence and Page 1994).

The proper bond is formed by mechanical interlocking of hydrated products in the pores of brick surface. The hydrated products are influenced by the chemistry of mortar composition and the presence of moisture throughout the period of cement hydration. The transport of cementitious material along with water to the interface through capillary suction provides continuity of contact along the two materials (Sugo et al. 2001). For adequate bond strength, an optimum amount of cementitious material is required at the interface. Insufficient amount will lead to adhesive failures at interface, whilst the excessive amount will lower the cohesive or tensile strength of mortar layer adjacent to the interface. To ensure the sufficient amount of cementitious material at the interface in the present work, a fresh cement slurry coating on the block surface has been applied prior to the mortar laying to enhance the masonry bond strength.

A thick sand-cement mortar layer (10–18 mm) is used to assemble the masonries of all kinds of bricks. The masonry specimen preparation using 10–12 mm thick sand-cement mortar joint is the general practice in India (Sarangapani et al. 2005, Reddy et al. 2008 and Sigh and Munjal 2017). In the modern repair works and construction industries, the role of polymers is increasing day by day (Aggarwal et al. 2007). Polymers are either mixed in a cement–aggregate mix or used as a single binder. The composites prepared using polymer along with cement and aggregates are called polymer modified mortars (PMM). The incorporation of polymers (liquid resins, latexes, redispersible powders and water-soluble homopolymers or copolymers) greatly improves strength, resilience, adhesion, impermeability, chemical resistance and durability properties of mortars (Mirza et al. 2002).

A thin layer (2–4 mm) of polymer modified mortar (PMM) is predominantly used to assemble the AAC masonry nowadays. Thamboo et al. (2013) carried out the characterisation of concrete masonry using the thin polymer based mortar of thickness 2 mm. Several researchers have carried out the masonry strength test using thin polymer based mortar (Thamboo et al. 2013 and Thamboo and Dhanasekar 2015). Although the compressive strength of the masonry increases with decrease in the joint thickness (Sarangapani et al. 2005 and Ferretti et al. 2015), but the shear and flexural bond strengths are unaffected by

varying the joint thickness (Dhanashekar and Da 2009). The compressive strength of masonry tends to approach the compressive strength of block for very thin mortar joint. However, the present work is mainly focussed on studying the bond strength with various joint materials and does not study the effect of joint thickness.

Compared to studies on the bond strength of clay bricks and cement-soil blocks, very few studies are available in the case of AAC masonry. Recently, Mallikarjuna (2017) examined the shear and tensile bond strengths of AAC masonry using a thick sand-cement mortar joint. Ferretti et al. (2015) studied the compressive and flexural strengths of AAC masonry based on thin glue joints of thickness 0.5–1 mm. However, the effect of joint strength on the overall performance of AAC masonry was not explored.

In this present study, the tensile and shear bond strengths of AAC masonry have been evaluated using the ordinary thick sand-cement mortar and a thin polymer modified mortar. Further, the enhancement of bond strength using cement slurry coating is explored. The results obtained using various joint materials are compared. Failure patterns during the AAC masonry bond strength tests are also studied. Based on the cost estimation of various joint materials and bond strength analysis, an optimised mortar type is suggested. The remaining sections of this chapter are arranged as follows. Section 6.2 describes materials (AAC block and different joint materials) used in this study. Section 6.3 presents the testing methods and specimen preparation to determine the shear and tensile bond strengths of AAC masonry. Section 6.4 discusses the results obtained from the experiments. The mortar cost estimation for AAC wall is also discussed in Section 6.4. Section 6.5 concludes the chapter.

6.2 Materials used in the Study

The main objective of this study is to understand the behavior of block-mortar bond strength in masonry for various joint materials. In the case of ordinary sand-cement mortar, the different proportions of sand-cement by weight were used. Subsequently, the bond strengths of AAC masonry using a polymer modified mortar (PMM), and sand-cement mortars used on the cement-slurry coated blocks were evaluated. The methods of preparing samples are explained in the following subsections.

6.2.1 Autoclaved aerated concrete (AAC) blocks

AAC blocks were collected from a local industry (KD Infra, Guwahati, India) to prepare the specimens. These blocks were used for preparing 18 cubic specimens of 200 mm side for measuring dry density, moisture content and compressive strength as per IS 6441.

The cubes were cut from bottom (the mold base side), middle and top (open side of the mold) portions of six AAC blocks of size 600×200×200 mm^3.

The compressive strength of 18 cubic AAC specimens lay within a range of 1.59–2.76 MPa with a mean of 2.07 MPa (CV = 0.15). However, taking the average compressive strength of cubes of side 200 mm extracted at the top, middle and base for each of 6 blocks, the CV for the compressive strength is 0.05 only with the same mean of 2.07 MPa. The average failure strain of the 18 AAC cubic specimens was 0.013 with a CV of 0.31. Mallikarjuna (2017) had obtained an average compressive strength of 2.61 MPa based on the compression tests on 12 AAC cubic specimens of average dry density of 746 kg/m^3, taken from a different lot. Ferretti et al. (2014) reported a compressive strength of 2.43 MPa for AAC block specimens having average density of 550 kg/m^3. It is to be noted that there are significant deviations of the compressive strength from lot to lot as well as within the lot. The testing methodology may also influence the test results to some extent. In fact, one random unconditioned AAC block from the same industry provided an average compressive strength of 3.23 MPa. For the present study, typical stress-strain responses for 6 specimens (2 specimens each from bottom, middle and top portions of the block) in compression test are depicted in Figure 6.1.

The splitting tensile strength test of the block was performed following the ASTM C1006-07 on six AAC block specimens of size 200×110×75 mm^3. In this test, the load is applied along a line on the bed surface of the specimen using a bearing rod. The bearing rod was kept along the width (110 mm) direction of the specimen during the test. The compressive load applied on the block produces tensile stress in the block. The splitting tensile strength of the blocks lay in the range of 0.19–0.32 MPa with an average of 0.26 MPa and CV of 0.20.

The AAC blocks are produced in different sizes with the maximum size of 625×200×300 mm^3. Testing a large sized block may not be feasible in some laboratories due to limitation of testing equipment. Conventionally, the triplet and cross-couplet masonry specimens are prepared with the standard clay bricks of size up to 220×110×70 mm^3. For better comparison with clay bricks, researchers prefer to use almost the same sized bricks to test the AAC blocks. For example, Ferretti et al. (2015) carried out the mechanical characterization of AAC masonry using the AAC unit of size 250×100×50 mm^3. Hence, in the work, it has been preferred to employ the non-standard AAC blocks of 200×100×70 mm^3 size for the masonry preparation.

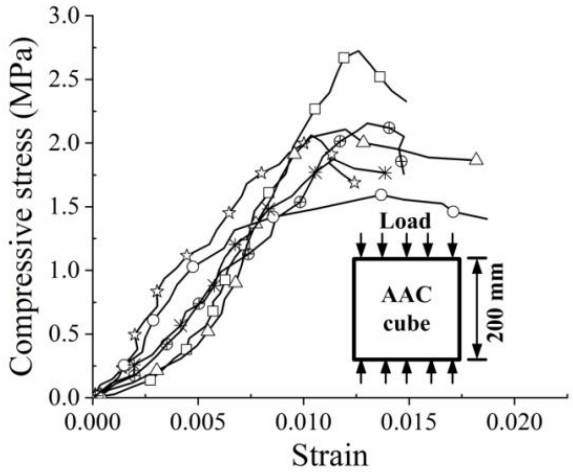

Figure 6.1 Stress-strain responses of AAC cubes during the compression test

6.2.2 Joint materials

Two types of joint materials (mortars) viz., sand-cement mortar (SCM) and polymer modified mortar (PMM) were used to determine the bond strength of AAC masonries. Three different types of sand-cement mortar combinations used in this study are as follows:

- SCM1 (strong mortar): cement to sand ratio by weight = 1/2
- SCM2 (medium strength mortar): cement to sand ratio by weight = 1/4
- SCM3 (weak mortar): cement to sand ratio by weight =1/6

A total of 18 mortar cube specimens with 70.6 mm edge length, 6 of each SCM1, SCM2 and SCM3 types were prepared. The Portland Pozzolana cement as a binder and local sand as a fine aggregate were used to prepare the mortar specimens. The cement was characterized by the compressive strength of 39.3 MPa, tested on three cubic specimens of size 70.6 mm as per the procedure available in IS 4031. The specimens were prepared by adding 0.33 kg water per kg of cement. The compression test was performed after curing the cement cube by immersing in water for 28 days. The sieve analysis was carried for the sand aggregate as per IS 2386. A total of 6 sieves were arranged in the descending order of size with the largest sieve on top. The sieve sizes were 4.75 mm, 2.36 mm, 1.18 mm, 0.6 mm, 0.3 mm and 0.15 mm. After placing the dry sand aggregate on the top sieve, the complete sieve stack was vibrated on a sieve shaker for 5 minutes. The relationship between the sieve size and the percentage passing by weight of sand aggregate is depicted in Figure 4.1. As obtained from the sieve analysis, most of the sand particles lay in the range of 0.3–0.6 mm. The fineness modulus of the sand was found to be 2.4, which corresponds to a fine sand aggregate. The

sand and cement were mixed in a dry condition for each types of sand-cement mortar, according to the required ratios by weight. To maintain a constant workable flow of 100%, the water-cement ratio of 58%, 70% and 91% was maintained for SCM1, SCM2 and SCM3, respectively. The compressive strength test of 70.6 mm cubes of these mortars was performed on a universal testing machine (UTM) of capacity 1000 kN after curing in water for 28 days and drying for 3 days. The sand-cement mortar specimen preparation and testing procedure were as per IS 2250.

The PMM mortar was prepared using sand, fly ash, cement and polymer additives. The composition was 66% fine sand, 23% cement, 9% fly ash, 1.5% thermoplastic polymers (vinyl acetates) and 0.5% methyl hydroxyl ethyl cellulose. The final PMM mortar is available in the market in fine powder form. The water to PMM powder ratio of 1:3 (by weight) was maintained during the specimen preparation of cubes of 50 mm size as per the manufacturer (KD Infra, Guwahati, India).

The compressive strength test of PMM mortar specimen was performed after the curing for 28 days in water and subsequent drying for 3 days. The stress and strain corresponding to the ultimate load was considered as the compressive strength and failure strain, respectively. The modulus of elasticity of the mortar was measured as the slope of the secant between 5% and 33% of the ultimate strength (Kaushik et al. 2007). The average compressive strength, average modulus of elasticity and average failure strains of the sand-cement mortars and PMM mortar based on six specimens are depicted in Table 6.1. The average compressive strength of the sand-cement mortar ranged from 9.40 MPa to 34.2 MPa as shown in Table 6.1, but the overall variation was from 7 MPa to 37 MPa. The compressive strength increases with the increase in cement content. The mortar SCM1 had the highest compressive strength of 37 MPa, while the least compressive strength of 7 MPa was observed in the case of SCM3 mortar. It is to be noted that the compressive strength of PMM mortar of 6 MPa is lesser than that of SCM3 mortar, the weakest sand-cement mortar in this study. The mortar bed joint thickness of 12 mm and 3 mm was maintained during the masonry specimen preparation using sand-cement and PMM mortar, respectively.

In order to enhance the masonry bond strength, the cement-water slurry (1 cement: 1 water, by weight) coating was applied on both the bed faces of the block. The thickness of the coating was maintained in the range of 0.6–0.8 mm. The sand cement mortar layer of thickness 12 mm was placed on the coated block surface during the specimen preparations. The coating was applied at all the block-mortar interfaces of the specimens. The different

combinations of cement slurry coatings with SCM1, SCM2 and SCM3 mortars were designated as CSCM1, CSCM2 and CSCM3, respectively.

Table 6.1 Compressive strength test results for mortars

Mortar designation	Average Compressive strength (MPa)	Modulus of elasticity (MPa)	Failure strain
SCM1	34.20 [0.09][a]	1913 [0.33]	0.021 [0.32]
SCM2	18.30 [0.10]	1046 [0.48]	0.020 [0.40]
SCM3	9.40 [0.20]	713 [0.28]	0.015 [0.43]
PMM	6.34 [0.08]	265 [0.18]	0.038 [0.23]

[a] Values in [ ] bracket indicate the coefficient of variation

6.3 Specimen Preparation and Testing Methods

The shear and tensile bond strengths of the masonry were tested on the triplet and cross-couplet masonry specimens. A dry AAC block can absorb most of the water content in mortar and retards the hydration process between cement and water. As a consequence, the weak and improper bonds are formed in the masonry. To alleviate this problem, prior to the preparation of AAC masonry specimens, the blocks were immersed in the water tub for 24 hours before laying, to ensure that the moisture content in the mortar did not get absorbed. Moreover, it simulated the prevailing condition in a high rainfall place like Assam, where most of the times, loose AAC blocks are already drenched with rain-water. Of course, after the construction of the wall, it is usually plastered and thus provides protection from heavy rain. All the triplets and cross couplet specimens were cured under moist condition using wet burlaps for 28 days. A total of 84 (42 triplet and 42 cross-couplet) masonry specimens were tested for the bond strength. A total of 6 specimens using each types of joining materials were tested for both the bond strengths. Three block units and two mortar layers were used to prepare the triplet specimens.

A uniform vertical (without pre-compression) load was applied on the middle block using 20 mm thick mild steel plate and two rollers of 12 mm diameter, as illustrated in Figure 3.7. In order to reduce the eccentricity, the two side blocks were supported by mild steel roller close to the mortar joint. The displacement controlled loading rate of 0.01 mm/s, corresponding to a strain rate of the order of 5×10^{-5} s^{-1}, was applied in a 250 kN servo

hydraulic actuator. A photograph and front view drawing of the triplet test setup are shown in Figure 3.7.

The shear bond strength was calculated corresponding to the peak load during the test. Loads coming on the block and the free body diagram of the middle block are shown in Figure 6.2. Using the free body diagram, the mathematical expression for shear bond strength is obtained as

$$\tau = \left(\frac{P_{\max}}{2A} \right), \tag{6.1}$$

where P_{max} is the peak shear load recorded at failure and A is the contact or bonding area of the joint.

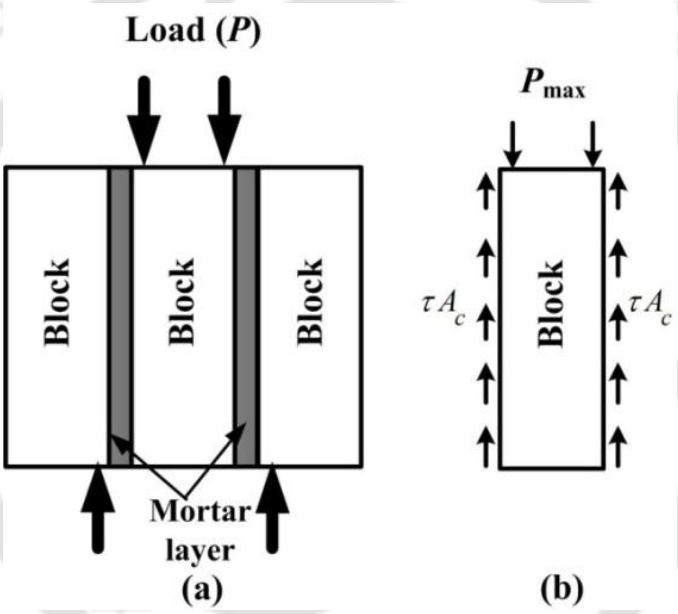

Figure 6.2 Schematic representation of a triplet test (a) the loading condition and (b) free body diagram of middle block

The tensile bond strength of block-mortar interface was determined using a cross-couplet test. The cross-couplet specimens were prepared using two block units and one mortar layer. Similar to the triplet specimens, equal number of cross-couplet specimens using all types of sand-cement mortars, PMM mortar and combination of sand-cement mortar with cement slurry coating were tested. Figure 3.8 shows a schematic view of the cross-couplet test setup. The specimen preparation and the testing procedure were carried as per the guideline available in ASTM C 952 (ASTM 1991).

During the test, the displacement controlled loading rate of 0.01 mm/s was adopted using a 250 kN servo hydraulic actuator, which provides a strain rate of order of 10^{-3} s^{-1}. The tensile bond strength was calculated corresponding to the peak load at the failure divided by block-mortar interface contact area. It is given by

$$\tau_t = \frac{(P_t)_{max}}{A}, \tag{6.2}$$

where $(P_t)_{max}$ is the peak load recorded at failure and A is the contact area of the joint.

6.4 Results and Discussion

The results of shear bond strength and tensile bond strength using different joining materials are presented and compared. However, construction industry looks for not only the strength but also economy. Cost plays a very crucial role in the acceptance of a new technology and a new material. the cost estimation results for mortar of various joining materials for an AAC wall are presented in Section 6.5.

6.4.1 Shear bond strength of the masonry triplet

Table 6.2 lists the triplet test results. The maximum, minimum and the mean value of shear bond strength using different joining materials are presented. The shear bond strength for all types of mortars lay in the range of 0.02– 0.43 MPa. The shear bond strength of AAC masonry using the ordinary sand-cement mortar was very less and lay in the range of 0.02–0.09 MPa. Comparatively higher shear bond strength in the range of 0.12–0.43 MPa was found using the mortar CSCM1, CSCM2, CSCM3 and PMM. As can be seen from Table 2, for all cement-coated specimens, shear bond strength was of the same order. To be precise, the relative difference in the shear bond strength for the mortar CSCM1 with CSCM2 and CSCM3 was 16% and 24%, respectively. Of course, the lowest shear bond strength of the CSCM3 is much less than that of CSCM1 and CSCM2. On the other hand, the significant difference of shear bond strength was observed using various ordinary sand-cement mortars; the relative difference in the shear bond strength for the mortar SCM1 with SCM2 and SCM3 was 43% and 57%, respectively. In general, the bond strength of masonry increases with the increase in the cement contents in a sand-cement mortar.

Since the bed face of AAC block is smooth unlike the clay brick, the shear bond strength using an ordinary sand-cement mortar is low (Sarangapani et al. 2005 and Singh and Munjal 2017). The use of cement slurry coating increases the shear bond strength significantly. As discussed in Section 6.1, an insufficient amount of cement will lead to the adhesive failures at the interface. The adhesive failure is the interfacial bond failure between the adherend (block) and adhesive (mortar).The shear bond strength with CSCM3 is significantly higher than that with ordinary sand-cement mortar. PMM also has almost same bond strength as CSCM3, it can sustain larger strain before failure.

A number of failure patterns of the triplet specimen were observed during the test. As expected, the joint failure in shear was sudden and brittle. The typical load-displacement curves obtained during the triplet test are depicted in Figure 6.3. Most of the triplet specimens exhibited the sliding failure at the block-mortar interface. The failure of the block-mortar interface using the triplet test can take place in any one of the following patterns:

1. Failure of block (Type A),
2. Failure of mortar (Type B),
3. Failure of block-mortar interface (Type C).

The failure patterns of the masonry triplets are shown in Figure 6.4, where the top views of the bed surface are depicted. The triplet failure of type A, was mostly found in the case of strong joint material i.e., for CSCM1, CSCM2 and PMM mortar (Figure 6.4 (a)). Here, the portion of block got sheared and stuck with the adjacent mortar layer. The failure of mortar (type B) was observed mostly in the specimens using CSCM3 mortar (Figure 6.4 (b)). Block-mortar interface failure (type C) was caused by the debonding of the block-mortar interface. This type of failure is predominantly observed in the weak joints i.e., for triplet specimens using ordinary sand-cement mortar i.e., SCM1, SCM2 and SCM3 (Figure 6.4 (c)) and occasionally in specimens using CSCM3.

Table 6.2 The triplet test results of AAC masonry (average of 6 specimens)

Joint material types	Mean failure load (kN)	Shear bond strength (MPa)			Triplet failure type
		Mean value	Range		
			Minimum	Maximum	
SCM1	2.72 [0.16]	0.07 [0.16]	0.06	0.09	In 6 triplets, type C
SCM2	1.70 [0.36]	0.04 [0.36]	0.02	0.07	In 6 triplets, type C
SCM3	1.02 [0.31]	0.03 [0.31]	0.02	0.04	In 6 triplets, type C
CSCM1	10.1 [0.37]	0.25 [0.37]	0.20	0.43	In 5 triplets, type A and in 1 triplet, type C
CSCM2	8.23 [0.10]	0.21 [0.10]	0.18	0.26	In 3 triplets, type A and in 3 triplets, type C
CSCM3	7.74 [0.20]	0.19 [0.20]	0.13	0.25	In 4 triplets, type B and in 2 triplets, type C
PMM	7.63 [0.22]	0.19 [0.22]	0.12	0.25	In 4 triplets, type A and in 2 triplets, type C

[a]Values in [ ] bracket indicate the coefficient of variation

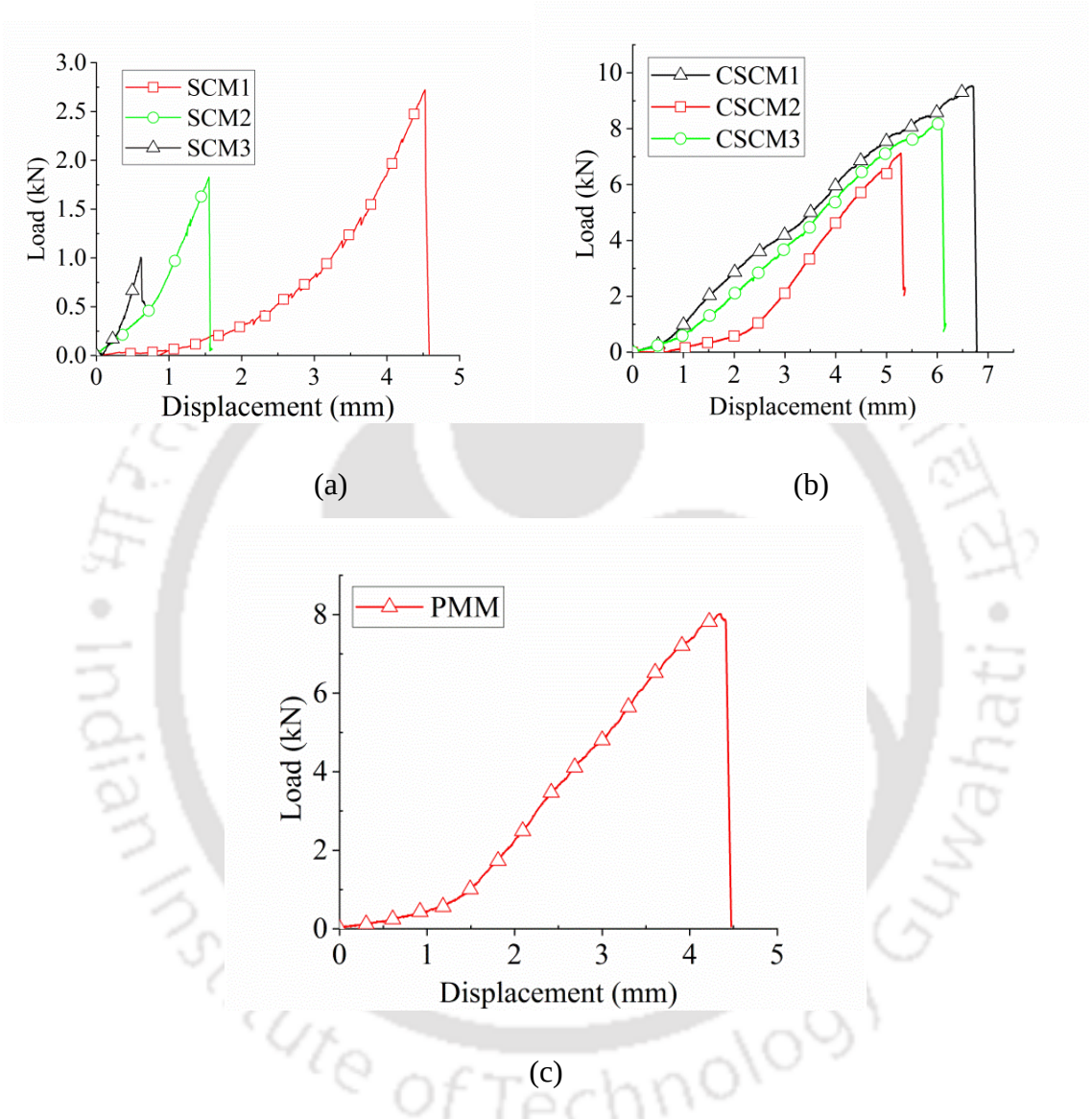

Figure 6.3 The load-displacement relationship during the triplet test for (a) sand-cement mortar, (b) combination of slurry coating with mortar and (c) polymer modified mortar

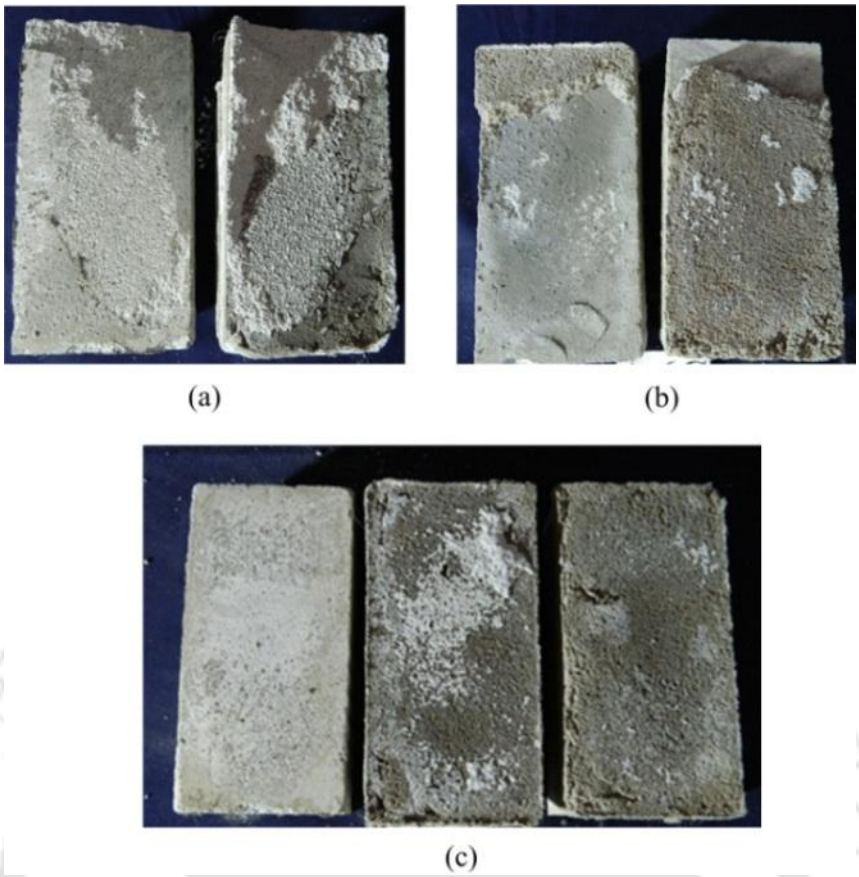

Figure 6.4 Different failure patterns of AAC triplet specimens: (a) type A, (b) type B and (c) type C

6.4.2 Tensile bond strength of the cross-couplet specimen

Table 6.3 presents the cross-couplet test results in the form of the maximum, minimum and mean values of tensile bond strength. The tensile bond strength using all types of mortars lay in the range of 0.01– 0.28 MPa. The typical load-displacement curve obtained during the test is shown in Figure 6.5. The tensile bond strength of the cross-couplet using the ordinary sand-cement mortar i.e., SCM2, SCM3 was very less and lay in the range of 0.01–0.07 MPa only. However, a significant increase in the tensile bond strength ranging from 0.16 MPa to 0.19 MPa was found in case of SCM1. Comparatively higher tensile bond strength in the range of 0.11–0.28 MPa was obtained using CSCM1, CSCM2, CSCM3 and PMM. As can be seen from Table 6.3, the differences in the tensile bond strength results using the cement slurry coating is very marginal, irrespective of the types of mortar used. On the other hand, a huge difference in the tensile bond strength among the different sand-cement mortars was observed.

The relative difference in the tensile bond strength for the mortar SCM1 with SCM2 and SCM3 was 67% and 88%, respectively; this much difference was not observed in the case of shear bond strength. The chemical bonding between cement and brick plays a major role in shear bond strength. Addition of extra cement in the mortar may not enhance the chemical reaction in that proportion. On the other hand, tensile bond strength increases with the addition of cement, largely following the rule of mixture.

The use of combination of cement slurry coating along with the ordinary mortar provides the sufficient amount of cementitious material for hydration at the block-mortar interface and hence, increases the bond strength. The failure patterns of the cross-couplet were observed during the test. The joint failure in tension was sudden and brittle. The failure of the block-mortar interface can take place in any of the following patterns:

1. Complete block-mortar interface failure (Type I),
2. Partial block-mortar interface failure (Type II),
3. Partial tensile failure of the block (Type III),
4. Complete tensile failure of block (Type IV).

The failure patterns during the tensile bond strength test of cross-couplet specimens are shown in Figure 6.6. The complete block-mortar interface failure (Type I), was mainly observed in the case of weak joint strength i.e., for SCM2 and SCM3 as shown in Figure 6.6 (a). This type of failure occurs due to weak interfacial bond strength as compared to the tensile strength of block. Partial interface failure (Type II) was mainly observed using the CSCM3 mortar and in some cases in SCM1. In this type of failure, a portion of either block or mortar gets stuck to each other (Figure 6.6 (b)). Partial tensile failure of the block (Type III) was observed for relatively stronger joint strength and was found in most of the couplet specimens using strong joint materials. In this type of failure, the joint does not fail, instead a portion of the block gets stuck on to the interface due to the partial tensile failure of the block (Figure 6.6 (c)). However, in case of complete tensile failure of block (Type IV) the block completely failed in tension and the joint remained intact (Figure 6.6 (d)). Both types of failure occur when the bond strength of block-mortar interface exceeds the tensile strength of block. Since the tensile strength (measured based on the splitting tensile strength) of the AAC block ranges from 0.19 MPa to 0.32 MPa, the failure pattern of type (III) and type (IV) was observed mainly using the mortar PMM, CSCM1, CSCM2 and SCM1.

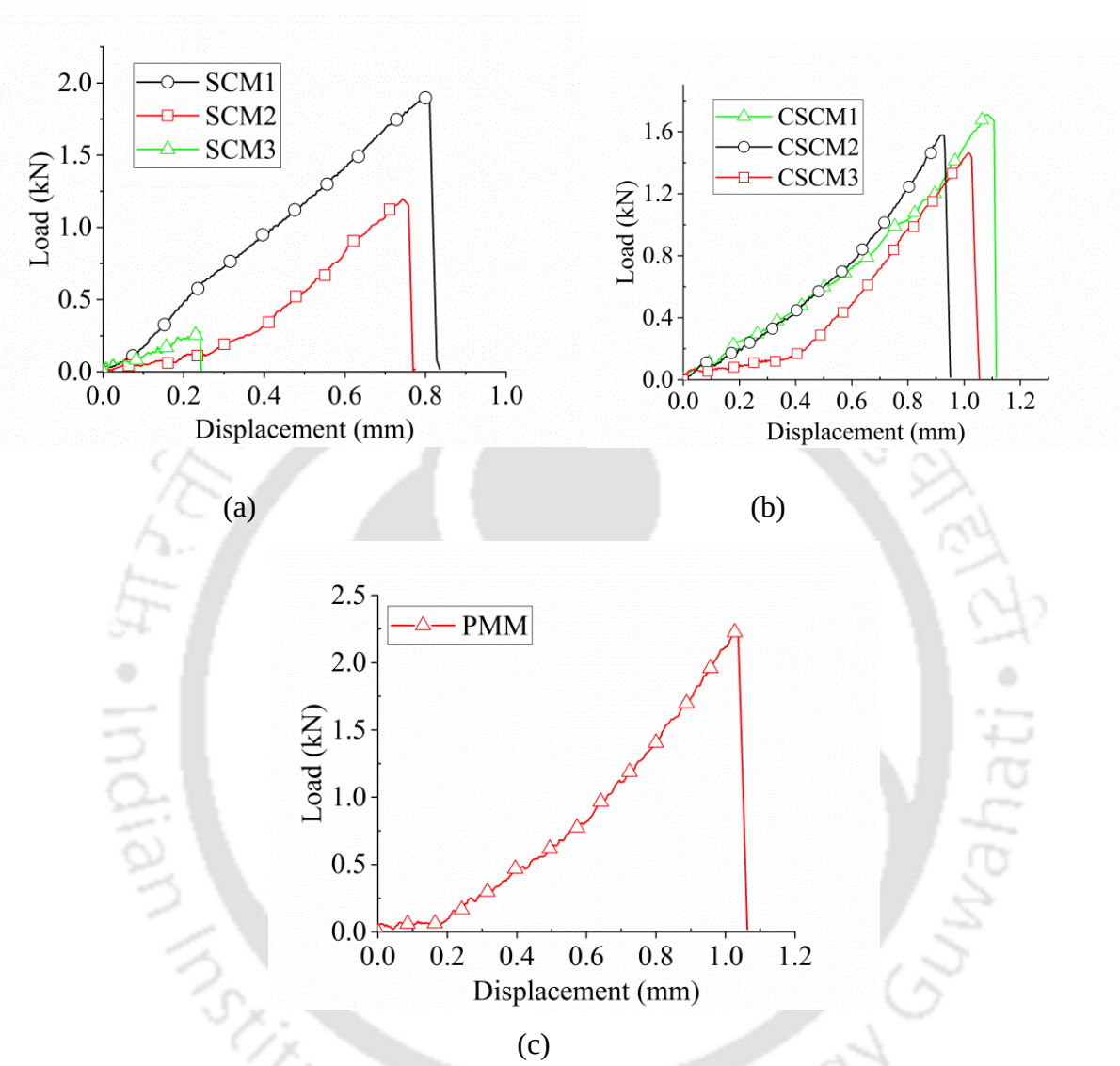

Figure 6.5 The load-displacement relationship during the cross-couplet test for (a) sand-cement mortar, (b) combination of slurry coating with mortar and (c) polymer modified mortar

Table 6.3 The cross-couplet test results of AAC masonry (average of 6 specimens)

Joint material types	Mean failure load (kN)	Tensile bond strength (MPa)			Cross-couplet failure type
		Mean	Range		
			Minimum	Maximum	
SCM1	1.75 [0.07]	0.18 [0.07]	0.16	0.19	In 5 couplets, type III and in 1 couplet, type IV
SCM2	0.56 [0.20]	0.06 [0.20]	0.05	0.07	In 4 couplets, type I and in 2 couplets, type II
SCM3	0.20 [0.47]	0.02 [0.47]	0.01	0.03	In 6 couplets, type I
CSCM1	1.90 [0.09]	0.19 [0.09]	0.18	0.22	In 6 couplets, type IV
CSCM2	1.70 [0.12]	0.17 [0.12]	0.15	0.21	In 4 couplets, type IV, in 2 couplets, type III
CSCM3	1.48 [0.17]	0.15 [0.17]	0.11	0.20	In 5 couplets, type II and in 1 couplet, type III
PMM	2.49 [0.16]	0.25 [0.16]	0.18	0.28	In 6 couplets, type IV

[a] Values in [ ] bracket indicate the coefficient of variation

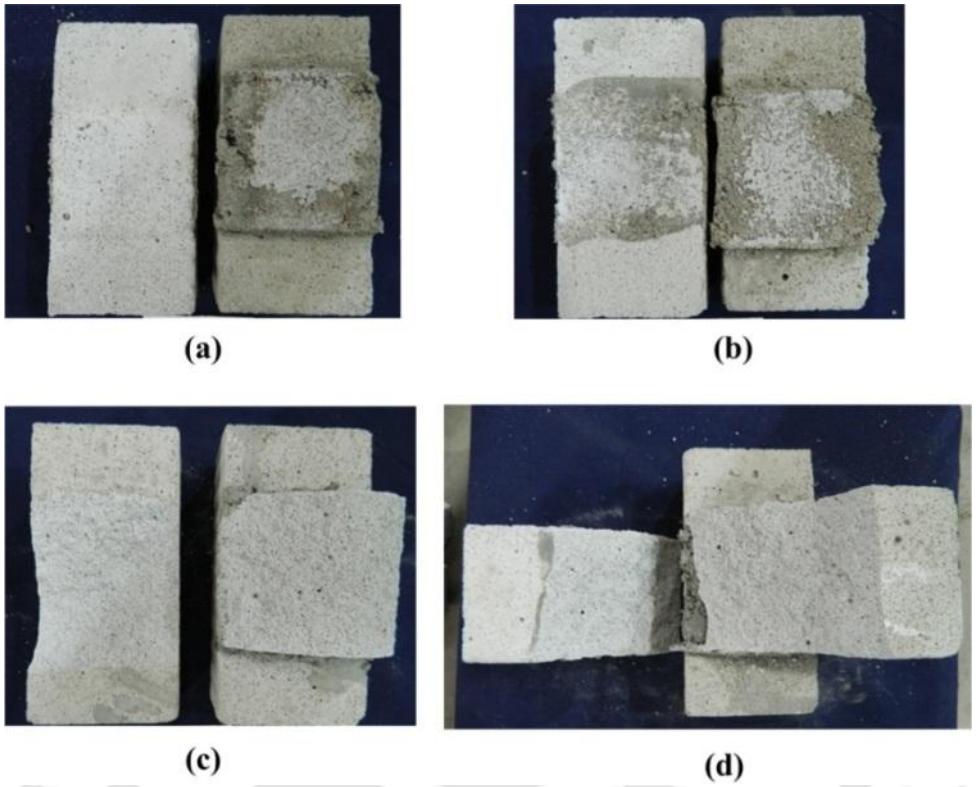

Figure 6.6 The different failure patterns of AAC cross-couplet specimens: (a) type I, (b) type II, (c) type III and (d) type IV

6.4.3 Comparison of observed bond strength of masonry employing various joining materials

As can be seen from Table 6.2 and Table 6.3, both shear and tensile bond strengths of the AAC masonry using the ordinary sand-cement mortar i.e., SCM2 and SCM3 are very less. Although the SCM1 mortar had a low shear bond strength, its tensile bond strength was significantly high. The bond strength (both tensile and shear) using polymer modified mortar (PMM) and the combination of slurry coating with mortar was found to be better as compared to the ordinary sand-cement mortars. During the bond strength test, the failure of the block instead of joint/interface failure was observed using the high strength mortar or mortar with rich cements content viz., CSCM1, CSCM2, PMM. However, the sufficient shear and tensile bond strengths with the joint failure were achieved using the mortar CSCM3.

Since the AAC block is a lightweight, porous and low density material, the use of mortar with high bonding strength is unwarranted. The bond strength increases abruptly by applying the cement slurry coating on the block during the masonry assemblage, irrespective of the mortar used. As evident from this study, good bond strength could be achieved using a combination of cement slurry coating with ordinary mortar of lean cement content.

6.4.4 Cost comparison

The cost incurred for the preparation and deployment of mortar used in AAC wall is estimated for the wall size of 1800×1000×200 mm^3. The detailed cost analysis is shown in Table 6.4. The wall considered has 3 blocks along length and 5 blocks along height and constitutes a total volume of 36×10^7 mm^3. A total of 15 AAC blocks of size 600×200×200 mm^3 and the 29 mortar joints (17 bed joints and 12 head joints) have been used for the wall assembly as shown in Figure 6.7. The volume occupied by the mortar layers in the wall system has been calculated by considering the bed joint and head joints separately. The bed area of the wall is considered to be 1800×200 mm^2.

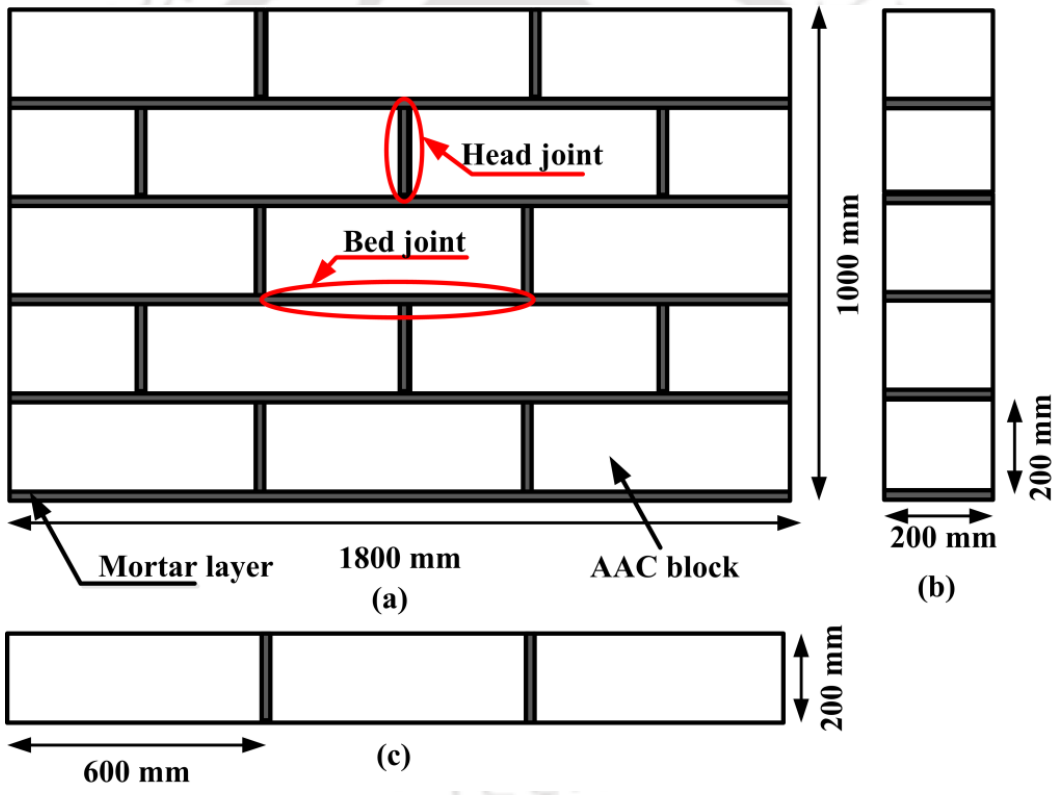

Figure 6.7 The schematic view of the AAC wall system: (a) front view, (b) side view and (c) top view

The joint thickness using sand-cement mortar and polymer modified (PMM) mortar is 12 mm and 3 mm, respectively. However, in case of combination of cement slurry coating and mortar, the total joint thickness is slightly increased from 12 mm to about 13.5 mm due to the addition of extra two coating layers.

The densities of mortars SCM1, SCM2, SCM3 and PMM are 2221 kg/m^3, 2159 kg/m^3, 1998 kg/m^3 and 1700 kg/m^3, respectively. Using the length of block as 600 mm, width as 200 mm, joint thickness as 12 mm, number of head joints as 12 and number of bed joints as 17, the total volume of sand-cement mortar occupied in the wall comes out to be 3×10^7 mm^3. A total volume of 3.3×10^7 mm^3 was calculated to be occupied by the combination of cement slurry coating and sand-cement mortar. Since the density of the individual sand-cement mortar is different, the total mass of the mortar SCM1, SCM2 and SCM3 consumed in the wall is 66.63 kg, 64.77 kg and 59.94 kg, respectively as shown in Table 6.4.

In case of combination of slurry coating with sand-cement mortar, the extra mass of cement (1.14 kg) consumed during the coating is added. During the study, a total of 30 gm cement was consumed by one block of surface area 600×200 mm^2 in the form of cement slurry coating. Similar to the sand-cement mortar, using same block, joint thickness as 3 mm, number of head joints as 12 and number of bed joints as 17, the total volume of PMM mortar occupied in the wall is calculated to be 0.7×10^7 mm^3. The total mass of the PMM mortar consumed in the wall is found to be 11.90 kg. The sand-cement mortar joints contribute 8.3% of the total wall volume, while the PMM mortar contributes only 2% of the total wall volume. The price of sand, cement and PMM powder were collected from the local market (Guwahati, Assam, India). The prices for 50 kg bag of cement, 1500 kg of sand and 30 kg bag of PMM powder are $ 6.10, $ 29.05 and $ 10.89, respectively.

Further, the labour cost incurred for the mortar preparation using all the joint materials was also considered. In India, in general practice, one mason and one helper are required to construct a complete AAC wall of 1 m^3 in 8 hours of working day. The daily wages of mason and helper is $ 6.97 and $ 4.88, respectively (CPWD 2014). In this analysis, one mason and one helper have been considered to construct the AAC wall using the mortar SCM1, SCM2, SCM3 and PMM, respectively. However, one extra helper is required to construct the wall using a combination of cement slurry coating and ordinary sand-cement mortar. From Table 4, it can be observed that using the SCM3 mortar, the total cost incurred is the least while the CSCM1 mortar costs the highest. Comparing the cost and strength of various mortars from Table 6.4, Table 6.3 and Table 6.2, the mortar CSCM3 is found to be the best choice in the building wall construction using AAC blocks.

Table 6.4 The mortar cost analysis for the AAC wall of size 1800×1000×200 mm^3

Mortar types	Sand (kg)	Cement (kg)	PMM (kg)	Cement in coating (kg)	Total mortar consumed (kg)	Mortar cost ($)	Labour cost ($)	Overall cost ($)
SCM1	44.42	22.21	Nil	Nil	66.63	3.58	4.27	7.85
SCM2	51.82	12.95	Nil	Nil	64.77	2.59	4.27	6.86
SCM3	51.37	8.56	Nil	Nil	59.94	2.04	4.27	6.31
CSCM1	44.42	22.21	Nil	1.14	67.77	3.72	6.02	9.74
CSCM2	51.82	12.95	Nil	1.14	65.91	2.73	6.02	8.75
CSCM3	51.37	8.56	Nil	1.14	61.08	2.18	6.02	8.20
PMM	Nil	Nil	11.90	Nil	11.90	4.33	4.27	8.60

The mortar CSCM1, CSCM2 and PMM can be compared with CSCM3. The total cost of using CSCM3 is the least when compared with CSCM1, CSCM2 and PMM. Although the shear and tensile bond strengths of masonry using CSCM1 and CSCM2 mortars are higher than CSCM3, but their total costs are higher. An equal average shear bond strength and higher tensile bond strength as compared to the CSCM3 is observed in case of using the PMM mortar. However, during the bond strength test, the complete block failure occurred rather than the interface or mortar failure in most of the masonries made of CSCM1, CSCM2 and PMM. This indicates that these masonries provide more bond strength than the required bond strength. On the other hand, the interface or mortar failure was observed in the masonry using CSCM3 mortar; however, the bond strength was still significantly higher than that of SCM1, SCM2 and SCM3. Moreover, the availability of CSCM3 mortar is not a problem. Thus, considering cost, supply chain aspect and bond strength, CSCM3 is an optimal choice. PMM mortar is also a good choice because the overall cost of wall-construction using PMM is only slightly more than that using CSCM3; however, its availability may be a problem in some cases. PMM mortar provides extra bond strength but overall cost of constructing a wall is lower than that by using CSCM1 and CSCM2 mortars.

6.5 Conclusions

The bond strength of the AAC masonry using triplet and cross-couplet specimens was studied. In order to study the masonry bond strength, the AAC masonries have been assembled using ordinary sand-cement mortar and polymer modified mortar. The combination of sand-cement mortar and cement slurry coating has been used to enhance the masonry bond strength. Further, the mortar cost estimation for various joint materials has been carried out. The following inferences are drawn from this study:

- The shear bond strength of the masonry using sand-cement mortar was less than that of the masonries using PMM or the combination of cement slurry coating with ordinary mortar.
- The sand-cement mortar with the leanest cement contents, viz. SCM3, provided the least shear bond strength, while the combination of the richest cement mortar and cement slurry coating, viz. CSCM1 has shown the highest shear bond strength. However, strengths of CSCM2 and CSCM3 were not far behind.
- The mortar SCM3 has shown the least tensile bond strength, while the PMM mortar has shown the highest tensile bond strength. Most of the cross-couplet specimens using PMM, SCM1, CSCM1 and CSCM2 have shown the complete tensile failure of the block instead of the joint failure. This is because of the lower tensile strength of the block as compared to the masonry joint strength.
- There is a huge difference of about 72% in the shear bond strength between SCM1 and CSCM1, but the cost difference between these two is less i.e., 19% only. Similar observations can be seen for other mortar with and without cement slurry coating. Hence, large enhancement in the bond strength can be achieved at a low cost by using the ordinary mortar with cement slurry coating.
- Since the AAC block is a lightweight, porous and low density material, use of mortar with ultra-high bonding strength is not preferable. The use of combination of lean cement mortar and cement slurry coating, viz., CSCM3 was found to be the best choice in terms of bond (both tensile and shear) strength and economy.
- PMM mortar provides more than desired bond strength. Moreover, the cost incurred for the mortar is the highest amongst all the mortars investigated in this study. However, unlike CSCM3 mortar, it does not require extra labor cost and hence the overall cost of wall-construction using PMM is only slightly higher than CSCM3.

Chapter 7

Finite Element (FE) Modeling of AAC Masonry for the Assessment and Analysis of Experimental Results

7.1 Introduction

In the earlier chapters, various experimental investigations on the strength of AAC masonry were discussed. Several methods for enhancing the strength of AAC masonry were suggested. Analytical models were developed to validate the experimental results. The statistical tools were used to check the efficacy of the obtained experimental findings. Since AAC block is a new product in India, it is essential to know its behavior, when used in the frame of building structure. Experimental studies on the behavior of AAC masonry structure when subjected to dynamic or in-plane load have been carried by a number of other investigators for many years (Alexendorson 1967, Narayanan and Ramamurthy 2000 and Bhosale et al. 2019). For a load bearing structure as well as framed structure, in-plane compression is an important mode of failure in the masonry walls. This chapter discusses the behavior of AAC masonry in compression using the finite element (FE) modeling method.

Mallikarjuna (2017) carried out a 2-dimensional linear elastic finite element analysis of a masonry shear wall under a pre-compression load of 0.1 MPa. In the masonry shear test, first the pre-compression load (normal stress) is applied in the horizontal direction and then the vertical shear load is applied to the masonry. The pre-compression load enhances the shear strength. By carrying out the shear test at two values of pre-compression load, the cohesion and internal-friction angle can be determined. The normal stress and shear stress distributions were studied. The potential failure mechanism and collapse load were estimated from the analysis. The micro-modeling (heterogeneous) and macro-modeling (homogeneous) are the two basic approaches to model the masonry structures using finite element method. The micro-modeling considers the masonry constituents (mortar and brick unit) as different materials. The brick-mortar bond is considered to be formed by a continuum brick-mortar interface layer. However, in a macro-modeling approach, the mortar joints and brick units are combined into a uniform composite material with average properties of brick and mortar. The micro-modeling is more accurate method to evaluate the actual behavior of masonry

(Bolhassani et al. 2015). The stiffness of the wall depends mainly on brick-mortar interface bond strength rather than the strength of the mortar.

Ferretti et al. (2014) investigated the tensile and compressive strength of AAC beams both experimentally and numerically. They studied the fracture mechanics of AAC by performing three-point bending tests on beams. Małyszko et al. (2015) numerically modeled the splitting tensile test on the cylindrical and cubic AAC specimen. (In splitting tensile test, a compressive line load is applied to the diametrically opposite side of the cylindrical surface that causes lateral tensile stresses.) The failure mechanisms were discussed based on finite element simulations and experiments with the digital image correlation. Ferretti et al. (2015) used the experimental results to calibrate a well-known macroscopic anisotropic constitutive model already developed for ordinary masonry. For both tension and compression, the behavior of AAC masonry as well as full-scale AAC masonry wall in uniaxial directions was simulated. It was concluded that the numerical anisotropic models proposed for traditional masonry can also be used for AAC masonry, if calibrated properly.

Although several researchers have studied the numerical modeling of AAC masonry strength such as compressive strength and bond strength, but none has modeled the development of lateral stresses corresponding to the applied axial compression load. However, it is difficult to obtain it experimentally. The aim of this chapter is to present finite element modeling of AAC masonry under compressive load. The nature of lateral stresses developed due to the application for an axial compressive stress are discussed and compared with that of clay brick masonry. In ordinary masonry system, the bricks and mortar expand laterally when the masonry is subjected to the axial compressive forces. However, both the constituent materials exhibit different mechanical properties. In case of clay brick masonry, the brick unit has higher modulus of elasticity and lower Poisson's ratio as compared to the mortar. As a result, when the masonry is subjected to an axial compressive force, higher lateral strain is developed in mortar as compared to the clay brick. Since the lateral deformation is constrained to be equal due to bond strength and friction at the brick-mortar interface, the lateral compressive stress and lateral tensile stress are induced in mortar and clay brick, respectively. Opposite is the case in AAC masonry. In the present study, a standard masonry prism using AAC unit and mortar (mix of cement and sand) has been modeled for estimating the compressive behavior.

In this chapter, the finite element micro-modeling, governed by plastic-damage constitutive relation in tension and compression (detailed discussion in Chapter 2, Section 2.5.1), has been used to model the AAC block and mortar, while cohesive zone modeling

strategy (detailed discussion in Chapter 2, Section 2.5.2) is adopted to model the block-mortar interface. The developed model has been used for the estimation of AAC masonry strength. The nature of lateral stress developed due the application of axial stress is discussed. The comparative study on stress distribution in AAC block and clay brick masonries is also presented. The results obtained from modeling have good agreement with the experimental results. FEM modelling helps in checking the consistency of the obtained experimental results. It is envisaged that AAC masonry can be a sustainable option for constructing buildings.

The remaining sections of this chapter are arranged as follows. Section 7.2 describes the finite element (FE) modeling of AAC masonry compressive strength using ABAQUS. Section 7.3 discusses the results obtained from the finite element simulation and the experimental validation. The behavior of AAC masonry subjected to uniaxial compressive load is discussed in this section. Section 7.4 concludes the chapter.

7.2 Finite Element Modeling of AAC Masonry Compressive Strength Using ABAQUS

The linear elastic model of the AAC masonry behavior was developed using the commercial finite element package ABAQUS version 6.14, which is capable of carrying out the elastic analysis. The modules of ABAQUS used during AAC masonry modeling process are as follows:

- Part module: This module is used to create a three dimensional shape of the workpiece. During modeling of masonry behavior, 3D geometric part was created using this module.
- Property module: The mechanical properties of the AAC block and mortar was assigned using this module.
- Assembly module: Used for assembly and placing the parts in a global coordinate system.
- Step module: It is used to create and define the analysis steps. Fixed time step increments were chosen for the analysis of elastic behavior of AAC masonry.
- Interaction module: In this module, surface-to-surface contact interaction was selected. The master and slave surfaces were defined to assign the interface properties. For cohesive behavior, the uncoupled stiffness coefficients were specified in this module.

- Load module: Load module was used to define and manage the loads, boundary conditions and predefined fields to view and manipulate the stepwise history of prescribed conditions. In order to model the AAC masonry compressive behavior, a vertical axial concentrated load was applied.
- Mesh module: Mesh module was used to generate finite element meshes on parts and assemblies. It provides tools for prescribing mesh density, element shape and element type. To assign the fine and coarse mesh region, partition toolset was used. The part was discretized with 8-node continuum element having three degree of freedom at each node (C3D8R).
- Job module: After finishing all the tasks involved in defining a model, job module was used to create a job, to submit it for analysis, and to monitor its progress. After the analysis, the different stresses developed were recorded.

A masonry prism is an assemblage of brick units and mortar, which is constructed to serve as a test specimen to determine the compressive strength of masonry. The micro-modeling of compression test of AAC masonry has been carried out. The individual properties of both AAC bricks and mortars used in this study are depicted in Table 7.1. The properties were experimentally evaluated based on the compressive strength test results of AAC blocks and mortar. The material properties for mortar corresponding to mortar grade 1:4 (cement: sand) was considered in this work. The block and mortar were modeled separately using concrete damage plasticity. The softening behavior of AAC block and mortar using the plastic stress-strain data were used as input parameter in the concrete damage plasticity modeling of block and mortar. The plastic stress-strain data of AAC block in compression and tension is depicted in Table 7.2. The plastic stress-strain data of mortar in compression is shown in Table 7.3. Tensile strength for mortar was taken as 3.51 MPa. It was evaluated based on the splitting tensile strength test of cylindrical specimen. The lateral displacement and hence, the Poison's ratio of AAC block and mortar was evaluated using laser extensometer (Make: Epsilon; Model: LE-15). The detailed discussion is presented in Chapter 3 (Section 3.2.3).

As discussed in Chapter 2 of Section 2.5.1, a non-associative flow rule is considered to define the plastic strain rate in CDP model. The multiple-hardening Drucker-Prager type surface is adopted as a yield surface. The yield surface is governed by dilation angle (φ), ratio of biaxial compressive strength to the uniaxial compressive strength (f_{b0}/f_{c0}) and a constant k (Lubliner et al. 1989, van Zijl et al. 2004 and Daltri et al. 2019). The dilation angle or

dilatancy is basically the measure of change in the volumetric strain with respect to the changes in shear strain. The dilation angle defines the amount of plastic volumetric strain induced in the body during the plastic shear. The constant k is the ratio of second stress invariant on tensile meridian to that on the compressive meridian at the failure point. The tensile and compressive meridians are the intersection curves between the plane (meridian plane) containing the hydrostatic axis and the failure surface (detailed discussion in Appendix A). For quasi-brittle material, such as masonry, the value of dilation angle (φ), f_{b0}/f_{c0} and k are generally taken as 10º, 1.16 and 2/3, respectively (Lubliner et al. 1989, van Zijl et al. 2004 and Daltri et al. 2019). Hence, for material modeling, the same values of the respective parameters have been considered in this work.

Surface based cohesive zone model has been used to model the block-mortar interface. Surface to surface interaction module with contact pairs available in finite element package ABAQUS/Standard was used. The following uncoupled stiffness coefficient were used: (a) Stiffness coefficient in normal or opening direction (K_{nn}), (b) Stiffness coefficient in in-plane shear direction (K_{ss}) and (c) Stiffness coefficient in out-of-plane shear direction (K_{tt}) (detailed discussion in Chapter 2 of Section 2.5.2) (Lizárraga and Pérez-Gavilán 2017). The values are provided in Table 7.1.

Table 7.1 The material and interface properties of AAC block and mortar

Material properties for FE modeling			**Interface properties** (Lizárraga and Pérez-Gavilán 2017)	
Properties	**AAC block**	**Mortar (1:4 grade)**	**Stiffness coefficient (N/mm^3)**	
Elastic modulus (MPa)	272.5	1046		
Poisson's ratio	0.14	0.22	K_{nn}	143
Yield strength in compression (MPa)	2.90	21.08	K_{ss}	85
Yield strength in tension (MPa)	0.50	3.51	K_{tt}	85

Table 7.2 The plastic stress-strain data for AAC block

Compression		**Tension**	
Plastic strain	Stress (MPa)	Plastic strain	Stress (MPa)
0	2.90	0	0.50
0.0008	2.89	0.0023	0.49
0.0012	2.86	0.0040	0.48
0.0014	2.82	0.0058	0.47
0.0016	2.77	0.0075	0.42
0.0019	2.71	0.0092	0.40

Table 7.3 The plastic compression stress-strain data for mortar

Plastic strain	Compressive stress (MPa)
0	21.08
0.0022	21.07
0.0050	20.10
0.0067	17.54
0.0084	16.39
0.0096	14.97

The masonry prism of size $210\times110\times398$ mm^3 was modeled with five AAC blocks ($210\times110\times70$ mm^3) and four mortar layers of 12 mm thickness as shown in Figure 7.1 (a). The 8-node continuum element having three degree of freedom at each node (C3D8R) element was used to model the masonry unit and mortar joint. The uniform mess element of sizes 8 mm and 2 mm was considered for block and mortar, respectively shown in Figure 7.1

(b). The bottom surface of the masonry was encastered.A vertical axial concentrated load of 65 kN was applied at the top block. The schematic representation of loading and the boundary conditions is presented in Figure 7.1.

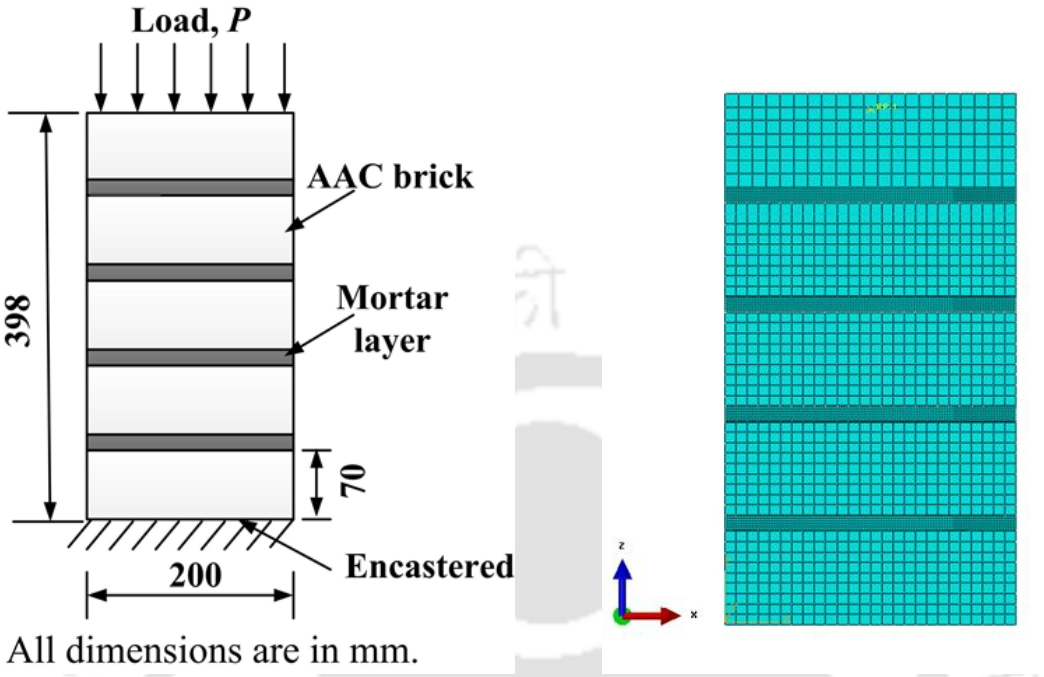

Figure 7.1 Masonry prism subjected to compressive load: (a) loading and boundary condition and (b) meshing of masonry prism adopted in FE modeling

7.3 Results and Discussion

Rankine theory also called maximum principal stress theory, has been used to estimate the masonry prism strength. This theory is basically applied for the brittle material. The principal stress distribution for the axial vertical load of 65 kN (*z*-direction) is shown in Figure 7.2 (a). The minimum and maximum principal stress developed in the block are 2.62 MPa and 2.96 MPa, respectively. Since the maximum principal stress developed in the prism model exceeds the AAC block yield strength i.e., 2.90 MPa, the failure takes in block region. Due to the stress concentration, the maximum principal stress of 3.63 MPa is observed at the corner of top and bottom block. This is also based on the elastic analysis and just indicates failure. Considering that the maximum stress with 65 kN load is 3.63 MPa, whilst the yield strength of the block is 2.90 MPa, a proportionate reduction in loading is needed to avoid failure. From that logic, the maximum load comes out to be 52 kN (without applying a factor of safety).

The obtained results have a good agreement when compared with the experimental results. In the experiment, the compressive strength of AAC masonry was evaluated using the same 1:4 (cement: sand) grade mortar. The geometrical properties of AAC block used to prepare the masonry prism specimens were also same. The specimens were prepared using one block in length and five blocks in height with four mortar layers of 12 mm thickness. The compressive strength test was performed on a total of three AAC prism specimens using the hydraulic universal testing machine of capacity 1000 kN. The test was performed after curing the specimens in moist condition for 28 days. The average compressive strength of individual AAC block and mortar was found to be 2.93 MPa and 24.22 MPa, respectively. However, in this modeling, the input value of individual compressive strength of AAC block and mortar has been considered to be 2.90 MPa and 21.08 MPa (values corresponding to a random specimen), with deviation from mean of 1% and 13%, respectively. The overall average masonry compressive strength of 2.53 MPa, corresponding to the peak load of 55.67 kN, was obtained in the experimental study. Hence, in this modeling work, the observed maximum load of 52 kN has the relative error of 7% with respect to the experimental result (i.e. 55.67 kN). This is a good agreement considering statistical variation.

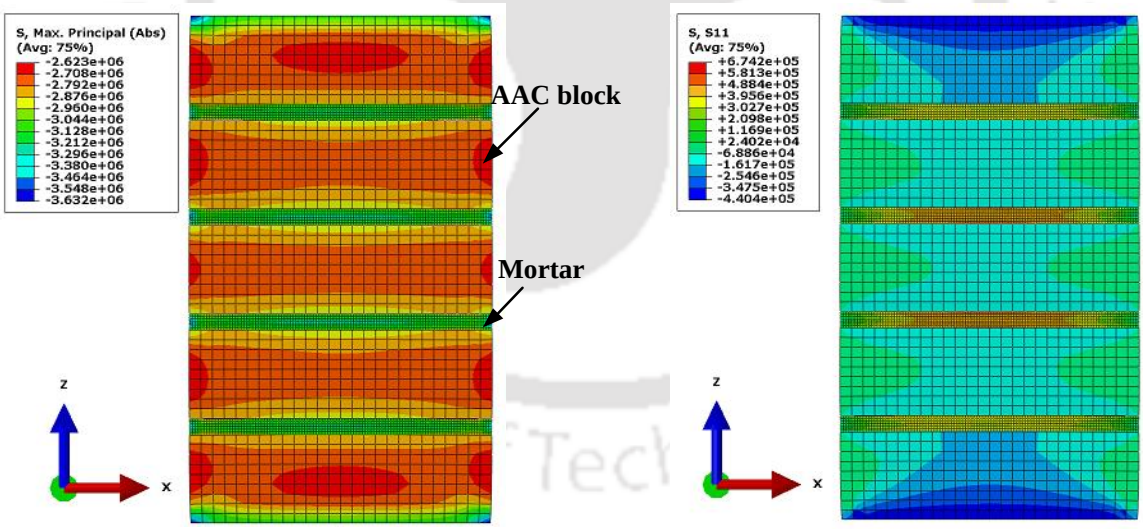

(a) (b)

Figure 7.2 Results of FE modeling of AAC masonry prism for a load of 65 kN: (a) maximum principal stress distribution and (b) lateral stress distribution (*x*-direction)

It is worthwhile to discuss the difference in stress distributions between clay brick and AAC masonries. In both types of masonries, the bricks and mortar expand laterally when the masonry is subjected to the compressive forces. However, both the constituent materials exhibit different mechanical properties. In case of clay brick masonry, the brick unit has higher modulus of elasticity and lower Poisson's ratio as compared to the mortar (Francis et al. 1971, Totaro 1994 and Sarangapani et al. 2005). As a result, when the masonry is subjected to an axial compressive force, higher lateral strain is developed in mortar as compared to the clay brick.

Since the lateral deformation is constrained to be equal due to bond strength and friction at the brick-mortar interface, the lateral compressive stress and lateral tensile stress are induced in mortar and clay brick, respectively (Francis et al. 1971). Therefore, the clay brick is subjected to combination of vertical compression and biaxial lateral tensions. Similarly, the mortar is subjected to the triaxial lateral compression. However, from this study, in case of AAC masonry, the nature of lateral stress developed is different for the same type of axial compression load. Since the modulus of elasticity of AAC block is less than that of mortar, although the Poisson's ratio is also less but its effect is less significant, the lateral stresses induced in the AAC unit and mortar are of opposite nature.

The AAC block is subjected to tri-axial lateral compressive stress, while the combination of vertical compressive and biaxial lateral tensile stress is developed in the mortar layer, as illustrated in Figure 7.3. In Figure 7.3 (b), σ_z is the vertical compressive stress applied to the AAC masonry in *z*-direction, σ_{xb} (compressive) and σ_{xm} (tensile) are lateral stresses developed in the block and mortar in *x*-direction. Similarly, σ_{yb} (compressive) and σ_{ym} (tensile) are the lateral stresses developed in block and mortar in *y*-direction.

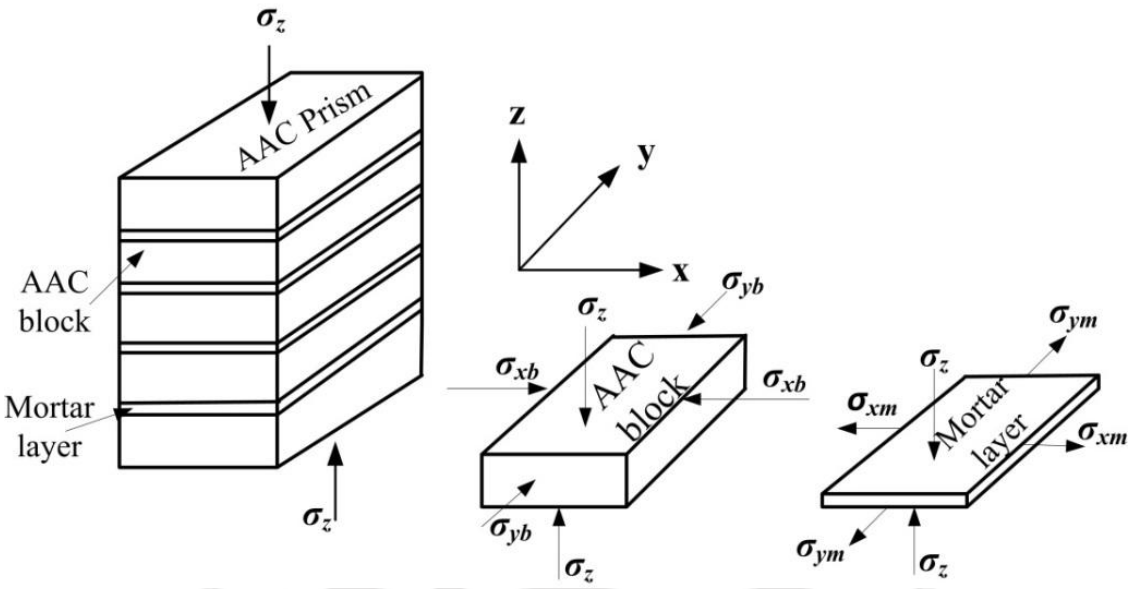

(a) (b)

Figure 7.3 The stress distribution in AAC masonry for axial vertical compression load (a) AAC masonry prism and (b) lateral stress distribution in block and mortar

Similar stress behaviors were observed during the FEM modeling of AAC masonry. As can be seen from Figure 3 (b), showing the lateral stress developed in *x*-direction for an axial vertical load of 65 kN (*z*-direction), the lateral compressive stress is developed in the block portion, while the lateral tensile stress is developed in mortar layer. Similar nature of lateral stress distribution for block and mortar was found in the *y*-direction as observed for *x*-direction.

7.4 Conclusions

FE modeling methodology to model the masonry strength has been discussed in detail. The concrete damage plasticity and cohesive zone model can be used to simulate the masonry behavior. The behavior of AAC masonry in axial compression loading has been discussed. The results obtained from modeling have good agreement with the experimental results. The nature of developed lateral stress due to the applied axial compressive stress has been studied and found different from that of clay brick masonry. For AAC masonry, the lateral compressive stress and lateral tensile stress was developed in AAC block and mortar, respectively. This is in contrast to clay brick masonry, where lateral compressive stress and lateral tensile stress are developed in mortar and brick, respectively.

Chapter 8

Epilogue

8.1 Introduction

Recently, autoclaved aerated concrete (AAC) blocks have appeared as a possible alternative to the clay as well as fly ash bricks. The density of AAC block is lower than that of conventional clay brick, which facilitates in building lighter structures. Autoclaved Aerated Concrete (AAC) blocks are used for both load bearing and non-load bearing masonry walls. The tensile bond and shear bond strengths of such walls are greatly affected by the bond strength of block-mortar interface. For a strong brickwork, a perfect bond between brickwork unit and mortar is crucial. The bond strength becomes significantly important when the masonry is subjected to in-plane and out-of-plane loading during seismic tremors. The masonry unit-mortar bond development is influenced by a large numbers of parameters related to the characteristics of masonry unit and mortar. Masonry unit surface characteristics include the surface roughness of the bonding surfaces and dimensions of the frog, if any, in the brick/block. The water absorption and moisture content of the brick/block also influence bond strengths. Mortar related salient parameters are water retention capacity, compositions and workability.The AAC blocks are wire-cut as per the industrial practice, which results in smooth surfaces. When the two blocks with smooth surfaces are joined with mortar, a high shear bond strength is not attained. The presence of frog in clay brick imparts higher masonry shear bond strength. Further, the proper bond is formed by mechanical interlocking of hydration products in the pores of brick surface. Hydration of products is influenced by the chemistry of mortar composition and the presence of moisture throughout the period of cement hydration. The transport of cementitious material along with water to the interface through capillary suction provides continuity of contact along the two materials.For adequate bond strength, an optimum amount of cementitious material is required at the interface. Insufficient amount will lead to adhesive failures at interface, whilst the excessive amount will lower the cohesive or tensile strength of mortar layer adjacent to the interface. Hence, the primary objective of the present thesis is to enhance the bond strength of AAC masonry.

For this, a grooved AAC block has been studied to enhance the shear bond strength of AAC masonry. Increasing the bond strength of AAC masonry using the combination of cement slurry coating and ordinary sand-cement mortar is another aspect of novelty/innovation in this research work. The thesis also reports the behavior of AAC masonry in compression using the finite element (FE) modeling method. The aim was to assess and analyze the experimental findings. The salient findings of the various subparts of the present work are summarized in the following sections. Finally, the overall conclusion and scope for the future work are presented.

8.2 Evaluation of Mechanical Properties of Autoclaved Aerated Concrete (AAC) Block and its Masonry

Detailed literature review on AAC and its masonry revealed that a large number of investigations on the physical, chemical and mechanical properties of AAC have been carried out in the past. The strength of AAC depends on the raw materials used and their proportions, processing methods and parameters, curing procedure, and atmospheric moisture content. AAC is a relatively new building material in Northeast India that falls in Seismic Zone-V. Hence, there is an urgent need to evaluate the performance of AAC block manufactured in this region. There is hardly any information available on the mechanical properties of AAC masonry based on a thick cement-sand mortar. Also, the effect of joint strength on the overall performance of AAC masonry has still not been presented in any literature. This subpart of the work fills up that gap. It discusses the useful mechanical and physical properties of AAC blocks. Furthermore, the experimental study on compressive strength, shear bond strength and tensile bond strength of AAC masonry using the thick conventional cement-sand mortar have been carried out.

A simple analytical model has also been proposed to evaluate the elastic modulus of masonry prism. The results indicate that there is a positive correlation between the strength of mortar and AAC masonry. The strength of AAC masonry increased with an increase in the strength of mortar. The elastic modulus of AAC masonry evaluated using one-dimensional analytical model is in close agreement with experimental finding. Since the present AAC blocks are smooth at all the six surfaces, the shear bond strength of AAC masonry is low as compared to the clay brick masonry, irrespective of mortar types. For the same cement-sand mortar, the shear bond strength of AAC masonry is 0.03 MPa, whereas for clay brick masonry, it is 0.05 MPa. It is suggested that high shear bond strength could be achieved by introducing the frog or rough textured bed face in the AAC block. Moreover, use of the

combination of cement slurry coating and cement-sand mortar can also result in enhanced shear bond strength. These aspects have been studied in the subsequent parts of the work.

8.3 Compressive and Shear Bond Strengths of Grooved AAC Block and its Masonry

The AAC blocks in vogue have smooth surfaces, due to which they have less bond strength than that of traditional clay bricks. The AAC blocks are wire-cut as per the industrial practice, which results in smooth surfaces. Shear bond strength was low when the two blocks with smooth surfaces were joined with mortar. The presence of frog in clay brick imparts higher masonry shear bond strength. Considering the present AAC manufacturing practice, it is difficult to produce AAC blocks with rough, textured or frogged bonding surface. However, the grooved bed face AAC block can be produced efficiently and economically. The grooved blocks will provide significant increase in shear bond strength as observed through experimentations in this part of study. This part of work reports rigorous experiments on the sliding shear bond (along the bed joint) and compressive strengths of grooved AAC masonry. The results are compared with those for conventional AAC blocks and masonry. Analytical models have been developed to estimate upper, lower and most likely estimates of strengths. Hypothesis testing has been carried out to support the experimental findings. The shear load carrying capacity of grooved AAC masonry triplet was 45.60% more than that of the existing/plain AAC masonry triplet. The percentage increase in compressive strengths of grooved AAC masonries over existing/plain AAC masonry is found to be 9.6%. However, Student's t-test indicated insignificant difference among these compressive strengths. Thus, the findings of this work strongly support the enhancement of shear load carrying capacity of a masonry employing grooved AAC blocks; however, no strong claim can be made for the enhancement of compressive strength.

8.4 Bond Strength of AAC Masonry Using Various Joint Materials

Subsequently, the bond strength of AAC block-mortar interface made of ordinary sand-cement mortar of different compositions and polymer modified mortars were studied. A method of improving the bond strength (both tensile and shear) of ordinary sand-cement mortar without altering the block surface characteristics is proposed. The enhancement of bond strength using cement slurry coating is explored. The shear bond and tensile bond strength of the masonry was studied for all types of interfaces. The failure patterns during the bond strength tests were studied. Afterward, costs were estimated for AAC walls of different types of interfaces. Considering the bond strength as well as cost, using a weak mortar (lean cement content) along with cement-slurry coating was found superior to the ordinary sand-cement mortar and polymer modified mortar.

8.5 Finite Element (FE) Modeling of AAC Masonry for the assessment and analysis of Experimental Results

The last part of this work deals with finite element modeling of AAC masonry for the estimation of compressive strength. The aim was to analyze the experimental findings. For a load bearing structure as well as framed structure, in-plane compression is an important mode of failure in the masonry walls. In this part of work, the finite element micro-modeling, governed by plastic-damage constitutive relation in tension and compression, has been used to model the AAC block and mortar, while cohesive zone modeling strategy is adopted to model the block-mortar interface. The developed model has been used for the estimation of compressive strength of AAC masonry. The nature of lateral stress developed due the application of axial stress is discussed. The comparative study on stress distribution in AAC block and clay brick masonries is also presented. The nature of lateral stress developed in the AAC masonry is different in comparison to clay brick masonry. The results obtained from modeling have good agreement with the experimental results.

8.6 Overall Conclusion

The salient conclusions and contributions are as follows:

- The mechanical properties of the existing AAC block and its masonry were investigated. The elastic modulus of AAC masonry evaluated using one-dimensional analytical model is in close agreement with experimental finding.

- Since the present AAC blocks are smooth at all the six surfaces, the shear bond strength of AAC masonry is low, irrespective of mortar types. A grooved AAC masonry was studied to enhance the shear bond strength.
- The shear load carrying capacity of grooved AAC masonry triplet was 45.60% more than that of the existing/plain AAC masonry triplet. The developed analytical models are capable of obtaining lower, upper and most likely estimates of strengths.
- The percentage increase in compressive strengths of grooved AAC masonries over existing/plain AAC masonry is found to be 9.6%. However, Student's t-test indicated insignificant difference among these compressive strengths. Thus, findings of this work strongly support the enhancement of shear load carrying capacity of a masonry employing grooved AAC blocks; however, no strong claim can be made for the enhancement of compressive strength.
- A technology of grooved AAC block overcomes the disadvantages of present/existing/plain AAC block. The technology is very simple and economical to implement in the present AAC manufacturing industry.
- Increasing the bond strength of AAC masonry using the combination of cement slurry coating and ordinary sand-cement mortar is also another aspect of novelty/innovation in this research work.
- The use of combination of lean cement mortar and cement slurry coating, viz., CSCM3 was found to be the best choice in terms of bond (both tensile and shear) strength and economy.
- The behavior of AAC masonry under compressive load was modeled using the finite element method. The nature of lateral stress developed in the AAC masonry was different to those of clay brick masonry. A good agreement was found between experimental and simulation results.

8.7 Scope for Future Work

Based on the work carried out in this thesis, there are several issues that need further investigations. Some of these are as follows:

- Although the experimental results of the proposed technology of grooved AAC block have been validated through developed analytical models, the numerical validation using finite element code will provide more reliable insight.

- The number of grooves can be optimised to obtain the optimum shear bond strength. Moreover, there is a need to implement the mold modification in the manufacturing industry to produce grooved AAC block of industrial size.
- Since the mortar joint thickness also affects the strength of ordinary masonry, the influence of mortar or glue thickness on the overall strength of AAC masonry should be studied in future.
- An appropriate failure criterion in presence of combined stresses for AAC masonry needs to be developed.

References

- A Petition letter to NarendraModi from AACPA, https://www.change.org/p/narendra-modi-fight-against-red-clay-bricks-promote-environment-friendly-fly-ash-bricks-blocks, Accessed on April 10, 2017.
- Abdul K.A., Mohajerani, A., Roddick, F. and Buckeridge, J., 2009. Density, strength, thermal conductivity and leachate characteristics of light-weight fired clay bricks incorporating cigarette butts. Proceedings of the World Academy of Science, Engineering and Technology, 53, 1035–1040.
- Abuku, M., Janssen, H. and Roels, S., 2009. Impact of wind-driven rain on historic brick wall buildings in a moderately cold and humid climate: Numerical analyses of mould growth risk, indoor climate and energy consumption. Energy and Buildings, 41(1), 101–110.
- Aggarwal, L.K., Thapliyal, P.C. and Karade, S.R., 2007. Properties of polymer-modified mortars using epoxy and acrylic emulsions. Construction and Building Materials 21(2), 379–383.
- Albayrak,M., Yörükog˘lu,A., Karahan,S., Atlıhan, S., Aruntas, H.Y.and Girgin, I., 2007. Influence of zeolite additive on properties of autoclaved aerated concrete. Building and Environment, 42, 3161–3165.
- Alberto, A., Antonaci, P. and Valente, S., 2011. Damage analysis of brick-to-mortar interfaces. Proceedia Engineering, 10, 1151–1156.
- Aldolsun, S., 2006. A Study on Material Properties of Autoclaved Aerated Concrete (AAC) and Its Complementary Wall Elements: Their Compatibility in Contemporary and Historocal Wall Sections, Master Thesis, Graduate School of Natural and Applied Sciences, Middle East Techical University, Turky.
- Alecci, V., Fagone, M., Rotunno, T. and De Stefano, M., 2013. Shear strength of brick masonry walls assembled with different types of mortar. Cons. and Build. Mater., 40, 1038–1045.
- Alexanderson, J., 1979. Relations between structure and mechanical properties of autoclaved aerated concrete. Cement and Concrete Research, 9, 507–514.
- American standard test method for bond strength of mortar to masonry units, ASTM C 952–91, United State, (1991)

- American standard test method for bond strength of mortar to masonry units, ASTM C 952–91, 1991. American Society for Testing and Materials (ASTM), United State
- American standard test method for splitting tensile strength of masonry units, ASTM C 1006-07, American Society for Testing and Materials (ASTM) West Conshohocken, United State, (2007)
- American standard test method for splitting tensile strength of masonry units, ASTM C 1006-07, 2007. American Society for Testing and Materials (ASTM) West Conshohocken, United State.
- American standard test methods for sampling and testing brick and structural clay tile, ASTM C67-00, 4th Edn., American Society for Testing and Materials (ASTM) Philadelphia, United State, (2001)
- ASTM C 1006-07, Standard Test Method for Splitting Tensile Strength of Masonry Units, American Society for Testing and Material (ASTM), West Conshohocken, United State, 2007.
- ASTM C 952-91, Standard Test Method for Bond Strength of Mortar to Masonry Units, American Society for Testing and Material (ASTM), Pennsylvania, United State, 1991.
- ASTM.2017a. Standard specification for autoclaved aerated concrete (AAC).ASTM C1693. West Conshohocken, PA, United State.
- Ayudhya, N. and Israngkura, B., 2011. Compressive and splitting tensile strength of autoclaved aerated concrete (AAC) containing perlite aggregate and polypropylene fiber subjected to high temperatures. Songklanakarin Journal of Science & Technology, 33 (5), 555–563.
- Basha, S.H. and Kaushik, H.B., 2014. Evaluation of nonlinear material properties of fly ash brick masonry under compression and shear. Journal of Materials in Civil Engineering, 27, 04014227.
- Bave, G., 1983. Climatic Conditions and Energy in autoclaved aerated concrete, Moisture and Properties, F.H. Wittmann, Ed., Elsevier, Amsterdam, 1–12.
- Bhosale,A., Zade,N. P., Davis,R., and Sarkar,P., 2019.Experimental Investigation of Autoclaved Aerated Concrete Masonry. Journal of Materials in Civil Engineering, 31, p.04019109.
- Bisceglie, F., Gigante, E. and Bergonzoni, M., 2014. Utilization of waste Autoclaved Aerated Concrete as lighting material in the structure of a green roof. Construction and Building Materials, 69, 351–361.

- Bolhassani, M., Hamid, A.A., Lau, A.C. and Moon, F., 2015. Simplified micro modeling of partially grouted masonry assemblages. Construction and Building Materials, 83, 159–173.
- Bories, C., Borredon, M.E., Vedrenne, E. and Vilarem, G., 2014. Development of eco-friendly porous fired clay bricks using pore-forming agents: A review. Journal of environmental management, 143, 186–196.
- Chen Y., Zhang Y., Chen T., Zhao Y. and Bao S., 2011. Preparation of eco-friendly construction bricks from hematite tailings. Construction and Building Material, 25, 2107–11.
- Chen, W.F., 2007. Plasticity in reinforced concrete. J. Ross Publishing, Cengage learning
- Comité euro-international du béton, 1978. Autoclaved aerated concrete: CEB manual of design and technology, Construction Press, 12.
- Costa A.A., Penna A., Magenes, G., Galasco, A., 2008. Seismic performance assessment of Autoclaved Aerated Concrete (AAC) masonry buildings. In Proc. 14th World Conference on Earthquake Engineering, Beijing, China, 05–04.
- Costa, A.A., Penna, A. and Magenes, G., 2011. Seismic performance of autoclaved aerated concrete (AAC) masonry: from experimental testing of the in-plane capacity of walls to building response simulation. Journal of Earthquake Engineering, 15(1), 1–31.
- Crisafulli F.J., 1997. Seismic behaviour of reinforced concrete structures with masonry infills, Ph.D. Thesis, University of Canterbury, Christchurch, New Zealand.
- D'Altri, A.M., Messali, F., Rots, J., Castellazzi, G. and de Miranda, S., 2019. A damaging block-based model for the analysis of the cyclic behavior of full-scale masonry structures. Engineering Fracture Mechanics, 209, 423–448.
- Dassault Systems. Abaqus analysis user's manual 6.13-3, 2013. RI2013; Dassault Systems Providence: Waltham, MA, USA.
- Demir, I., 2006. An investigation on the production of construction brick with processed waste tea. Building and Environment, 41(9), 1274–1278.
- Dhanasekar M. and Porto Da F., 2009. Review of the progress in thin bed technology for masonry construction. In Proceedings of the 11th Canadian Masonry Symposium , Toronto, Canada.
- Dixit, P.M. and Dixit, U.S., 2008. Modeling of metal forming and machining processes: by finite element and soft computing methods. Springer, London.

- Dugdale, D.S., 1960. Yielding of steel sheets containing slits. Journal of the Mechanics and Physics of Solids, 8(2), 100–104.
- Eliche-Quesada, D., Corpas-Iglesias, F.A., Pérez-Villarejo, L. and Iglesias-Godino F.J., 2012. Recycling of sawdust, spent earth from oil filtration, compost and marble residues for brick manufacturing. Construction and Building Material, 34, 275–84.
- Farid, A.B.E.D.,Aidan,A., Ibrahim, T., Hegazi, N. and Saif, A.D., 2017.Preparation of a new AAC-concrete sandwich block and its compressive behavior at quasi-static loading.Engineering Transactions, 65, 371–389.
- Ferretti, D., Michelini, E. and Rosati, G., 2014. Cracking in autoclaved aerated concrete: Experimental investigation and XFEM modeling.Cement and Concrete Research, 67, 156–167.
- Ferretti, D., Michelini, E. and Rosati, G., 2015. Mechanical characterization of autoclaved aerated concrete masonry subjected to in-plane loading: Experimental investigation and FE modeling. Construction and Building Materials, 98, 353–365.
- Francis A.J., Horman C.B. and Jerrems L.E., 1971. The effect of joint thickness and other factors on compressive strength of brickwork. In: Proceedings of 2nd International Brick Masonry Conference, H. W. H. West, ed., British Ceramic Association Stoke-on-Trent, 31–37.
- Francis, A. J., Horman, C. B., and Jerrems, L. E., 1971. The effect of joint thickness and other factors on the compressive strength of brickwork. Proc., 2nd Int. Brick Masonry Conf. H. W. H. West, ed. British Ceramic Association, Stoke-on-Trent. U.K., 31–37.
- Frey, E. and Briesemann, D., 1985. More Recent calculations of the primary energy costs of autoclaved aerated concrete. Betonwerk and Fertigteil-Technik, No. 79, 468–472.
- Groot, C.J.W.S., 1993. Effects of water on mortar brick bond, (PhD thesis), University of Delft, Delft, Netherland.
- Habib, A., Begum, H.A. and Hafiza, E. R., 2015. Study on production of Aerated concrete block in Bangladesh. International Journal of Innovative Science, Engineering & Technology, 2, 200–203.
- Hamad, A.J., 2014. Materials, production, properties and application of aerated lightweight concrete. International Journal of Materials Science and Engineering, 2(2), 152–157.
- Holt, E. and Raivio,P., 2005. Use of gasification residues in aerated autoclaved concrete, Cement and Concrete Research, 35, 796–802.

- Houst,Y., Alou, F. and Wittmann, F.H., 1983.Influence of moisture contenton the mechanical properties of autoclaved aerated concrete. In:Wittmann FH, editor. Proceedings Autoclaved Aerated Concrete, Moisture and Properties. Amsterdam: Elsevier; 219–33
- https://www.indiatoday.in/india/story/india-s-trash-bomb-80-of-1-5-lakh-metric-tonne-daily-garbage-remains-exposed-untreated-1571769-2019-07-21, Accessed on June 29, 2020.
- Hu, W.Y. and Neufeld,D., 1997. Strength properties of autoclaved cellular concrete with high volume fly ash. Journal of Energy Engineering, 123, 44–54.
- India Standard Code of Practice [IS: 1077-1992, Reaffirmed 2002] for Common burnt clay building bricks-specifications (Fifth Revision), New Delhi, India.
- Indian standard code of practice [IS 1828-1999, Reaffirmed 2005] for Tension/Compression Testing Machines — Verification and Calibration of the Force-Measuring System (Third Revision), New Delhi, India.
- Indian standard code of practice [IS 1905-1987, Reaffirmed 2002] for structural use of unreinforced masonry (Third Revision), New Delhi, India
- Indian standard code of practice [IS 2250-1981, Reaffirmed 2002] for preparation and use of masonry mortars (First Revision), New Delhi, India.
- Indian Standard Code of Practice [IS: 2386 (Part I)-1963, Reaffirmed 2002] for standard methods of test for aggregates and concrete, New Delhi, India.
- Indian Standard Code of Practice [IS: 3495-1976, Reaffirmed 2002] for testing burnt clay building bricks (Third Revision), New Delhi, India.
- Indian Standard Code of Practice [IS: 4031 (Part VI)-1988, Reaffirmed 2005] for determination of compressive strength of hydraulic cement other than masonry cement, New Delhi, India.
- Indian Standard Code of Practice [IS: 6441-1972, Reaffirmed 2001] for testing autoclaved cellular concrete products (Fifth Revision), New Delhi, India.
- Kaushik, H.B., Rai, D.C. and Jain, S.K., 2007. Stress-strain characteristics of clay brick masonry under uniaxial compression. Journal of materials in Civil Engineering, 19, 728–739.
- Kayali, O., 2005, April. High performance bricks from fly ash. In Proceedings of the World of Coal Ash Conference,Vol. 11, Lexinton, Kentucky, United State.

- Khalaf, F.M., 2005. New test for determination of masonry tensile bond strength. Journal of Materials in Civil Engineering, 17, 725–732.
- Kinniburgh, W., 1965. Moisture Content and Moisture Migration in Aerated Concrete," in Proceedings, Symposium on Autoclaved Calcium Silicate Building Products, University of London, Society of the Chemical Industry, 174–181.
- Kowalewski, Ł. and Gajewski M., 2015. Determination of failure modes in brick walls using cohesive elements approach, Proceeding Engineering, 111, 454–461.
- Kunchariyakun,K., Asavapisit,S., and Sombatsompop,K., 2015. Properties of autoclaved aerated concrete incorporating rice husk ash as partial replacement for fine aggregate. Cement Concrete and composite, 55, 11–16.
- Kurama, H., Topcu, I.B. and Karakurt, C., 2009. Properties of the autoclaved aerated concrete produced from coal bottom ash. Journal of Materials Processing Technology, 209(2), 767–773.
- Lam, K.M., Leung, M.Y.H. and Zhao, J.G., 2008. Interference effects on wind loading of a row of closely spaced tall buildings. Journal of Wind Engineering and Industrial Aerodynamics, 96(5), 562–583.
- Lawrence, S.J. and Page, A.W., 1994. Scientific bond studies in masonry. CSIRO, Division of Building. Construction and Engineering, North Ryde, Australia.
- Limbachiya M.C. and Roberts J.J. (Eds.), 2005. Proceeding of 4th International Conference on AAC—Autoclaved Aerated Concrete: Innovation and Development Taylor & Francis, London.
- Lin, K.L., 2006. Feasibility study of using brick made from municipal solid waste incinerator fly ash slag. Journal of hazardous materials, 137(3), 1810–1816.
- Lingling X., Wei Go, Tao W. and Nanru Y., 2005. Study on fired bricks with replacing clay by fly ash in high volume ratio. Construction and Building Material, 19 (3), 243–247.
- Lizárraga, J.F. and Pérez-Gavilán, J.J., 2017. Parameter estimation for nonlinear analysis of multi-perforated concrete masonry walls. Construction and Building Materials, 141, 353–365.
- Longarini, N., Cabras, L., Zucca, M., Chapain, S. and Aly, A.M., 2017. Structural improvements for tall buildings under wind loads: comparative study. Shock and Vibration, 2017, 1–19.

- Lourenco PB., 1994. Analysis of masonry structures with interface elements. Rep. No. 03-21-22-0.
- Lourenco, P.B. Milani, G., Tralli, A. and Zucchini, A., 2007. Analysis of masonry structures: review of and recent trends in homogenization techniques. Canadian Journal of Civil Engineering, 34, 1443–1457.
- Lubliner, J., Oliver, J., Oller, S. and Oñate, E., 1989. A plastic-damage model for concrete. International Journal of solids structures, 25 (3), 299–326.
- Mallikarjuna, S., 2017. Experimental Determination of Parameters for a Micro-Modeling based Failure Criterion for AAC Block Masonry Shear Wall, M.Tech. Thesis, Indian Institute of Technology, Guwahati, India.
- Małyszko, L.,Kowalska, E.,Bilko, P., 2017. Splitting tensile behavior of autoclaved aerated concrete: Comparison of different specimens' results. Construction and Building Materials, 157, 1190–1198.
- Mathey R.G. and Rossiter W.J., 1988. A review of autoclaved aerated concrete products. US Department of Commerce, National Bureau of Standards.
- Mathey R.G. and Rossiter W.J., 1990. A summary of the manufacture, uses, and properties of autoclaved aerated concrete. In Insulation Materials, Testing and Applications. ASTM International.
- Menezes, R.R., Ferreira, H.S., Neves, G.A., Lira, H.D.L. and Ferreira, H.C., 2005. Use of granite sawing wastes in the production of ceramic bricks and tiles. Journal of the European Ceramic Society, 25(7), 1149–1158.
- Miccoli, L., Garofano, A., Fontana, P. and Müller, U., 2015. Experimental testing and finite element modeling of earth block masonry. Engineering Structure, 104, 80–94.
- Minaie, E., Mota, M., Moon, F.L., Hamid, A. A., 2010. In-plane behavior of partially grouted reinforced concrete masonry shear walls. Jornal of Structural Engineering, 136, 1089–1097.
- Mirza, J., Mirza, M.S. and Lapointe R., 2002. Laboratory and field performance of polymer-modified cement-based repair mortars in cold climates. Construction and Building Materials, 16, 365–74.
- Moslemi, M. and Khoshravan, M., 2015. Cohesive zone parameters selection for mode-I prediction of interfacial delamination. Strojniškivestnik Journal of Mechanical Engineering, 61(9), 507–516.

- Mostafa, N.Y., 2005. Influence of air-cooled slag on physicochemical properties of autoclaved aerated concrete. Cement and Concrete Research, 35 (7), 1349–1357.
- Nambiar, E.K. and Ramamurthy, K., 2007. Air-void characterization of foam concrete, Cement and Concrete Research, 37, 221–230.
- Narayanan, N. and Ramamurthy, K., 2000. Structure and properties of aerated concrete: a review, Cement and Concrete Composite, 22, 321–329.
- Qu, X. and Zhao X., 2017. Previous and present investigations on the components, microstructure and main properties of autoclaved aerated concrete–A review. Construction and Building Materials, 135, 505–516.
- Rahman, M.A. and Anand, S.C., 1994. Empirical Mohr-Coulomb failure criterion for concrete block-mortar joints. Journal of Structural Engineering, 120, 2408–2422.
- Rajamane, N.P., Nataraja, M.C., Lakshmanan, N. and Ambily, P.S., 2012. Literature survey on geopolymer concretes and a research plan in Indian context. The Masterbuilder, 148–160.
- Ramamurthi, M., Lee, J.S., Yang, S.H. and Kim, Y.S., 2013. Delamination characterization of bonded interface in polymer coated steel using surface based cohesive model. International Journal of Precision Engineering and Manufacturing, 14(10), 1755–1765.
- Rao, K.V.M., Reddy, B.V.V. and Jagadish, K.S., 1996. Flexural bond strength of masonry using various blocks and mortars. Materials and Structures, 29 (2), 119–124.
- Reddy, B.V. and Jagadish K.S., 2003. Embodied energy of common and alternative building materials and technologies. Energy and buildings, 35(2), 129–137.
- Reddy, B.V.V., and Vyas, C.V.U., 2008. Influence of shear bond strength on compressive strengthand stress-strain characteristics of masonry. Materials and Structures, 41 (10), 1697–1712.
- Reddy, B.V.V., Lal, R. and Rao, K.S.N., 2007. Enhancing bond strength and characteristics of soil-cement block masonry. Journal of Materials in Civil Engineering, 19 (2), 164–172.
- Retrieved August 31, 2019, from https://cpwd.gov.in/Publication/DAR14-Vol2.pdf.
- RILEM. 1993. Autoclaved aerated concrete: Properties, testing and design. London: Taylor & Francis.

- Sarangapani, G., Reddy, B.V.V. and Jagadish, K.S., 2005. Brick-mortar bond and masonry compressive strength. Journal of Materials in Civil Engineering, 17 (2), 229–237.
- Sejnoha, J., Sejnoha, M., Zeman, J., Sykora, J. and Vorel, J., 2008. Mesoscopic study on historic masonry. Structural Engineering and Mechanics, 30, 99–117.
- Singh S.B. and Munjal, P., 2017. Bond strength and compressive stress-strain characteristics of brick masonry, Journal of Building Engineering, 9, 10–16.
- Sinha, B.P., 1983. Factors affecting the brick/mortar interface bond strength. International Journal of Masonry Construction, 3, 14–18.
- Stathopoulos, T. and Zhu, X., 1988. Wind pressures on building with appurtenances. Journal of Wind Engineering and Industrial Aerodynamics, 31(2-3), 265–281.
- Sugo, H.O., Page, A.W. and Lawrence, S.J., 2001.The development of mortar/unit bond.In 9ème Symposium surla maçonnerie Canadienne, Fredericktown, Canada.
- Svanholm, G., 1983. Influence of water content on properties of aerated concrete. In: Wittmann FH, editor. Proceedings Autoclaved Aerated Concrete, Moisture and Properties. Amsterdam: Elsevier; 119–29
- Thamboo J.A. and Dhanasekar M., 2015. Characterisation of thin layer polymer cement mortared concrete masonry bond. Construction and Building Materials, 82, 71–80.
- Thamboo J.A., Dhanasekar M. and Yan C., 2013. Flexural and shear bond characteristics of thin layer polymer cement mortared concrete masonry, Construction and Building Materials, 46, 104–113.
- Totaro, N., 1994. A hybrid elastic theory for evaluation of compressive strength of brick masonry. In Proc., 10th Int. Brick and Block Masonry Conf. 1443–1451.
- Turgut, P. and Algin, H.M., 2007. Limestone dust and wood sawdust as brick material. Building and Environment, 42(9), 3399–3403.
- Turon, A., Davila, C.G., Camanho, P.P. and Costa, J., 2007. An engineering solution for mesh size effects in the simulation of delamination using cohesive zone models. Engineering fracture mechanics, 74 (10), 1665–1682.
- Valore, R.C., 1954. Cellular concretes part 2 physical properties. In Journal Proceedings, 50 (60), 817–836.
- Walker, P., 1999. Bond characteristics of earth block masonry. Journal of Materials in Civil Engineering, ASCE, 11 (3), 249–256.

- Wittmann F.H. (Ed.), 1992. Proceeding of 3rd RILEM International Symposium on AAC — Advances in Autoclaved Aerated Concrete, Balkema, Rotterdam, Netherland.
- Zhang, L., 2013. Production of bricks from waste materials–A review.Construction and building materials, 47, 643–655.
- Zhang, S., Mousavi, S.M.T., Richart, N., Molinari, J.F. and Beyer, K., 2017. Micro-mechanical finite element modeling of diagonal compression test for historical stone masonry structure, International Journal of Solids and Structures, 112, 122–132.

Appendix

Appendix A

Tensile and Compressive Meridians

The failure of concrete under multiaxial loading is quite complex and is studied by observing its behaviour on deviatoric and meridian planes (Chen, 2007). Deviatoric planes are perpendicular to the hydrostatic axis, while meridian planes are the planes containing the hydrostatic axis in the principal stress space as depicted in Figure A.1. In the figure, the compressive stress is treated as positive. If the meridian plane contains uniaxial tensile or compressive stress, it is called tensile meridian or compressive meridian, respectively. The behaviour of concrete on tensile and compressive meridian differs. The hydrostatic axis in the principal stress space is equally inclined to all the principal stress axes. It has been observed that the failure of concrete is dependent on the hydrostatic pressure (mean of the three principal stresses taking compressive stresses as positive). The failure of concrete on a deviatoric plane changes from triangular at low hydrostatic pressure (compressive) to circular at high hydrostatic pressure (Chen, 2007). In Figure A.1, *P* represents the stresses point in principal stress space in the Haigh–Westergaard coordinate system, in which axes are represented by principal stresses, σ_1, σ_2 and σ_3.

The stress point in the deviatoric plane is represented by three parameters (ξ, r, θ). These parameters are defined as

$$\xi = \frac{I_1}{\sqrt{3}} \tag{A.1}$$

$$r = \sqrt{2J_2} \tag{A.2}$$

$$\theta = \frac{1}{3}\sin^{-1}\left(-\frac{3\sqrt{3}}{2}\times\frac{J_3}{J_2^{\frac{3}{2}}}\right), \tag{A.3}$$

whereI_1 is the first stress invariant of the stress tensor, equal to the sum of the principal stresses. J_2 and J_3 are the second and third stress invariants of deviatoric stress tensor, respectively. They are expressed in terms of principal deviatoric stress as

$$J_2 = \frac{1}{2}\left(s_1^{\,2} + s_2^{\,2} + s_3^{\,2}\right) \tag{A.4}$$

$$J_3 = \frac{1}{3}\left(s_1^{\,3} + s_2^{\,3} + s_3^{\,3}\right), \tag{A.5}$$

where s_1, s_2 and s_3 are the major, intermediate and minor principal deviatoric stresses, respectively; ξ is the distance from origin to the projection of point P on hydrostatic axis (OO'=ξ), while r represents the distance between the stress point P from the hydrostatic axis Also, ξ and r represents the stress invariant measures of hydrostatic and deviatoric stress components, respectively; θ denotes the angle of similarity and is the invariant, which is controlled by the relationship of intermediate principal stress to the major and minor principal stresses. When the intermediate principal stress, σ_2, is equal to the minor principal stress, σ_3, the value of θ becomes 60º, which corresponds to tensile meridian. Similarly, when the intermediate principal stress, σ_2, is equal to the major principal stress, σ_1, the value of θ becomes 0º, which corresponds to compressive meridian. Hence, the value of similarity angle, θ varies only between 0º and 60º. Further, considering the failure surface in the (ξ, r) plane, also called meridian plane, the two extreme plane corresponding to θ=0º and θ=60º are called compressive meridian and tensile meridian, respectively. The compressive meridian and tensile meridian can been seen as the plane bounded by ΔOO′A in Figure A.1 (a) and Figure A.1 (b), respectively. The major principal stress (σ_1), intermediate principal stress (σ_2) and minor principal stress (σ_3) in terms of (ξ, r, θ) are given as (Chen, 2007)

$$\begin{bmatrix}\sigma_1\\ \sigma_2\\ \sigma_3\end{bmatrix} = \sqrt{\frac{2}{3}}r\begin{bmatrix}\sin\left(\theta+\frac{2\pi}{3}\right)\\ \sin\theta\\ \sin\left(\theta-\frac{2\pi}{3}\right)\end{bmatrix} + \frac{\xi}{\sqrt{3}} \tag{A.6}$$

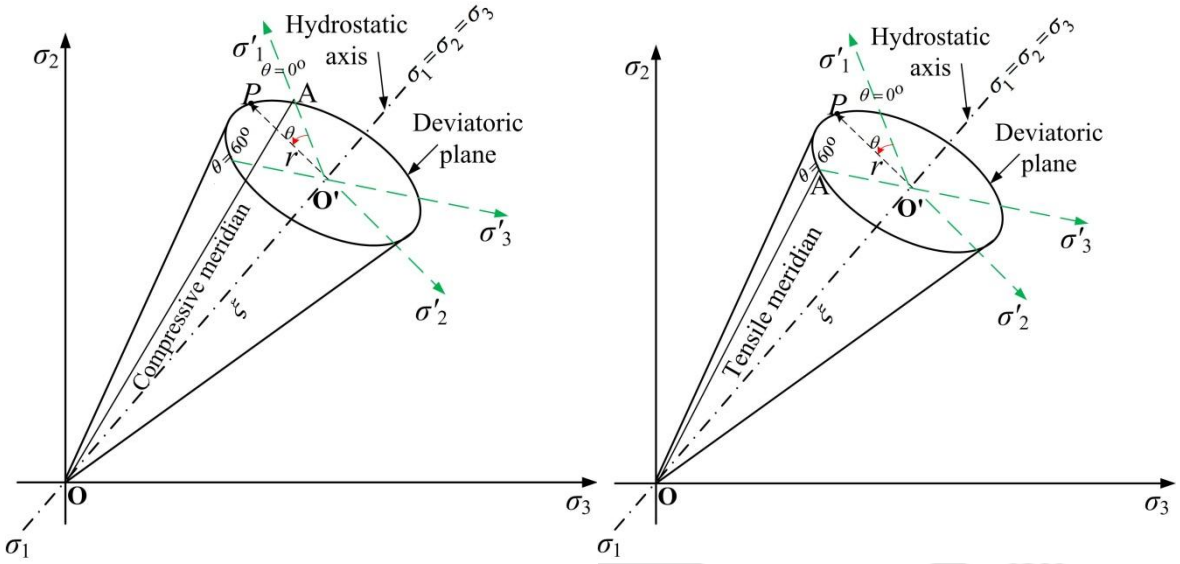

(a) (b)

Figure A.1 Concrete failure envelope in the principal stress space representing (a) compressive meridian and (b) tensile meridian

Appendix B

Important Specification of Universal Testing Machine (UTM)

Make	: Fine Testing Instrument (India)
Model	: TUE-C-1000
Measuring Capacity(kN)	: 1000
Measuring Range (kN)	: 0-1000
Least Count (kN)	: 0.1
Load Range in kN with accuracy of measurement ± 1%	: 20-1000
Resolution of Piston Movement (mm)	: 0.1
Over all dimensions approx. (in mm)	: $2350 \times 800 \times 2700$
Weight approx. (kg)	: 4100

Appendix C

Important specification of Hydraulic Actuator

Make	: MTS, USA
Model	: 243.30T
Measuring Capacity(kN)	: 250 kN
Measuring Range (kN)	: 0–250
Least Count (kN)	: 0.1
Load Range in kN with accuracy of measurement ± 1%	: 01–250
Resolution of Piston Movement (mm)	: 0.1
Load cell and mounting hardware length (mm)	: 267
Swivel head length (mm)	: 264
Weight approx. (kg.)	: 450

Appendix D

Important Specification of Laser Extensometer

Make	: Epsilon Technology Corporation
Model	: LE-15
Measuring Range (mm)	: 8 to 381
Maximum Resolution (mm)	: 0.01 mm
Linearity (mm)	: ±0.04
Repeatability (mm)	: ±0.04
Maximum Scan Rate	: 100 scans/second
Analog Output:	: 16 bit, ±10 VDC standard
Digital Communications	: RS-232 serial communications, standard 3 wire
Display	*:* 2 line, 16 character digital display, backlit LCD
Power Input (VAC)	:230 VAC ±10%, 50/60 Hz optional
Size (in mm):	: 668 L ×457 H × 196 W mm
Weight (kg)	: 20.4
Mounting Provisions	: 1/4-20 UNC tapped holes in base (4)
Laser Source	:Diode laser, 670 nm, <1 mW maximum scanned output CDRH Certified Class II laser instrument

Appendix E

Data of Compressive Load Carrying Capacity of the AAC Blocks

Compressive test result data for AAC block and masonry are presented in Tables E.1 and E.2. The values in square bracket represent percentage coefficient of variation. A large statistical variation is observed.

Table E.1 The compressive strength test results for AAC blocks

Block type	**Load carrying capacity (kN)**	**Compressive strength (MPa)**	**Average load carrying capacity (kN)**	**Average compressive strength (MPa)**
PB1	55.70	2.11		
PB2	77.35	2.93		
PB3	56.23	2.13		
PB4	66.53	2.52		
PB5	56.50	2.14		
PB6	60.19	2.28	62.04 [12.52]	2.35 [12.52]
SGB1	58.87	2.23		
SGB2	63.62	2.41		
SGB3	65.73	2.49		
SGB4	100.58	3.81		
SGB5	53.33	2.02		
SGB6	44.08	1.67	64.42 [27.40]	2.44 [27.40]
DGB1	72.86	2.76		
DGB2	63.88	2.42		
DGB3	78.40	2.97		
DGB4	71.28	2.7		
DGB5	66.26	2.51		
DGB6	69.38	2.62	70.22 [6.6]	2.66 [6.6]

Table E.2 The compressive strength test results for AAC masonry prisms

Masonry prism types	**Load carrying capacity (kN)**	**Compressive strength (MPa)**	**Average load carrying capacity (kN)**	**Average compressive strength (MPa)**
PB1	30.36	1.15		
PB2	29.57	1.12		
PB3	46.46	1.76		
PB4	38.02	1.44		
PB5	23.76	0.90		
PB6	26.93	1.02	32.52 [23.35]	1.23 [23.35]
SGB1	32.21	1.22		
SGB2	40.39	1.53		
SGB3	32.47	1.23		
SGB4	43.30	1.64		
SGB5	25.08	0.95		
SGB6	29.30	1.11	33.79 [26.57]	1.28 [26.57]
DGB1	33.00	1.25		
DGB2	31.94	1.21		
DGB3	31.15	1.18		
DGB4	44.08	1.67		
DGB5	40.92	1.55		
DGB6	34.84	1.32	35.99 [13.42]	1.36 [13.42]

Publications from This Thesis

Patent

[1] Dixit US, Borsaikia AC, Raj A (2018) Autoclaved Aerated Concrete (AAC) Block unit comprising in built anchorage/frog on surface for enhancement of bonding and lateral/shear strength in masonry wall system, Published in the India Patent Office Journal No. 36/2018, application No. 201831028883, Dated: 07/09/2018 **(first examination response report submitted)**

Journal papers

[1] Raj A, Borsaikia AC, Dixit US (2019) Compressive and shear bond strengths of grooved AAC blocks and masonry, Journal of Materials and Structures, 52 (6), 116.https://doi.org/10.1617/s11527-019-1428-8

[2] Raj A, Borsaikia AC, Dixit US (2019) Bond strength of Autoclaved Aerated Concrete (AAC) masonry using various joint materials, Journal of Building Engineering, 28, 101039.https://doi.org/10.1016/j.jobe.2019.101039

[3] Raj A, Borsaikia AC, Dixit US (2020) Evaluation of Mechanical Properties of Autoclaved Aerated Concrete (AAC) Unit and its Masonry, Journal of Institution of Engineers (series A), 101 (2), 315–325. https://doi.org/10.1007/s40030-020-00437-5.

[4] Raj A, Borsaikia AC, Dixit US (2020) Physical and Mechanical properties of Autoclaved Aerated Concrete (AAC) Block used in the building wall system: A review, Manufacturing Technology Today (to be publish in November 2020 issue)

Book chapters

[1] Raj, A, Borsaikia, AC, and Dixit, US, (2020) Finite Element Modeling of Autoclave Aerated Concrete (AAC) Masonry for Estimation of Strength. In *Manufacturing Engineering* (pp. 511–524). Springer, Singapore.https://doi.org/10.1007/978-981-15-4619-8_37.

[2] Raj, A, Borsaikia, AC and Dixit, US, (2019) Manufacturing of Autoclaved Aerated Concrete (AAC): Present Status and Future Trends. In *Advances in Simulation, Product*

Design and Development (pp. 825–833). Springer, Singapore.https://doi.org/10.1007/978-981-32-9487-5_69

Conference papers

[1] Raj A, Borsaikia AC and Dixit US (2018) Manufacturing of Autoclaved Aerated Concrete (AAC): Present Status and Future Trends, 7th International and 28th All India Manufacturing Technology, Design and Research Conference, Anna University, Chennai, India.

[2] Raj A, Borsaikia AC, Dixit US (2019) Finite Element Modeling of Autoclave Aerated Concrete (AAC) Masonry for Estimation of Strength, 6th International Conference on Production and Industrial Engineering (CPIE-2019), DR BR Ambedkar National Institute of Technology, Jalandhar, India.

[3] Raj A, Borsaikia AC and Dixit US (2019) Physical and mechanical properties of Autoclaved Aerated Concrete (AAC) used in the building wall system: A review, 7th International Conference on Advancements and Futuristic Trends in Mechanical and Materials Engineering, Indian Institute of Technology Ropar, India.

[4] Raj A, Barman S, Borsaikia AC, Dixit US (2017) Stress-strain behavior of materials used in a building wall system made of AAC blocks, proceeding of the National Conference on Sustainable Mechanical Engineering Today and Beyond, Tezpur University, India.